MARTIN-LUTHER-UNIVERSITÄT
HALLE-WITTENBERG

Bioenergetik des Wasserstoff-Stoffwechsels

Dr. Constanze Pinske

Habilitation

Constanze Pinske

Habilitation   2021

MARTIN-LUTHER-UNIVERSITÄT

HALLE-WITTENBERG

HYDROGEN

Bioenergetik des

Wasserstoff-Stoffwechsels

Dr. Constanze Pinske

"Bioenergetik des Wasserstoff-Stoffwechsels"

Kumulative
H a b i l i t a t i o n s s c h r i f t

zur Erlangung des akademischen Grades

doctor rerum naturalium habilitatus (Dr. rer. nat. habil)

vorgelegt der

Naturwissenschaftlichen Fakultät I (Biowissenschaften)
der Martin-Luther-Universität Halle-Wittenberg

von

Frau Dr. rer. nat. Constanze Pinske
geb. am 24.12.1983 in Berlin

Gutachter /in

1. Prof. Dr. R. Gary Sawers

2. Prof. Dr. Andrea Sinz

3. Prof. Dr. Gottfried Unden

Halle (Saale), 22. Juni 2021 und 02. Dezember 2021 (Probevorlesung)

Vorwort

Die Menschheit steht vor vielen Herausforderungen, um sich eine komfortable Zukunft mit den jetzigen Lebensstandards zu sichern. Neben Überalterung, Krankheiten und Pandemien ist eines der größten hausgemachten Probleme der Erdbevölkerung der Klimawandel. Durch übermäßigen Ausstoß von Kohlenstoffdioxid (CO_2) hat sich das Klima in einem Maße erwärmt, dass ein anthropogener Einfluss nicht mehr bestreitbar ist und zu Recht fordern daher junge Generationen ein rasches Umdenken in Bezug auf Verbrennungsmotoren, Konsumverhalten und Nachhaltigkeit.

Mit ihrer Forschung versuchen Wissenschaftler weltweit einen Beitrag zu leisten, um Alternativen zu ergründen, die diese Probleme adressieren. Eine Trennung der Wissenschaft von politischen Zielen ist dabei weder wünschenswert noch ökonomisch erstrebenswert. Eine Lösung der politisch angestrebten Energiewende stellt die Nutzung von molekularem Wasserstoff (H_2) als alternative Energiequelle dar. H_2 kann mit Sauerstoff unter Zündung in der Knallgasreaktion Energie von 289,5 kJ mol^{-1}/141,8 MJ kg^{-1} freisetzen, wobei diese Energie alternativ mit Hilfe einer Brennstoffzelle in Elektrizität umgewandelt werden kann (**Abbildung 1**). Um die Nachhaltigkeit zu garantieren, muss der dafür benötigte H_2 aus erneuerbaren statt wie im Moment aus fossilen Rohstoffen hergestellt werden. Für „grünen" H_2 existiert die aktuell im Labormaßstab angewandte Elektrolyse, wenn der Strom aus ökologisch sinnvollen erneuerbaren Quellen wie Sonnen-, Wind- oder Gezeitenkraftwerken stammt. Zusätzlich kann CO_2-neutraler „blauer" H_2 aus fossilen Quellen durch Abscheidung und Speicherung von CO_2 gewonnen werden (Referenz: BMBF). Ein Bedarf von 45 Millionen Tonnen H_2 wird für Deutschland bis 2050 erwartet.
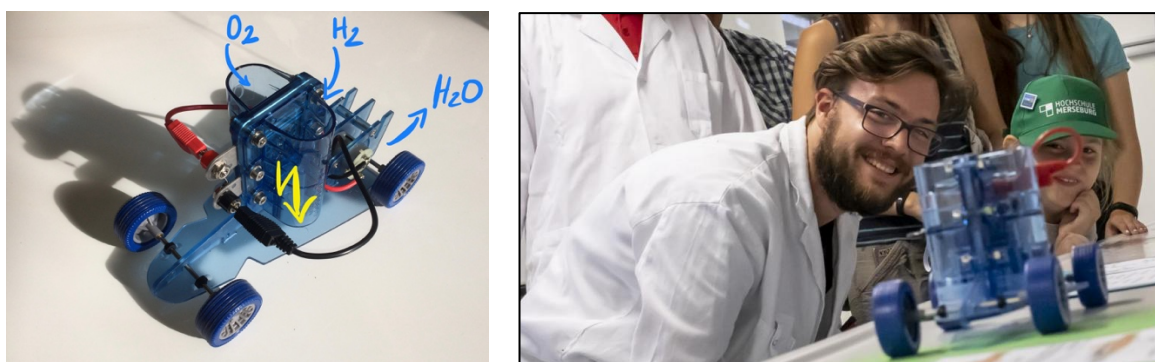
Abbildung 1: Modell-Wasserstoff Brennstoffzelle für den Antrieb eines Spielzeugautos (Cornelsen Experimenta Set Energieumwandlung 3) und dessen Anwendung bei der langen Nacht der Wissenschaften 2018 (Foto: Constanze Pinske und Maike Glöckner).

Der Wechsel zu H_2 als Energieträger wird jedoch nur dann stattfinden, wenn Verfügbarkeit verbunden mit Erzeugung und Lagerung sowie der damit einhergehenden Technik ökonomisch vertretbar werden. Die große Vision von Wissenschaftlern, die an Hydrogenasen forschen, ist es daher, eine enzymatische Version der Biokatalysatoren bereitzustellen, die stabil und langfristig H_2 erzeugt und somit wirtschaftlich konkurrenzfähig ist. Man stelle sich vor, dass jeder Haushalt seinen Abfall in einen kleinen Fermenter wirft und durch Kopplung an eine Brennstoffzelle eigenen, sonnenunabhängigen Strom generiert. Hilfreich hierbei könnten Bakterien sein, die in der Lage sind Kohlenhydrate zu zersetzen und deren Endprodukt H_2 für uns nutzbar gemacht werden könnte.

Mikrobiologie ist die Wissenschaft der Bakterien und der Sinn dieser Forschung liegt auf der Hand: Wir nutzen Mikroben für unsere Zwecke, obwohl sie gleichzeitig unsere Feinde sind. Schon Louis Pasteur hielt fest, dass ein Leben ohne Mikroorganismen nicht lange möglich wäre (Gilbert & Neufeld, 2014). Damit beschrieb er auf einfache Weise die Symbiose mit Mikroorganismen zum Zweck der Bereitstellung von Nährstoffen für Organismen. Dies ist in unserer Hygienegesellschaft jedoch in Vergessenheit geraten und den meisten Menschen bereitet der Gedanke an unsichtbare kleine Mitbewohner eher Unbehagen. Tatsächlich listet die Weltgesundheitsorganisation (WHO) die zunehmende Resistenz von Mikroorganismen als Gefahr für die Gesundheit und damit als neue Herausforderung, der wir uns stellen müssen. Mikroorganismen, die früher leicht mit Antibiotika bekämpft werden konnten, sind aufgrund des umfangreichen Gebrauchs dieser Medikamentenklasse und der dauerhaften Verbreitung in unserer umgebenden Umwelt resistent geworden. Antibiotika sind nicht nur in der Apotheke zu finden, sondern mittlerweile auch in unseren Abwässern, in unserem Nutzvieh und im Boden und somit letztendlich in unserer Nahrung. Dadurch können Mikroorganismen durch horizontalen Gentransfer Resistenzen gegen Antibiotika erwerben und weitergeben. Wenn diese „aufgerüsteten" Bakterien eine Infektion verursachen, sind dringend alternative Medikamente mit neuen Wirkmechanismen erforderlich. Demgegenüber steht, dass die Forschung nach neuartigen antimikrobiellen Wirkstoffen in den letzten Jahrzehnten aufgrund hoher Forschungsinvestitionen und niedriger Margen ins Stocken geraten ist. Stattdessen verlagert sich der Schwerpunkt der aktuellen Forschung auf alternative Strategien wie Phagentherapie oder den Einsatz von Nutz-

Mikroben, die ihre Feinde mit hochspezifischen Verbindungen, die auf bestimmte Bakterienmerkmale abzielen, abtöten können.

Eine der Eigenschaften, die es Bakterien ermöglicht während des Infektionsprozesses erfolgreich zu gedeihen, ist ihr spezifischer Stoffwechsel und die Fähigkeit im Wirt vorhandene Substanzen für ihr eigenes Wachstum zu nutzen. Das Verständnis der Grundprinzipien des Metabolismus und insbesondere der detaillierten Unterschiede zwischen Prokaryoten und Eukaryoten ist die Grundlage für die Entwicklung von hochspezifischen und innovativen Arzneimitteln, die auf diese physiologischen Prozesse abzielen und Bakterien bekämpfen. Meine Forschung wird somit möglicherweise ein Puzzlestück innerhalb dieser beiden Zukunftsszenarios, Energiewende und alternative Medikamente, beisteuern und damit einen Beitrag für eine lebenswerte Zukunft der Menschheit schaffen.

Vorbemerkung

Für die Darstellung der hier vorliegenden Forschungsergebnisse wurde die kumulative Form der Habilitationsschrift gewählt. Die ausgewählten Veröffentlichungen sind als Anlage in der Druckfassung beigefügt und enthalten die experimentellen Daten sowie eine ausführliche Diskussion der entsprechenden Ergebnisse. In dieser Arbeit wurden, unter Verweis auf die jeweiligen relevanten Publikationen, die wesentlichen Aspekte kurz dargestellt und diskutiert. Für gegebenenfalls vorhandene *Supporting Information* zu den entsprechenden Publikationen sei auf die Online-Veröffentlichungen verwiesen.

Halle, den 24.12.2020

Dr. Constanze Pinske

Inhaltsverzeichnis

Verzeichnis der zugrunde liegenden Original-Veröffentlichungen:

Lindenstrauß U & Pinske C* (2019) Dissection of the hydrogen metabolism of the enterobacterium *Trabulsiella guamensis*: Identification of a formate-dependent and essential formate hydrogenlyase complex exhibiting phylogenetic similarity to complex I. *J Bacteriol* **201:** 1480

Lindenstrauß U, Skorupa P, McDowall JS, Sargent F & Pinske C* (2017) The dual-function chaperone HycH improves assembly of the formate hydrogenlyase complex. *Biochem J* **474:** 2937–2950

Lubek D, Simon AH & Pinske C* (2019) Amino acid variants of the HybB membrane subunit of *Escherichia coli* [NiFe]-hydrogenase-2 support a role in proton transfer. *FEBS Lett* **156:** 2194–2203

Marloth JT & Pinske C* (2020) Susceptibility of the formate hydrogenlyase reaction to the protonophore CCCP depends on the total hydrogenase composition. *Inorganics* **8:** 38

Pinske C, Thomas C, Nutschan K & Sawers RG* (2019) Delimiting the function of the *C*-terminal extension of the *Escherichia coli* [NiFe]-hydrogenase 2 large subunit precursor. *Front Microbiol* **10:** 2223

Skorupa P, Lindenstrauß U, Burschel S, Blumenscheit C, Friedrich T & Pinske C* (2020) The *N*-terminal domains of the paralogous HycE and NuoCD govern assembly of the respective formate hydrogenlyase and NADH dehydrogenase complexes. *FEBS Open Bio* **10:** 371–385

Übersichtsartikel:

Pinske C*. 2019. Bioenergetic aspects of archaeal and bacterial hydrogen metabolism. *Adv Microb Physiol* **74**:487–514.

Sawers RG*, Pinske C. 2017. [NiFe]-Hydrogenase Assembly, in 'Metalloprotein Active Site Assembly', edited by Michael K. Johnson and Robert A. Scott. Chichester, UK: John Wiley & Sons, Ltd, pp. 1-11.

Pinske C, Sawers RG*. 2016a. Anaerobic Formate and Hydrogen Metabolism. *EcoSal Plus* **7**:ESP–0011–2016.

* Korrespondierende(r) Autor(in)

Abkürzungsverzeichnis

ADP/ATP	– Adenosindiphosphat/Adenosintriphosphat
CISM	– *complex iron–sulfur molybdoenzyme*
$E^{0'}$	– biologisches Standardredoxpotenzial/-spannung (pH 7,0, 25 °C, 1 atm, 1 M)
Fdh-H	– Formiatdehydrogenase H, mit FHL assoziiert, kodiert vom *fdhF* Gen
[FeS]	– Eisen-Schwefel (Cluster), zum Elektronentransfer innerhalb von Proteinen
FHL	– Formiat Hydrogenlyase, bestehend aus HycE/HyfG, Fdh-H u. a.
H_2	– molekularer Wasserstoff
Hyc	– Proteine des FHL-1-Komplexes mit Hydrogenase 3
Hyd	– Hydrogenase(n)
Hyf	– Proteine des FHL-2 Komplexes mit Hydrogenase 4
Hyp	– *hydrogen pleiotropic*, Reifungsproteine der [NiFe]-Hydrogenasen
Komplex I	– NADH:Ubichinon Oxidoreduktase (Nuo) der mitochondrialen Atmungskette
MBH	– Membrangebundene Hydrogenase, Typ 4b aus *Pyrococcus furiosus*
MRP	– *multiple resistance and pH adaptation,* Klasse von Na^+/H^+-Antiportern
[NiFe]	– Nickel-Eisen; aktives Metallzentrum einer Klasse von Hydrogenasen
PFL	– Pyruvat Formiatlyase, PflB Protein
pmf	– protonenmotorische Kraft (*pmf – proton motive force*)
Q/QH_2	– Chinon/Chinol, Elektronencarrier in der Membran
SAXS	– Röntgenkleinwinkelstreuung (*small angle X-ray scattering*)
spec.	– vom lateinischen Wort *species* (deutsch: Spezies, Art)

Tabellen- und Abbildungsverzeichnis

Einleitung

Die Lebensenergie wird auf Sanskrit Prana genannt. Der aus dem esoterischen Kontext entlehnte Begriff beschreibt, wie wir Kraft in uns finden können. Abseits von dieser eher philosophischen Bedeutung gibt es in jeder lebenden Zelle eine messbare Energie. Diese besteht darin, dass das Innere der Zelle von der äußeren Umgebung durch eine Membran abgetrennt ist, welche sich wie ein Kondensator verhält der Energie speichert. Die Grundeigenschaft dieser Membran ist die räumliche Trennung von Stoffen, insbesondere Ionen des Zellinneren vom -äußeren. Das Leben basiert darauf, diesen Ionengradienten an der Membran aufrecht zu erhalten und dieses Potenzial bei Bedarf in nutzbare Energie umzuwandeln. Nach z. B. einem Herzstillstand tritt durch Energiemangel bedingt innerhalb kürzester Zeit ein Zusammenbruch des Gradienten bei Nervenzellen ein und eine wellenartige Depolarisation breitet sich im Gehirn aus, welche im Falle einer Wiederbelebung sogar Nahtoderfahrungen erklären könnte aber ansonsten den Tod einleitet (Dreier *et al*, 2018). Ein Überschuss von Kationen wird an der Außenseite generiert, was letztlich das Membranpotenzial durch die Separierung von Ladungen bildet. Zusätzlich zu dieser Ladungstrennung wirkt ein pH-Gradient an der Membran, bei dem Außen ein Protonenüberschuss aufgebaut wird, während im Cytoplasma in der Regel ein annähernd neutraler pH-Wert vorliegt. Diese beiden Komponenten ergeben zusammen die **protonenmotorische Kraft (*pmf – proton motive force*)**, die durch den reduktiven Teil des Stoffwechsels etabliert wird; wobei bei einigen Organismen ein Natrium-Ionen (Na^+) Gradient (*sodium motive force*) den pH-Gradienten ersetzt.

1. Atmung

Der Energiestoffwechsel besteht grundsätzlich darin, dass Reduktionsäquivalente/Elektronen entsorgt werden müssen. Bei der Atmung werden diese Elektronen über eine **Elektronentransportkette** auf externe Elektronen-akzeptoren übertragen. Wenn der externe Elektronenakzeptor Sauerstoff ist und zu Wasser reduziert wird, wie es bei der Atmungskette in Mitochondrien stattfindet, handelt es sich um eine aerobe Atmung. Im Gegensatz dazu ist eine Atmung anaerob, wenn andere externe Elektronenakzeptoren als Sauerstoff reduziert werden. Dabei werden Verbindungen mit niedrigem Standard-Redoxpotenzial ($E^{0'}$), welche als Elektronendonatoren dienen, mit solchen mit höheren Redoxpotenzialen, die als Elektronenakzeptoren dienen, miteinander kombiniert (Thauer *et al*, 1977).

Die am Elektronentransfer beteiligten Enzymkomplexe können über verschiedene Mechanismen während der Redoxreaktion Protonen über die Membran translozieren und den Gradienten generieren, der wiederum das Leben der Zelle ermöglicht und sie wachsen lässt. Dieses Grundprinzip gilt für alle Lebewesen und wurde ursprünglich von Peter Mitchell in den 60er-Jahren formuliert (Mitchell, 1961). Energie für die Zelle bedeutet in diesem Zusammenhang die Synthese von **ATP (Adenosintriphosphat)**, welches für chemische Reaktionen benötigt wird. Der Membrangradient wird dafür von membranständigen ATPasen genutzt und durch mechanische Rotation die Energie des Gradienten an die Biosynthese von ATP aus ADP (Adenosindiphosphat) und Phosphat gekoppelt (chemiosmotische Kopplung). Ein Teil der Energie wird dabei in Wärme umgewandelt. Man geht davon aus, dass Energiekonservierung in chemotrophen Organismen ausschließlich über diese Art von Reaktionen stattfindet. Neben der Synthese von ATP wird der Membrangradient zum Transport von Molekülen über die Membran oder die Rotation der (Bakterien-) Flagellen genutzt.

2. <u>Fermentation</u>

Bakterielle Fermentationen gelten als Ausnahme zu dieser Generalisierung, denn dort fehlt eine Elektronentransportkette und ATP wird über einen zweiten Mechanismus hergestellt: der **Substratkettenphosphorylierung** (Herrmann *et al*, 2008). Diese Art der chemischen Reaktion nutzt energiereiche chemische Verbindungen, um Phosphatgruppen auf das energieärmere ADP zu übertragen. Typische Reaktionen sind solche der 3-Phosphoglycerat-Kinase, der Pyruvat-Kinase und der Acetat-Kinase, wie in **Abbildung 2** dargestellt. Erstere Reaktionen sind Teil des weit-verbreiteten Stoffwechselweges der Glykolyse (Embden-Meyerhof-Parnas-Weg) und des Entner-Doudoroff-Weges, während die Reaktion der Acetat-Kinase direkt für die Bildung des Gärungsproduktes Acetat verantwortlich ist (Fuchs, 2017). Der hier ebenfalls benötigte Membrangradient wird umgekehrt unter Hydrolyse von ATP durch eine andere Sorte von ATPasen (P-Typ-ATPasen) etabliert. Während manche Bakterien obligate Fermentierer sind (*Clostridium spec.*, Milchsäurebakterien) nutzen andere fakultative Anaerobier (*Enterobacteriacea*) diesen Mechanismus nur unter bestimmten anaeroben Bedingungen, wenn keine externen Elektronenakzeptoren verfügbar sind. Allerdings zeichnet sich inzwischen ab, dass dieses Konzept nur vordergründig zutrifft. Es gibt vielmehr eine Reihe von Vorgängen, die auch während der Fermentation dazu beitragen, dass Protonen aus der Zelle transportiert werden.

Dies sind z. B. Reaktionen von Enzymen (z. B. Hydrogenase 2, **Kapitel I**) oder Export von Reaktionsprodukten mit Protonensymport (Konings, 2002).
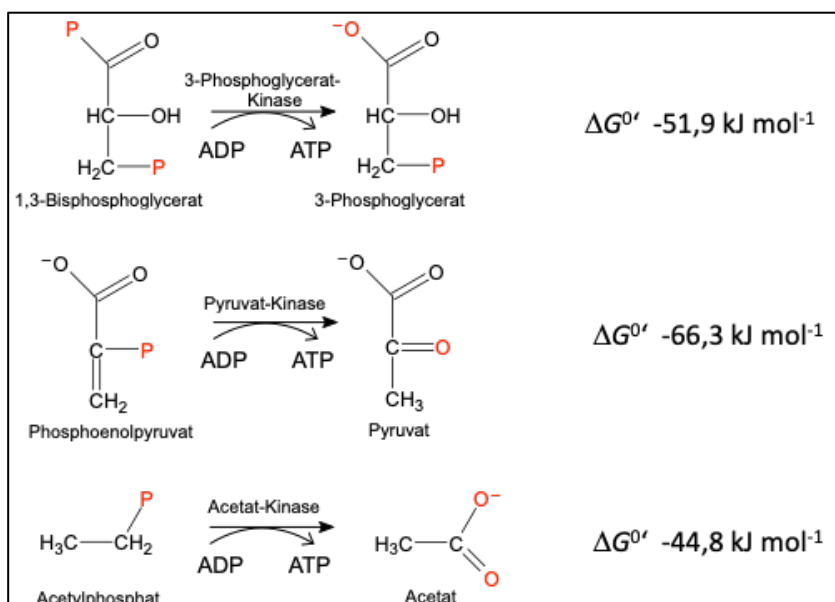
Abbildung 2: Reaktionen, die der Substratkettenphosphorylierung dienen.

3. <u>Wasserstoff-Stoffwechsel</u>

Molekularer Wasserstoff (H_2) kann sowohl zur Energiekonservierung während der Fermentation als auch der Atmung verwendet werden. Dabei nutzen Mikroorganismen H_2 entweder als energiereiche Verbindung ($E^{0'}$ = -414 mV) mit H_2-oxidierenden Enzymen als Elektronendonator, um externe Elektronenakzeptoren während der anaeroben Atmung zu reduzieren. Oder Mikroorganismen entsorgen überschüssige Elektronen auf Protonen indem sie H_2 produzieren, wenn während der Fermentation keine externen Elektronenakzeptoren verfügbar sind. Für diese verschiedenen Stoffwechselprozesse können Mikroorganismen verschiedene **Hydrogenasen (Hyd)** synthetisieren, die ihnen breite metabolische Flexibilität verleihen (Greening *et al*, 2016).

Die atmosphärische Konzentration von H_2 beträgt 0,53 ppm (*parts per million*) aber Organismen in dem Boden sind in der Lage, diese geringen Konzentrationen direkt zu verwenden (Bay *et al*, 2021). Dazu gehören Aktinobakterien wie *Mycobacterium smegmatis* und Knallgasbakterien wie *Cupriavidus necator* (Greening *et al*, 2014; Schäfer *et al*, 2013). Deren Hydrogenasen besitzen besonders hohe H_2-Affinität und koppeln H_2 Oxidation mit O_2-Reduktion. Diese aerobe Atmung dient der Aufrechterhaltung der *pmf*, welche jedoch nicht genügend Energie für das Wachstum liefert. H_2 wird in größeren Mengen durch bakterielle und vulkanische Tätigkeiten im

Boden und an Orten, wo Biomasse zersetzt wird, freigesetzt und vor Ort auch ebenso schnell wiederverwendet (**Abbildung 3**). Neben abiotischen Prozessen und Bildung durch menschliche Aktivität werden jedes Jahr 0,3 Gt (Gigatonnen) H_2 durch bakterielle Fermentation gebildet. Die anschließende Acetogenese oder Methanogenese wären ohne fermentativen H_2 nicht durchführbar und damit wäre auch die Umsetzung von Kohlenstoff als Kreislauf unterbrochen (Thauer, 2011). Diese beiden Prozesse sind eine CO_2-Atmung, bei der H_2 als Reduktionsmittel dient (**Abbildung 3**). Durch Interspezies-Wasserstofftransfer sorgen diese Stoffwechselwege für den Verbrauch von H_2 aus Fermentationen, halten den H_2-Partialdruck gering (<100 Pa) und ermöglichen damit Zersetzungsprozesse, bei denen H_2-Akkumulation energetisch ungünstig wären (Thauer, 2011). Die Acetogenese nutzt den reduktiven Acetyl-CoA-Weg (Wood-Ljungdahl-Weg) und verwendet CO_2 für die Umsetzung zu Essigsäure. Bei der Methanogenese ist das Endprodukt Methan. Das Schlüsselenzym beider Wege ist das Nickel-Enzym Kohlenmonoxid-Dehydrogenase (CODH) /Acetyl-CoA Synthase (ACS) (Burton *et al*, 2018). Reduktionsäquivalente werden u. a. von H_2 mittels Ferredoxin auf dieses Enzym übertragen.
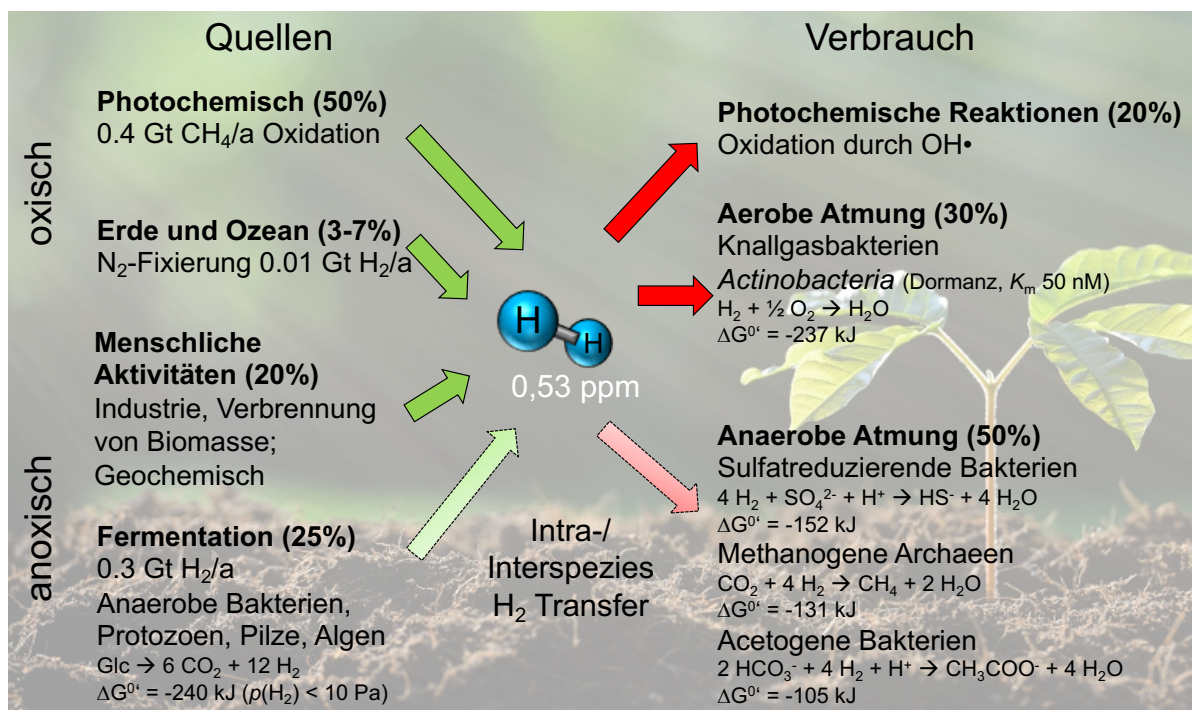
Abbildung 3: Biogeochemischer H_2-Kreislauf. Eine ungefähre Schätzung der Mengen an H_2, die jährlich durch photochemische Prozesse, menschliche und geochemische Aktivitäten, mikrobielle Fermentation und Stickstofffixierung gebildet und durch aerobe und anaerobe Atmung sowie photochemische Reaktionen verbraucht werden. Einige Prozesse nehmen direkt auf den atmosphärischen H_2 Gehalt von 0,53 ppm Einfluss, während Fermentation und anaerobe Atmung durch Intra- und Interspezies H_2-Transfer direkt miteinander verbunden sind. (Zahlen nach Chris Greening und (Thauer, 2011)).

Bei pathogenen Organismen ist H_2 zudem ein essentieller Faktor während der Infektion eines Wirtes (Benoit *et al*, 2020). Wegen seines niedrigen Redoxpotenzials kann es mit der Reduktion aller physiologischen Elektronenakzeptoren (z. B. Nitrat, Nitrit, O_2, Fumarat, Tetrathionat) kombiniert werden. Da H_2 frei im Gewebe diffundiert, beträgt die Konzentration in der Maus ca. 168 µM im Dünndarm und ca. 43 µM im Magen (Benoit *et al*, 2020). Bei *Helicobacter pylori*, *Campylobacter jejuni* und *Salmonella enterica* serovar Typhimurium sind H_2-oxidierende Hyd essentiell für die Infektion des Wirtes und die Proliferation im Gewebe (Benoit *et al*, 2020; Maier *et al*, 2013).

4. <u>Hydrogenasen (Hyd)</u>

Biologischer Wasserstoff kann durch Hyd gebildet werden, welche die reversible Umwandlung von Protonen und Elektronen in H_2 katalysieren. Es sind drei phylogenetische Klassen bekannt ([Fe], [FeFe], [NiFe]), die sich durch den Aufbau ihrer aktiven Zentren voneinander unterscheiden (Thauer *et al*, 2010; Vignais *et al*, 2001). Effiziente Wasserstoffproduzenten finden sich sowohl in der Klasse der [FeFe]-Hyd als auch der [NiFe]-Hyd (**Abbildung 4**). Bisher konnten [FeFe]-Hyd in niederen eukaryontischen Algen und Bakterien identifiziert werden, von denen solche aus *Chlamydomonas*, *Clostridia* und *Desulfovibrio* bislang am besten charakterisiert wurden (Lubitz *et al*, 2014). Ihr aktives Zentrum wird als H-Cluster bezeichnet und umfasst zwei Eisenatome mit diatomaren Liganden (Cyanid- und Carbonylreste), die über ein Cystein direkt mit einem **Eisen-Schwefel ([FeS])-Cluster** verbunden sind (**Abbildung 4**). Die Anzahl der weiteren [FeS]-Cluster variiert je nach Enzym. Die Enzyme nutzen oftmals reduziertes Ferredoxin als Elektronendonator für die H_2-Produktion oder sind an der Elektronenbifurkation beteiligt. Bei der Bifurkation werden z. B. von den zwei Elektronen des NADH eines über einen Flavin-Kofaktor auf H^+ übertragen (endergon) und mit einem zweiten Transfer auf Ferredoxin gekoppelt (exergon) (Buckel & Thauer, 2018; Schut & Adams, 2009).

Im Gegensatz zu den [FeFe]-Hyd, konnte das Vorkommen von [NiFe]-Hyd ausschließlich in Bakterien und Archaeen belegt werden, was die Schlussfolgerung nach sich zog, dass dieses Enzym bereits in LUCA (*last universal common ancestor*) vorhanden gewesen sein muss (Peters *et al*, 2015). Bis vor kurzem waren die [Fe]-Hyd auf Archaeen beschränkt, konnten jedoch von Watanabe *et al*, in einer homologen und Tetrahydrofolat-abhängigen Form in Bakterien nachgewiesen werden

(Watanabe *et al*, 2019). In Archaeen werden [Fe]-Hyd als alternative Enzyme unter Nickel-Mangel synthetisiert und nutzen H_2 als Reduktant für Tetrahydromethanopterin, welches einen Zwischenschritt bei der Reduktion von CO_2 zu Methan in der Methanogenese darstellt (s. o.) (Shima & Thauer, 2007).

Obwohl die Reaktion der Hyd reversibel ist, katalysiert das jeweilige Hyd-Enzym unter physiologischen Bedingungen nur eine Reaktionsrichtung und besitzt daher unterschiedliche Funktionen im mikrobiellen Metabolismus. Diese katalytische Präferenz wird durch die Architektur der sekundären Koordinationssphäre des Cofaktors und der [FeS]-Cluster determiniert, welche die Elektronen leiten (Abou Hamdan *et al*, 2012; Adamson *et al*, 2017).
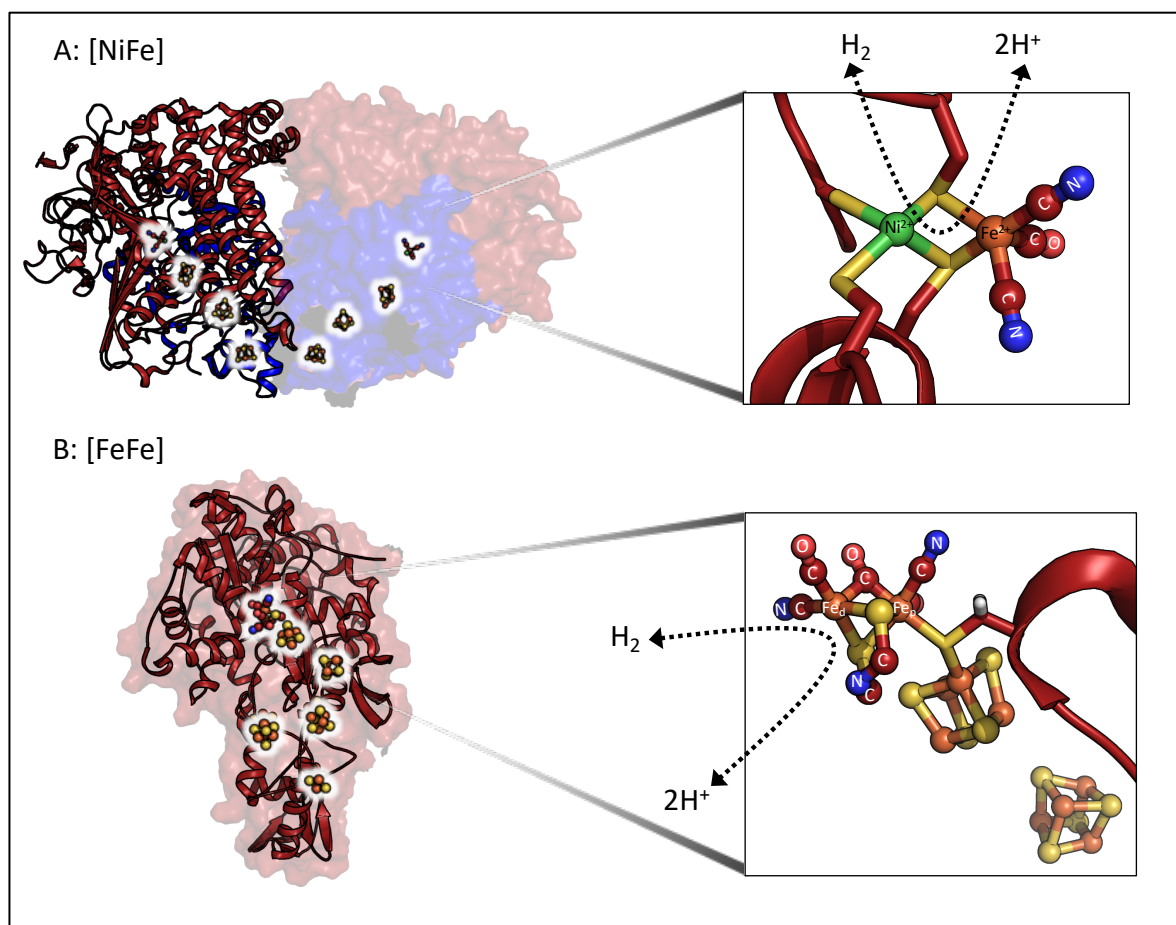
Abbildung 4: Aufbau der [NiFe]- und [FeFe]-Hydrogenasen. A: Dargestellt ist die *Dimer-of-Dimer*-Struktur der [NiFe]-Hydrogenase 5 aus *Salmonella enterica* serovar Typhimurium (PDB: 4C3O) mit den katalytischen Untereinheiten in Rot und den kleinen Elektronentransfer-Untereinheiten in Blau. Das aktive Zentrum und die FeS-Cluster sind als Stäbchen und Kugeln dargestellt. Die Nahaufnahme des aktiven Zentrums zeigt das Ni^{2+} (grün), das Fe^{2+} (orange), die diatomaren Liganden CN^- (rot/blau) und CO (rot/rosa) und der Schwefel der koordinierenden Cysteinreste (gelb). B: Die [FeFe]-Hydrogenase aus *Clostridium pasteurianum* CpI (PDB 4XDC) ist als kombinierte Cartoon-Darstellung mit teilweise transparenter Oberfläche dargestellt. Die Atome des aktiven Zentrums haben die gleichen Farben wie oben, die Eisenatome sind mit Fe_d für distal und Fe_p für proximal zum FeS-Cluster gekennzeichnet (entnommen aus (Benoit *et al*, 2020)).

5. [NiFe]-Hydrogenasen

Die [NiFe]-Hyd zeichnen sich ebenso wie die [FeFe]-Hyd durch ein Eisenatom mit den gebundenen diatomaren Carbonyl- (CO) und Cyanid- (CN⁻) Liganden aus (**Abbildung 4**). Zusammen mit Ni^{2+} stellen die Metalle das aktive Zentrum in der großen oder katalytischen Untereinheit dar. Diese katalytischen Untereinheiten werden mit [FeS]-haltigen Untereinheiten kombiniert und können sowohl solubel sein oder über weitere membrangebundene Untereinheiten an der Membran vorliegen. Entsprechend ihrer Funktion können sie in die Untergruppen 1 bis 4 eingeteilt werden (Vignais *et al*, 2001). Die Gruppen 1 und 2 bilden die respiratorischen H_2-Aufnahme Hyd mit einer periplasmatischen Lokalisation, Gruppe 3 umfasst bidirektionale, Kofaktor-gekoppelte (z.B. F_{420}, NADP) Hyd und Gruppe 4 beinhaltet die H_2-bildendenden Hyd, welche gemäß HydDB weiter unterteilt werden können (Søndergaard *et al*, 2016). Die **Formiat Hydrogenlyase (FHL)**-Komplexe klassifizieren sich phylogenetisch mit anderen H_2-bildenden Hyd in Gruppe 4 der [NiFe]-Hyd. Einige weitere Beispiele gemäß HydDB umfassen die Ferredoxin-gekoppelten MRP-ähnlichen Hydrogenasen (*multiple resistance and pH*) oder die Ech-Hydrogenasen (*energy converting*) (Auszug in **Tabelle 1**) (Søndergaard *et al*, 2016).

Tabelle 1: Gruppe 4 der [NiFe]-Hyd.

Gruppe	Name	Funktion	Taxonomische Verteilung
4a	Formiat hydrogenlyase	Koppelt Formiatoxidation mit fermentativer H_2-Produktion. Könnte H^+-translozierend sein.	Hauptsächlich Gammaproteobacteria z.B. Enterobacteria
4b	Formiat Atmung	Veratmet Formiat oder CO und nutzt H^+ als Elektronenakzeptor. Na^+-transloziierend via MRP.	*Thermococci, Thermoprotei,* und *Thermodesulfovibrio*
4c	Kohlenstoffmonoxid Atmung	Veratmet CO mit H^+ als Elektronenakzeotor. H^+-Translozierend.	Ausschließlich in carboxydotrophen Proteobacteria
4d	Ferredoxin-gekoppelt, MRP-ähnlich	Koppelt Fd_{red} Oxidation mit H^+ Reduktion. Na^+-transloziierend via MRP Komplex.	Ausschließlich in *Thermococci* und *Aciduliprofundi*
4e	Ferredoxin-gekoppelt, Ech-Typ	Koppelt Fd_{red} Oxidation mit H^+ Reduktion. Physiologisch reversibel via H^+/Na^+ Translokation.	Kodiert in verschiedenen Methanogenen und anaeroben Bakterien.
4f	Formiat-gekoppelt (putativ)	Unbekannte Funktion. Könnte Formiatoxidation mit H_2 Produktion koppeln und H^+ translozierend sein.	Kodiert in verschiedenen Firmicutes
4g	Ferredoxin-gekoppelt (putativ)	Unbekannte Funktion. Könnte Fd_{red} Oxidation mit H^+-Reduktion koppeln und H^+/Na^+transloziierend sein.	Sporadisch verteilt in anaeroben Bakterien und Archaeen
4h	Ferredoxin-gekoppelt, Eha-Typ	Koppelt Fd_{red} Oxidation mit H^+ Reduktion in anapleurotischen Reaktionen. H^+/Na^+-transloziierend.	Sporadisch verteilt in anaeroben Bakterien und Archaeen
4i	Ferredoxin-gekoppelt, Ehb-Typ	Koppelt Fd_{red} Oxidation mit H^+ Reduktion in anabolen Prozessen. H^+/Na^+-transloziierend.	Kodiert in verschiedenen Methanogenen

Das Archäon *Thermococcus onnurineus* wächst bei erhöhten Temperaturen von 80 °C mit Formiat als einziger Energiequelle. Es kombiniert ein separates Formiatdehydrogenaseenzym, eine H$^+$-translozierende [NiFe]-Hyd (Gruppe 4b), einen Na$^+$/H$^+$-Antiporter und die ATP-Synthese über eine Na$^+$-abhängige ATPase, um die Energie zu konservieren (Kim *et al*, 2010; Lim *et al*, 2014). Ein weiteres Beispiel ist die Struktur des membrangebundenen Hydrogenasekomplexes (MBH, Gruppe 4d) aus *Pyrococcus furiosus*, die eine Kopplung der H$^+$- und Na$^+$-Ionentranslokation während der H$_2$-Produktion suggeriert (Yu *et al*, 2018) und eine nächste evolutionäre Entwicklung bei der Kombination dieser getrennten Proteine zu einem Komplex darstellt (**Abbildung 5**).

Allerdings reicht die phylogenetische Verwandtschaft weit über Hyd-Enzyme hinaus und bereits mit der Entdeckung der Nukleotidsequenz des FHL-Operons konnte ein Zusammenhang zu **Komplex I** der Atmungskette hergestellt werden (Böhm *et al*, 1990; Volbeda & Fontecilla-Camps, 2012). Diese Verwandtschaft basiert wahrscheinlich auf gemeinsamen evolutiven Vorgängerkomplexen von FHL und Komplex I (Friedrich & Scheide, 2000; Marreiros *et al*, 2012). Alle Komplexe besitzen als Gemeinsamkeit Membranuntereinheiten vom **MRP-Typ (*multiple resistance and pH adaptation*)** (Batista *et al*, 2013)**.** MRP-Antiporter dienen im Allgemeinen dazu, die Kationenhomöostase und in untergeordneter Rolle auch die pH-Homöostase von Zellen und Organellen aufrecht zu erhalten (Padan & Landau, 2016). Die dabei beobachtete Stöchiometrie liegt bei mindestens 2H$^+$ je Na$^+$ (Taglicht *et al*, 1993):

$$NhaA: Na^+ \text{ (innen)} + 2H^+ \text{ (außen)} \rightleftharpoons Na^+ \text{ (außen)} + 2H^+ \text{ (innen)}$$

Den MRP-**Na$^+$/H$^+$-Antiportern** liegt ein Kopplungsmechanismus zugrunde, der in den Membrandomänen dieser phylogenetisch verwandten Komplexe weitgehend konserviert zu sein scheint (Friedrich & Scheide, 2000; Pinske, 2019). Jede Protonen-translozierende Untereinheit besitzt zwei Halb-Kanäle, die Lysinreste in einer unterbrochenen Helix enthalten welche wiederum miteinander über eine Reihe geladener Reste mittig in der Membran (Lysine und Glutamate) verbunden sind. Die unterbrochenen Helices lassen auf eine konformationelle Kopplung schließen. Der Mechanismus von Komplex I involviert eine Bewegung der cytoplasmatischen Domäne, wobei die 120° Drehung einer Helix in der Membran den Ladungstransfer der Redoxreaktion in die Membrandomäne über die geladenen Aminosäuren ermöglicht (Kampjut & Sazanov, 2020). Die Reihe geladener Reste kann damit eine weit entfernte Ladungsänderung (Kationentransport bei MRP oder Elektronentransfer

bei Redoxkomplexen) in die Membrandomäne weiterleiten und an die Protonen-translokation koppeln (Kampjut & Sazanov, 2020; Steiner & Sazanov, 2020; Zickermann *et al*, 2015). Die Gruppe von Sazanov schlug den MRP-Mechanismus als universellen Mechanismus für die gesamte Klasse redoxgetriebener Protonenpumpen vor (Steiner & Sazanov, 2020).

Die **NADH-Ubichinon Oxidoreduktase (**auch **NADH-Dehydrogenase oder Komplex I)** der Atmungskette pumpt bis zu 4 H$^+$ durch die Membran, je ein Proton pro Na$^+$/H$^+$-Antiporter-Membranuntereinheit vom MRP-Typ (**Abbildung 5**). Die Protonen werden während der Ladungsübertragung aus dem Cytoplasma aufgenommen und über Halb-Kanäle auf der Außenseite wieder abgegeben. Der Komplex nutzt dafür die Redoxenergie des Elektronentransfers von NADH ($E^{0'}$= -320 mV) zu Ubichinon (ca. $E^{0'}$ = +113 mV). Das Vorhandensein von Protonophoren erhöht seine Aktivität, da es den *pmf*-Gegendruck während der Protonentranslokation reduziert.
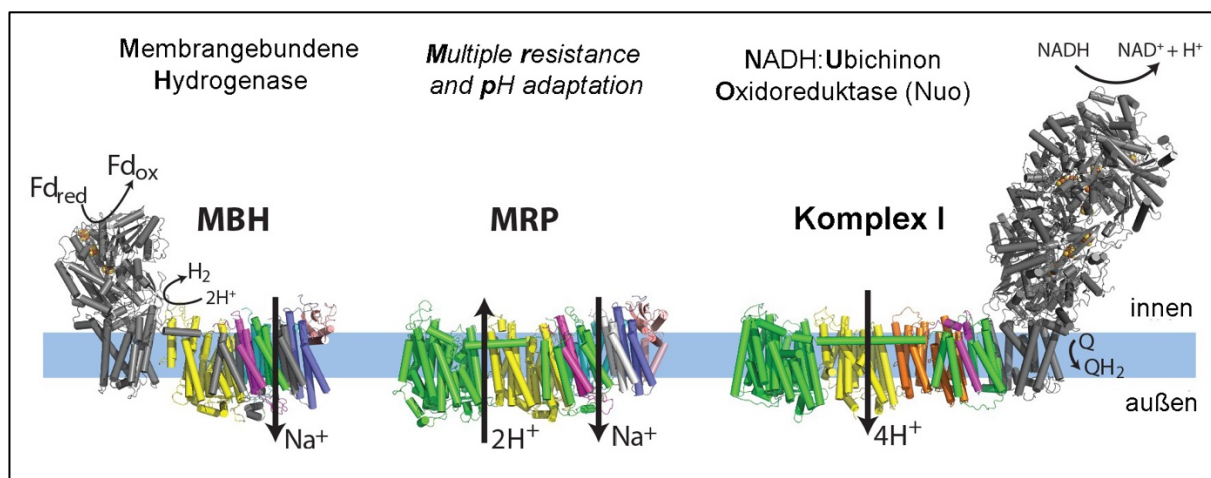
Abbildung 5: Strukturvergleich zwischen MBH (Membrangebundene Hyd, *membrane bound hydrogenase*), MRP (*multiple resistance and pH adaptation*) Na$^+$/H$^+$ Antiporter und Respiratorischem Komplex I. Abbildung modifiziert nach (Steiner & Sazanov, 2020). Homologe Untereinheiten sind identisch angefärbt.

Da im FHL-Komplex Aminosäurepositionen für die Protonentranslokation von Komplex I konserviert sind, wurde eine Energiekonservierung lange vorhergesagt und untersucht (Andrews *et al*, 1997; Böhm *et al*, 1990; Pinske & Sargent, 2016). Dies gilt ebenso für das HycE Protein, welches wie die Ech-(*energy converting hydrogenase*) Hyd zur Klasse 4 der [NiFe]-Hyd gehört, bei denen teilweise bereits eine Energiekonservierung bestätigt werden konnte (Hedderich & Forzi, 2005).

6. __Weitere Mechanismen der Energiekonservierung__

Redoxenzyme nutzen neben dem Protonenpumpen verschiedene Mechanismen zur Energiekonservierung. Eine Redoxschleife aus zwei divergent angeordneten Komplexen, wie Formiatdehydrogenase N und Nitratreduktase, setzt voraus, dass die Membranuntereinheiten die Elektronen durch die 6-8 nm dicke Cytoplasmamembran leiten (Jormakka *et al*, 2003). Beide Komplexe sind fast identisch aufgebaut und besitzen eine katalytische Untereinheit mit einem Molybdän-Kofaktor. Sie gehören zur Gruppe der **CISM (*complex iron–sulfur molybdoenzyme*)**-Komplexe. Elektronen werden vom aktiven Molybdän-Zentrum über [FeS]-Cluster, die in einem Abstand von bis zu 13 Å in der kleinen Untereinheit gebunden sind, zur Membran geleitet und dort über eine membranintegrale Untereinheit mittels zweier Häm-Kofaktoren zur gegenüberliegenden (cytoplasmatischen) Membranseite gebracht. Dort nimmt ein frei durch die Membran diffundierendes Chinon während der Reduktion Protonen aus dem Cytoplasma auf, diffundiert auf die periplasmatische Seite der Membran und gibt die Protonen während der Re-Oxidation am zweiten Komplex ins Periplasma ab. Obwohl die Hyd-1 kein Molybdän besitzt, ist sie phylogenetisch mit CISM-Komplexen verwandt und kann zur Energiekonservierung mittels Redoxschleifen beitragen (Pinske, 2019).

Ein unabhängiger Mechanismus konnte für Hyd 2 vorgeschlagen werden (**Kapitel I**). Hyd-2 gehört zur Klasse 2 der [NiFe]-Hyd und katalysiert die H_2-Oxidation, gekoppelt an z. B. die Reduktion von Fumarat (Pinske & Sawers, 2016; Unden & Bongaerts, 1997). Dieser Enzymkomplex besteht aus einer katalytischen Untereinheit HybC und dazugehöriger kleiner Untereinheit HybO (Menon *et al*, 1994; Sargent *et al*, 1998). Weiterhin sind diese über eine Ferredoxin-ähnliche Untereinheit HybA an die Membranuntereinheit HybB gebunden (Beaton *et al*, 2018; Dubini *et al*, 2002). Die HybB Untereinheit beinhaltet keine weiteren Kofaktoren, sie besitzt jedoch die Chinon-Bindestelle, wo Elektronen aus der H_2-Oxidation auf Chinon übertragen werden. Für die nicht-physiologische Rückreaktion konnte eine Abhängigkeit von der *pmf* nachwiesen werden, was zunächst zur Hypothese einer Protonenpumpe führte (Pinske *et al*, 2015a). Allerdings konnte für die homologe Untereinheit QrcD des phylogentisch verwandten Qrc (*Quinone-reductase complex*)-Komplexes während der Sulfatatmung ein elektrogener Mechanismus postuliert werden (Duarte *et al*, 2018). Dabei werden nicht wie bei der Redoxschleife die Elektronen auf die andere Membranseite gebracht, sondern die Protonen durch die Membran ‚gezogen'.
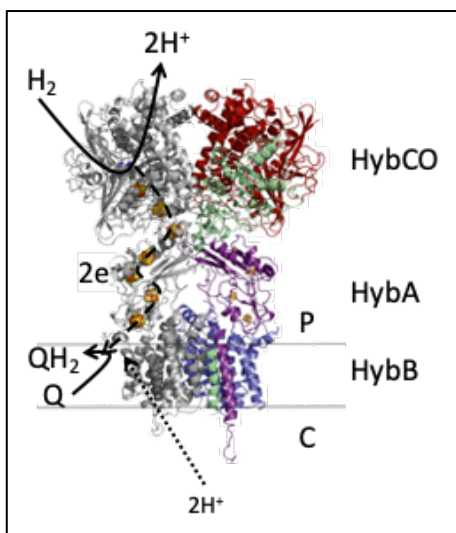
Abbildung 6: Schema der Hyd-2 Reaktion. Die katalytische Untereinheit HybC spaltet H_2 in $2H^+$ und $2e^-$. Die kleine Untereinheit HybO, sowie die Ferredoxin-ähnliche Untereinheit HybA sind im Periplasma lokalisiert (P). Die membranintegrale Untereinheit HybB ist am elektrogenen Mechanismus beteiligt und durch die Reduktion des Chinons (Q) zum Chinol (QH_2) werden Protonen aus dem Cytoplasma (C) auf das Q übertragen. Der heterotetramere Komplex liegt dimerisiert in der Membran vor. Abbildung modifiziert nach (Beaton *et al*, 2018).

Eine bioinformatische Analyse der Membranuntereinheit HybB ergab, dass in einem mit Wasser gefüllten Kanal Protonen aus dem Cytoplasma mittels Hydronium-Ionen (Grotthuß-Mechanismus, Wraight, 2006) auf die periplasmatische Seite der Membran transportiert werden. Dort werden sie jedoch nicht in das Periplasma entlassen, was dem Mechanismus einer Protonenpumpe entspräche, sondern sie werden gemeinsam mit den Elektronen auf das Chinon übertragen (**Abbildung 6 und 17**). Damit bleibt die Reaktion elektroneutral und es werden trotzdem Protonen aus dem Cytoplasma entfernt und eine *pmf* generiert. Dies konnte durch Mutagenesestudien verifiziert werden (Lubek *et al*, 2019) (**Kapitel I**), wobei als treibende Kraft der Elektronentransfer identifiziert wurde.

Der Vollständigkeit halber sei hier noch der grundlegend verschiedene Q-Zyklus des mitochondrialen bc_1 Komplex III der Atmungskette erwähnt. Dieser Komplex überträgt Elektronen von Ubichinol auf Cytochrom *c* und transferiert dabei Protonen über die Cytoplasmamembran (Brandt & Trumpower, 1994). Es ist jedoch keine Hyd bekannt, die diesen oder einen ähnlichen Mechanismus verwendet.

7. <u>Gemischte Säuregärung</u>

Enterobakterien können in Abwesenheit von Sauerstoff und anderen externen Elektronenakzeptoren ihren Stoffwechsel von Atmung auf Fermentation umstellen. Dabei gibt es eine Reihe von Enterobakterien, die bevorzugt neutrale Stoffwechselprodukte produzieren. Das namensgebende Endprodukt für diese 2,3-Butandiolgärung ist 2,3-Butandiol. Beispiele sind die Enterobakteriengattungen *Klebsiella* spec., *Enterobacter* spec., *Citrobacter* spec., *Erwinia* spec. sowie *Serratia* spec. (Brenner *et al*, 2006). Zucker werden hauptsächlich über den Weg der Glykolyse

zu Pyruvat abgebaut, wobei in oben genannten Reaktionen Substratketten-phosphorylierung stattfindet (**Abbildung 2**). Im weiteren Verlauf kondensieren zwei Moleküle Pyruvat unter CO_2-Abspaltung zu Acetyllactat, welches nach nochmaliger Decarboxylierung über Acetoin zu 2,3-Butandiol umgesetzt wird. Es entstehen zusätzlich in geringen Mengen Ethanol und Formiat, welches über die Reaktion der **FHL (Formiat Hydrogenlyase)** zu CO_2 und H_2 disproportioniert wird. Das Zwischenprodukt Acetoin kann mittels des Voges-Proskauer Tests mit Kreatin und α-Naphthol als roter Farbstoff nachgewiesen werden (**Anhang**). Dieser Test dient zur Unterscheidung der zweiten Form der Ameisensäuregärung, bei welcher eine Reihe von organischen Säuren produziert wird, aber insgesamt weniger Gas (CO_2) akkumuliert wird.
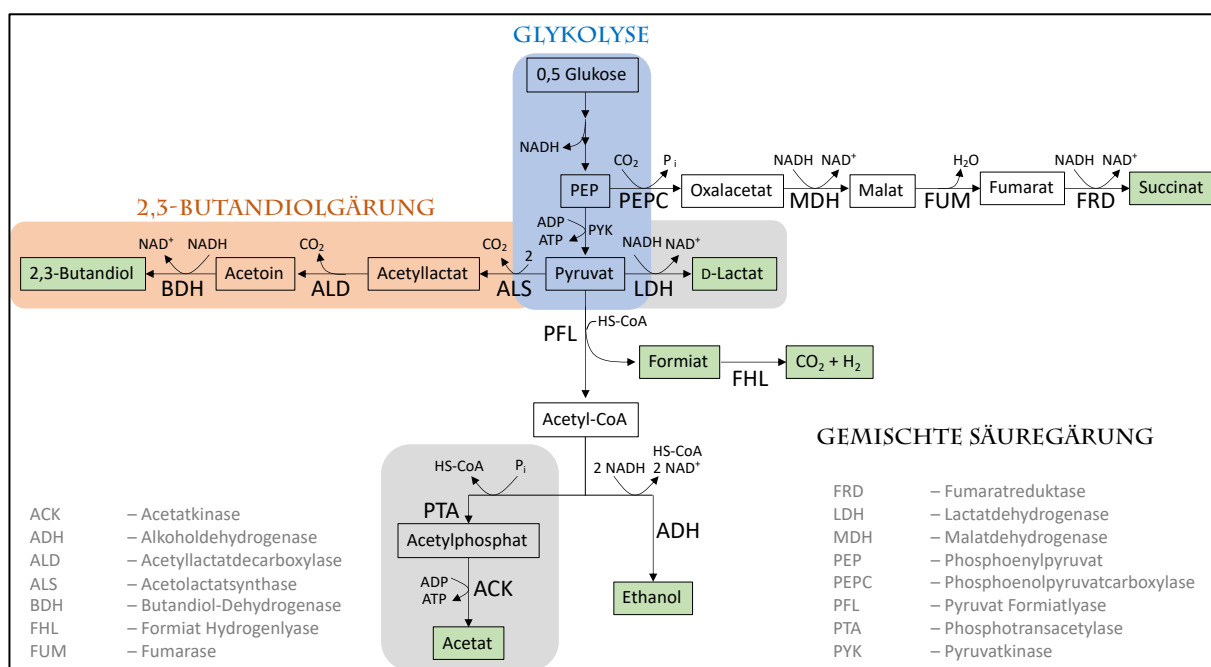
Abbildung 7: Reaktionen der gemischten Säuregärung. Reaktionen, die identisch zur Glykolyse sind, sind blau unterlegt. Reaktionen, die ausschließlich bei der 2,3-Butandiolgärung vorkommen sind orange unterlegt. Reaktionen, die in der 2,3-Butandiolgärung eine untergeordnete Rolle spielen, sind grau unterlegt. Endprodukte sind grün unterlegt. Abkürzungen der Enzymnamen sind angegeben. Abbildung basierend auf Angaben der Wikipedia.

Zu den Produkten der gemischten Säuregärung gehören Acetat, Formiat, Laktat, Succinat und ebenfalls Ethanol und CO_2/H_2, welche aus Formiat gebildet werden (**Abbildung 7**). Zu diesen Enterobakterien gehören *Escherichia coli* und *Trabulsiella guamensis,* die Gattungen *Salmonella* spec., *Shigella* spec. und auch *Yersinia* spec. (Brenner *et al*, 2006). Diesen Bakterien fehlt die Acetolactatsynthase und Acetoin ist nicht nachweisbar (Vivijs *et al*, 2015). Stattdessen wird bevorzugt aus Pyruvat entweder über eine NADH-abhängige Lactatdehydrogenase Lactat oder über die

Pyruvat-Formiatlyase (PFL) Formiat und Acetyl-CoA gebildet. Das Acetyl-CoA kann entweder für die Reoxidation von NADH durch die Alkoholdehydrogenase zu Ethanol umgewandelt werden oder zur Synthese von ATP über die Reaktionen der Phosphotransacetylase und Acetat-Kinase zu Acetat umgesetzt werden (Sawers & Clark, 2004).

8. Formiatstoffwechsel

Eine besondere Bedeutung im Stoffwechsel hat Formiat, das Produkt der PFL-katalysierten Reaktion. Diese C_1-Verbindung hat einen pKa-Wert von 3,75 und das Potenzial das Cytoplasma soweit anzusäuern, dass es durch Destabilisierung der *pmf* zytotoxisch wirken kann (Sawers, 2005). Deshalb wird es zunächst in der frühen exponentiellen Phase durch den Formiattransporter FocA exportiert (**Abbildung 8**), der dabei ein Proton symportiert, welches zusätzlich dem Aufbau der *pmf* dient.
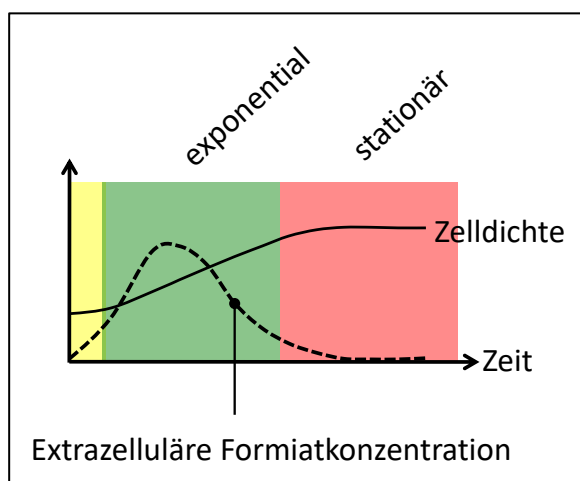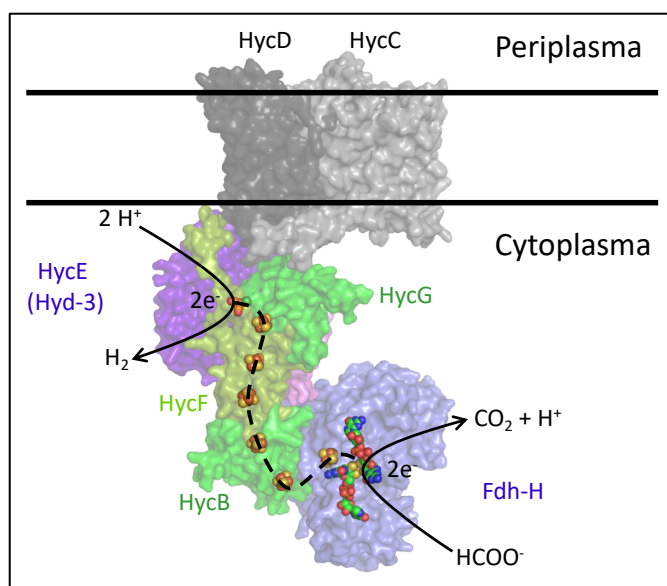
Abbildung 8: Anaerobe Wachstumsphasen einer *E. coli* Kultur (Latenzphase gelb, exponentielle Phase grün und stationäre Phase rot) mit paralleler Darstellung der extrazellulären Formiatkonzentration (gestrichelte Linie). Abbildung basierend auf Daten von (Beyer *et al*, 2013) und entnommen aus (Pinske & Sawers, 2016).

Im Periplasma steht Formiat für respiratorische Prozesse den periplasmatischen Formiat-Dehydrogenasen N und O zur Verfügung. Diese oxidieren es in CO_2 und leiten die Elektronen in die Membran auf den Chinonpool, von wo sie auf terminale Elektronenakzeptoren wie Sauerstoff und Nitrat übertragen werden könnten. In der späten exponentiellen Wachstumsphase wird Formiat gezielt von FocA importiert (**Abbildung 8**) und dient cytoplasmatisch als Induktor für die Gene des FHL-Komplexes und als Substrat für die **Formiatdehydrogenase H (Fdh-H)**, die eine der beiden katalytischen Untereinheiten des FHL-Komplexes darstellt. Der Mechanismus des Reimportes durch FocA ist noch nicht geklärt. Klar ist, dass Formiat nicht als Anion ($HCOO^-$) die Membran passieren kann. Deshalb wäre für den Import ebenfalls ein Protonensymport denkbar. Daten von Beyer *et al*, zeigten, dass Formiataufnahme anscheinend nur dann stattfindet, wenn funktionaler FHL-Komplex gebildet werden
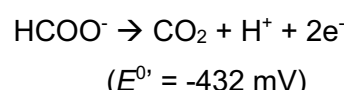
kann (Beyer *et al*, 2013). Diese Abhängigkeit lässt vermuten, dass Energiekonservierung in irgendeiner Art involviert ist, sonst wäre der Import energetisch nachteilig. Damit lassen die Daten ebenfalls die Schlussfolgerung zu, dass der Formiatimport konzentrationsgetrieben ist.

9. Aufbau des FHL-Komplexes

Die Produktion von CO_2 und H_2 aus der Disproportionierung von Formiat wird durch den membrangebundenen FHL-Komplex katalysiert (**Abbildung 9**). Die Fähigkeit zur H_2-Produktion von Enterobakterien wurde bereits 1932 von Marjory Stephenson und Leonard Hubert Stickland beschrieben und als Hydrogenlyase Reaktion benannt (Stephenson & Stickland, 1932). Allerdings konnte erst viel später genau definiert werden, dass *E. coli* drei aktive Hyd Komplexe synthetisieren kann und welcher davon für die H_2-Produktion aus Formiat verantwortlich war (Sawers *et al*, 1985).

Gleichung 1:

$HCOO^- \rightarrow CO_2 + H^+ + 2e^-$

$(E^{0'} = -432 \text{ mV})$

Gleichung 2:

$2H^+ + 2e^- \rightarrow H_2$

$(E^{0'} = -414 \text{ mV})$
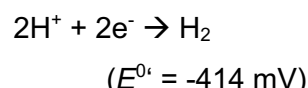
Abbildung 9: Schematische Darstellung des Formiat-Hydrogenlyase Komplexes (FHL). Basierend auf Strukturvorhersagen und Alignment zu Komplex I (pdb 4HEA) wurde diese Vorhersage erstellt. Erläuterungen zum Komplex folgen im Text.

Die cytoplasmatische Domäne des FHL-Komplexes umfasst die Molybdän- und Selen- abhängige Fdh-H, das [NiFe]-Hyd Protein HycE und drei [FeS]-haltige Elektronentransfer Proteine (HycB, HycF, HycG), die den Elektronentransfer zwischen den Domänen ermöglichen (**Abbildung 9**). Dieser verläuft über insgesamt acht [FeS]-Cluster (1x HycG, 2x HycF, 4x HycB, 1x Fdh-H). Die aus der Formiatoxidation zu CO_2 stammenden Elektronen (**Gleichung 1**) gelangen von der Fdh-H zunächst zur kleinen Untereinheit HycB, dann zu einer weiteren elektronentransferierenden Untereinheit HycF und schließlich zur kleinen Untereinheit der Hyd-3, HycG, um durch HycE zur Reduktion von Protonen zu H_2 genutzt zu werden (**Gleichung 2**). Zusätzlich ist die cytoplasmatische FHL-Domäne an eine Membrandomäne gebunden, die zwei als

HycC und HycD bezeichnete Untereinheiten umfasst. Die Membrandomäne ist nicht am Elektronentransfer beteiligt, jedoch für die katalytische Aktivität des Gesamtkomplexes zwingend erforderlich (Pinske & Sargent, 2016; Sauter *et al*, 1992). Gleichzeitig bleiben die beiden separaten Enzymaktivitäten der Hyd-3 und Fdh-H in Abwesenheit der Membrandomäne als Reduktion von Redoxfarbstoffen nachweisbar. Auch eine isolierte lösliche Domäne alleine zeigt, dass beide Reaktionen durchgeführt werden können, jedoch nicht miteinander gekoppelt werden können. Meine derzeitige Hypothese ist, dass nur die Membrananbindung die Kopplung der beiden Halbreaktionen von Fdh-H und HycE aktiviert oder ermöglicht.

Bei einigen Bakterien wie *E. coli* und *Citrobacter* spec. kodiert das Genom für einen weiteren FHL-Komplex (**FHL-2, Hyf-Proteine, Hyd-4**). Die beiden FHL-Komplexe können anhand des Vorhandenseins eines Hyd-4-spezifischen Membranproteins HyfE eindeutig unterschieden werden (**Tabelle 2**). Allerdings konnte in *E. coli* die Aktivität des FHL-2 Komplexes bisher nicht direkt nachgewiesen werden. Der Komplex wurde ausschließlich durch Genomanalyse entdeckt (Andrews *et al*, 1997), aber seine Aktivität konnte in Stämmen ohne die anderen Hyd nicht detektiert werden (Redwood *et al,* 2008). Lediglich indirekt in Anwesenheit von entweder FHL-1 oder Hyd-2, die unter bestimmten Bedingungen ebenfalls H_2 produziert, wurde auf H_2-Produktion von FHL-2 geschlossen (Bagramyan *et al*, 2001; 2002). Als Gründe für die Abwesenheit von FHL-2 Aktivität in *E. coli* wurde vermutet, dass der *hyf*-Promoter zu schwach für die Expression ist (Self *et al*, 2004; Skibinski *et al*, 2002) oder weil in dem Operon keine Endoprotease für die Prozessierung zur Verfügung steht (Finney *et al*, 2020). Die Frage, warum der FHL-2 Komplex in *E. coli* inaktiv ist, konnte bisher nicht abschließend geklärt werden. So konnten auch Experimente mit Promoteraustausch oder Mutagenese zur Spezifität durch die HycI-Protease des FHL-1 Komplexes keine Erklärung liefern (Finney *et al*, 2020; Finney & Sargent, 2019).

Im Vorhandensein der FHL-Komplexe zeigt sich bereits innerhalb der Enterobakterien große Variabilität (**Anhang**). Es existieren Stämme wie *E. coli* Nissle 1917 (O6:K5:H1) und dessen uropathogenen Verwandten CFT073, bei denen die Gene für den FHL-2 Komplex nicht vorkommen oder Stämme wie *E. coli* BL21 (Gruppe B), bei denen Mutationen den FHL-2 Komplex inaktivieren. Andere Enterobakterien wie *S. enterica*, *Enterobacter* spec. und *Klebsiella* spec. kodieren ausschließlich den FHL-1 (Hyc)-Komplex. Andere dahingegen haben keinen der beiden Komplexe (*Yersinia pestis* –

Familie *Yersiniaceae* und *Providencia stuartii* - Familie *Morganellaceae*,) (Benoit *et al*, 2020). Und weitere haben nur den FHL-2 Komplex (*Proteus* spec., *Morganella morganii* – beide Familie *Morganellaceae*, *Yersinia enterocolitica* – Familie *Yersiniaceae*) (Benoit *et al*, 2020). Während H$_2$-Oxidation die Pathogenität bei *S. enterica* fördert, war die FHL-Reaktion (FHL-1) nicht essentiell, während FHL-Deletion bei *Proteus mirabilis* (FHL-2) eine Attenuierung hervorruft (Lin & Liaw, 2020; Maier et al, 2013). Dies suggeriert eine unterschiedliche Involvierung der beiden Komplexe in die Energiekonservierung.

Auch *T. guamensis* kodiert ausschließlich den FHL-2$_{Tg}$-Komplex und produziert damit nachweislich H$_2$ (Lindenstrauß & Pinske, 2019) (**Kapitel II**). Das langsam wachsende pflanzenpathogene Enterobakterium *Pectobacterium atrosepticum* codiert ein identisches Hydrogenase-Komplement wie *T. guamensis* und seine H$_2$-Produktion, aber noch nicht seine Bioenergetik wurden charakterisiert (Finney *et al*, 2019). Beide Organismen stellen durch ihre genetische Zugänglichkeit hervorragende Kandidaten zur Untersuchung der Funktion des FHL-2 Komplexes dar, wobei *T. guamensis* den Vorteil hat nicht-pathogen zu sein und einen schnell wachsenden Lebensstil zu haben. Als dieses Bakterium 1992 aus einem Staubsaugerbeutel der Bibliothek auf Guam isoliert wurde, wurde es zunächst für eine Unterart von *S. enterica* gehalten, weil es z. B. auch H$_2$S Produktion aufwies, jedoch im Gegensatz zu *Salmonella* Cellobiose verstoffwechselte und im ONPG (*o*-Nitrophenol-β-D-galactopyranosid)-Test negativ war (McWhorter *et al*, 1992).

Tabelle 2: Homologe Membranuntereinheiten zu FHL-Komplexen.

FHL-1	FHL-2	Komplex I (*E. coli*)	Anzahl der Transmembranhelices	MRP
HycC	HyfB	NuoL	14+2, inklusiver langer transversaler α-Helix und Anker	MrpA (transportiert H⁺)
HycD	HyfC	NuoH	8	Nicht vorhanden
Nicht vorhanden	HyfD/F	NuoM/N	14	MrpD (transportiert H⁺)
Nicht vorhanden	HyfE	NuoK	3	MrpC (transportiert Na⁺)
Nicht vorhanden	Nicht vorhanden	NuoJ	5	*C*-Terminus von MrpA

FHL-2 Komplexe weisen einen bedeutenden Unterschied zu FHL-1 Komplexen auf: Sie besitzen fünf vorhergesagte Membranuntereinheiten (**Tabelle 2**). Die FHL-Komplexe enthalten bis zu drei Membranuntereinheiten vom **Na⁺/H⁺-Antiporter-MRP-Typ (*multiple resistance and pH adaptation*)** (HycC in FHL-1 und HyfB, D und F in FHL-2), die möglicherweise die gegenseitige Umwandlung von H^+- und Na^+-Gradienten während der Katalyse ermöglichen. Die Funktion der überzähligen Membranuntereinheiten ist Gegenstand meiner derzeitigen Forschung.

10. Genetische Organisation der FHL-Operons

Die Proteine der Hyd-3 (FHL-1) sind innerhalb des *hycA-I*-Operons kodiert, wobei ergänzend zu den oben genannten Strukturproteinen das regulatorische Protein HycA, die HycE-spezifische Endoprotease HycI und das HycE-spezifische Chaperon HycH kodiert sind (Sauter *et al*, 1992; Pinske & Sawers, 2016; Lindenstrauß *et al*, 2017) (**Abbildung 10**). Es gibt eine Reihe von *hyc*-Operons, die einen weiteren Leserahmen enthalten, der von uns als *hycJ* bezeichnet wird und von dem nachgewiesen wurde, dass Kotranskription mit *hycI* stattfindet (**Anhang**). Allerdings konnten Studien in *E. coli* Nissle bisher keinen weiteren Phänotyp aufzeigen.
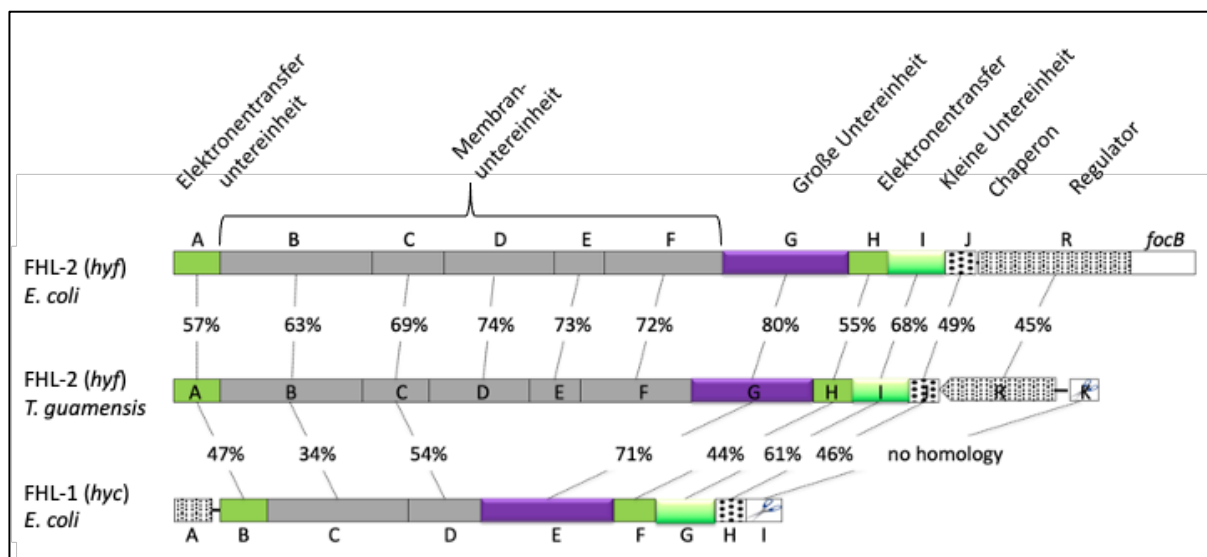
Abbildung 10: Aufbau der FHL-Operons (*hyc* und *hyf* Gene) aus *E. coli* K-12 und *T. guamensis*.

Das *hyc*-Operon befindet sich in unmittelbarer Nähe der *hyp*-Gene, die für die Reifung des [NiFe]-Kofaktors aller Hyd benötigt werden. Bemerkenswerterweise ist das Fdh-H-kodierende Gen *fdhF* jedoch an einer anderen Stelle auf dem Chromosom lokalisiert. Die unterschiedlichen Loci der *fdhF* und *hyc* Gene haben zu erheblichen Spekulationen über den Grund für diese genetische Trennung geführt. Eine Hypothese für diese Separation ergibt sich aus der Identifikation der Gene eines

zweiten FHL-2-Komplexes, der vom *hyf*-Operon kodiert wird (Andrews *et al*, 1997). Es wurde spekuliert, dass Fdh-H auch der Elektronendonator für den FHL-2-Komplex ist (Andrews *et al*, 1997). Dies liefert eine Erklärung für die Expression von *fdhF*, welche mit der von *hyc*- und *hyf*-Operons koordiniert aber unabhängig sein muss. Für *E. coli* ist die Assoziation von Fdh-H mit dem FHL-2 jedoch nie direkt nachgewiesen worden, hauptsächlich weil die FHL-2-Aktivität nicht eindeutig detektierbar ist (Redwood *et al*, 2008; Self *et al*, 2004). In einem unabhängigen Experiment konnten wir allerdings zeigen, dass die Aktivität des heterologen FHL-2 Komplexes aus dem Enterobakterium *Trabulsiella guamensis* von der Anwesenheit der *E. coli* Fdh-H abhängig war (Lindenstrauß & Pinske, 2019). Beide Organismen haben für die Proteine der FHL-Komplexe im Durchschnitt eine Aminosäureidentität von 80%, mit Ausnahme des Fdh-H-Proteins, das eine 95%ige Identität zwischen *E. coli* und *T. guamensis* aufweist (**Kapitel II**).

Die *hyf*-Operon-Zusammensetzung von *T. guamensis* ähnelt insgesamt jener von *E. coli*, weist jedoch signifikante Unterschiede in der Organisation der assoziierten Transkriptionsregulatoren, Proteinreifungsfaktoren und des umgebenden Genomkontexts auf (Lindenstrauß & Pinske, 2019). Beispielsweise kodiert es eine Endoprotease im Gen *hyfK*, dessen Genprodukt nach Abschluss der Metall-Kofaktor-Insertion für die Prozessierung der katalytischen Untereinheit benötigt wird aber im *E. coli hyf*-Operon fehlt (Finney *et al*, 2020; Sawers & Pinske, 2017).

11. Membranuntereinheiten der FHL-Komplexe

Vorangegangene Charakterisierungen der FHL-1$_{Ec}$-Reaktion ergaben, dass ihre partielle *pmf*-Abhängigkeit hauptsächlich auf das Vorhandensein weiterer H$_2$-oxidierender Hyd-Enzyme zurückzuführen war und die H$_2$-Produktion invers von der Konzentration der extrazellulär vorhandenen einwertigen Kationen abhing (**Kapitel III**). Dies ließ den Schluss zu, dass die FHL-1$_{Ec}$-Reaktion eng an den Protoneneinstrom und den Na$^+$-Export der Zelle gekoppelt ist (Marloth & Pinske, 2020). Der zugrunde liegende molekulare Mechanismus wurde noch nicht aufgeklärt. In homologen Komplexen konnte ein Na$^+$-Antiport beobachtet werden, der jedoch nur eine sekundäre Funktion haben könnte (Vignais, 2008). Aktuelle Studien beschäftigen sich mit der Verbindung der Na$^+$-Homöostase und der FHL-Aktivität. So wird die Aktivität des FHL-2$_{Tg}$-Holoenzyms im homologen und heterologen Wirt in Gegenwart des Protonophors **Carbonylcyanid *m*-Chlorphenylhydrazon (CCCP)** oder bei

Überschuss von NaCl oder wenn beide Bedingungen kombiniert wurden, leicht verringert (**Abbildung 11A**).

Deletionen einzelner Membranuntereinheiten aus dem *T. guamensis* heterolog exprimierten *hyf*-Operon in *E. coli* zeigten, dass der akkumulierte H_2 im Gasraum schrittweise abnahm, sodass die ungefähre Reihenfolge der Untereinheiten in der Membran abgeleitet werden konnte (**Abbildung 11B).** Deletionen der Gene für *hyfB* und *hyfC* waren inaktiv in der H_2-Produktion und verursachten damit einen $\Delta hycC$- und $\Delta hycD$-ähnlichen Phänotyp wie im FHL-1$_{Ec}$-Komplex. Damit befinden sich HyfB und HyfC proximal zur löslichen Domäne. Eine *hyfD* Deletion zeigte allein keinen Einfluss auf die Aktivität und wir nahmen zunächst an, dass diese Untereinheit distal zur löslichen Domäne liegen müsse. Während *hyfE* und *hyfF* Deletionen die Aktivität um ca. 40% senkten, hatten die beiden Deletionen in Kombination mit $\Delta hyfD$ kaum eine Verringerung der Aktivität zur Folge. Damit war die Deletion von *hyfD* dominant über $\Delta hyfEF$ weshalb die Untereinheiten HyfD zentral in der Membrandomäne und HyfE mit HyfF distal von der löslichen Domäne aus liegen. Durch Deletion der Gene für die HyfDE- und F-Untereinheiten entspricht der FHL-2$_{Tg}$ Komplex theoretisch dem FHL-1$_{Ec}$ und wies auch eine ähnliche Aktivität wie FHL-1$_{Ec}$ auf (**Abbildung 11B**).
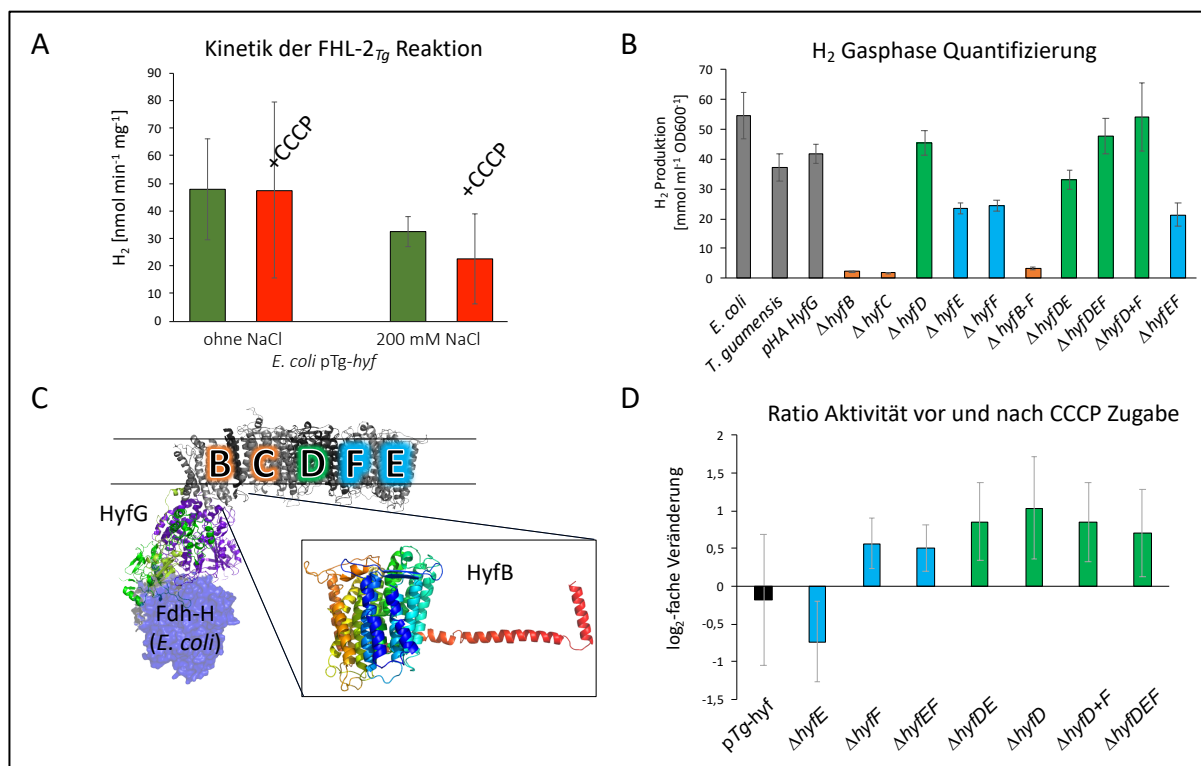
Abbildung 11: H_2-Produktion aus heterologen *T. guamensis-hyf*-Genen in Hoch- und Niedrig-Salzpuffer aus Formiat und die Reaktion auf CCCP und NaCl (A) H_2-Produktion aus Varianten ohne die angegebenen Membranuntereinheiten (B) und das abgeleitete Modell des FHL-2-Komplexes (C). Die Reaktion als log$_2$-fache Änderung auf CCCP nach Zugabe von Formiat (D).

Vorhersagen zur Struktur basieren auf den Kristallstrukturen des Komplex I (Batista *et al*, 2013; Marreiros *et al*, 2012). Auffällig bei FHL-2$_{Tg}$ ist, dass die proximal zur löslichen Domäne vorhergesagte Untereinheit HyfB die lange transversale Helix besitzt, die typisch für die distale Membranuntereinheit des Atmungskomplexes I (NuoL/Nqo12) ist (**Abbildung 11C** und **Tabelle 2**). Die Komplex I-ähnliche Hydrogenase aus *Pyrococcus furiosus* ist die erste Kryo-EM Struktur, welche dieselbe inverse Anordnung der Membrandomäne im Vergleich zum Komplex I aufweist (Yu *et al*, 2018).

Experimente mit Konstrukten der verkürzten Membrandomäne ließen eine Veränderung der Reaktionsgeschwindigkeit in Gegenwart des Protonophors CCCP erkennen. Dieses Protonophor reduziert den Gegendruck auf die Protonenpumpen-Untereinheiten und erleichtert dadurch Protonentransfer durch die Membran. Im Gegensatz zum Holoenzym reagierten die Membrandeletionsvarianten unterschiedlich auf die CCCP-Zugabe in der Formiat-initiierten Reaktion. Unter diesen Umständen zeigte CCCP in allen außer der Δ*hyfE*-Variante und dem Holokomplex eine Aktivierung anstelle der Hemmung (**Abbildung 11D**). HyfE ist kein Antiporter sondern ähnlich zur Na$^+$-translozierenden Untereinheit des MRP-Komplexes und deshalb ist eine zusätzliche Kopplung eventuell an Na$^+$-Translokation denkbar. Wenn diese Kopplung durch Deletion entfällt, könnten die verbliebenen Untereinheiten ausschließlich Protonen translozieren und durch CCCP enthemmt werden. Überraschenderweise war die CCCP-Aktivierung nicht sichtbar, wenn Glucose die H$_2$-Produktion initiierte. Daher könnte zusätzlich die Formiat-Aufnahme über den Formiat-Kanal FocA (in beiden Organismen konserviert) bioenergetisch beteiligt sein.

Obwohl dieser Befund neue Fragen zur Stöchiometrie der Anzahl der pro Molekül Formiat gepumpten Protonen, zur bioenergetischen Kopplung und zum Vorhandensein von zwei FHL-Komplexen in *E. coli* aufwirft, sind erste Rückschlüsse auf die Funktion der Membrandomäne möglich. Allein die Anwesenheit von drei zusätzlichen Membranuntereinheiten vom MRP-Typ in den FHL-2$_{Tg}$-Komplexen impliziert eine weitere energetische Kopplung an den Na$^+$-Antiport.

12. Reifung der katalytischen Untereinheit HycE

Die Synthese aktiver Hyd benötigt eine Reihe akzessorischer Reifungsproteine, die die Metall-haltigen Kofaktoren mit ihren diatomaren Liganden synthetisieren. Bei den [FeFe]-Hyd konnten die Reifungsproteine HydE, F und G für die Synthese des H-Clusters identifiziert und deren Beteiligung bei der CO und CN^--Synthese aus Tyrosin über Radikal-SAM Mechanismen inzwischen geklärt werden (Kleinhaus *et al*, 2020; Kuchenreuther *et al*, 2011; Peters *et al*, 2015; Shepard *et al*, 2014). Ebenso wurden bei den [Fe]-Hyd Reifungsproteine identifiziert und weitestgehend über die Aufklärung der HcgB, C und D (*Hmd co-occurring genes*) Kristallstrukturen auf den Mechanismus geschlossen werden (Fujishiro *et al*, 2016; 2014; 2013). Der Mechanismus der Reifung (Maturation) der [NiFe]-Hyd unterscheidet sich diesen beiden grundlegend.

An der Maturation der [NiFe]-Hyd sind mindestens sechs sogenannte **Hyp (*hydrogen pleiotropic*)** Proteine beteiligt. Einige detaillierte Übersichtsartikel zur weiterführenden Information wurden von uns und anderen verfasst: (Böck *et al*, 2006; Forzi & Sawers, 2007; Lacasse & Zamble, 2016; Peters *et al*, 2015; Pinske & Sawers, 2016; Sawers & Pinske, 2017). Zusätzlich zu den Hyp-Proteinen katalysieren Enzyme die Synthese und den Einbau der [FeS]-Cluster in die Elektronentransfer-Untereinheiten (Pinske & Sawers, 2014; Py & Barras, 2015). Und letztendlich werden spezifisch für die Fdh-H des FHL-Komplexes noch die Maschinerien für den Einbau von Selenocystein (Böck *et al*, 1991) und die Synthese des Molybdopterin-Dinukleotid-Kofaktors benötigt (Magalon & Mendel, 2015) auf die hier nicht näher eingegangen wird.
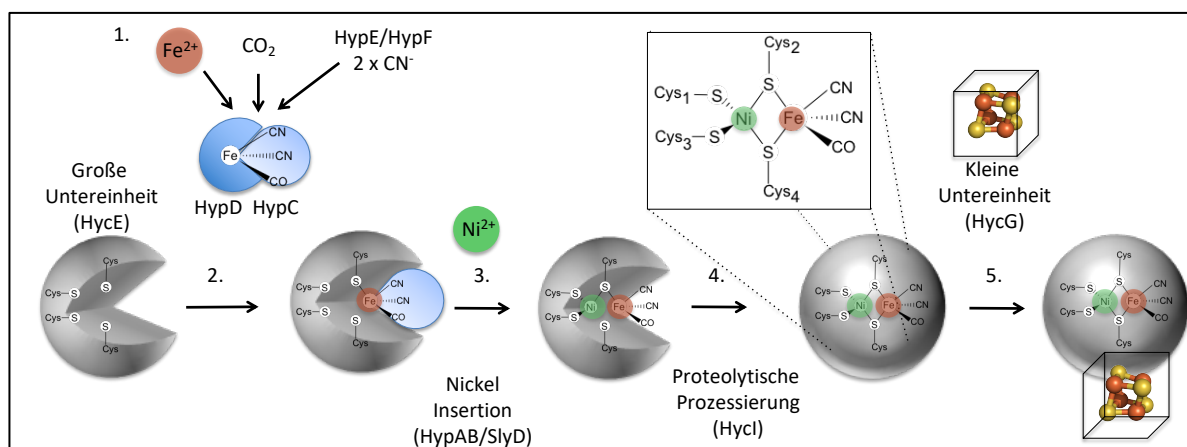
Abbildung 12: Schematischer Ablauf der HycE-Reifung. 1. Synthese von $Fe(CN)_2CO$; 2. Kofaktorinsertion in die große Untereinheit; 3. Nickelinsertion; 4. *C*-terminale proteolytische Prozessierung; 5. Assemblierung. [FeS]-Cluster werden durch braune und gelbe Kugeln dargestellt. Modifiziert nach (Sawers & Pinske, 2017).

Während der Maturation der [NiFe]-Hyd wird zunächst der $Fe(CO)CN_2$-Kofaktor synthetisiert (**Abbildung 12/1.**). Carbamoylphosphat dient als Substrat von HypF, wird von diesem ATP-abhängig aktiviert und als Thiocarboxamid auf das *C*-terminale Cystein von HypE übertragen. Dieses wird unter Verbrauch eines weiteren ATP von HypE weiter zu (Iso)thiocyanat dehydratisiert. Die so gebildete Cyano-Gruppe wird anschließend von HypE auf den HypCD-Komplex übertragen, wo vermutlich bereits das Eisenatom durch Cys_2 von HypC und Cys_{41} von HypD koordiniert wird. Sowohl HypF als auch HypE liegen als Dimer vor, in der Kristallstruktur des HypCDE-Komplexes bleibt die Dimerbildung von HypE erhalten und ließe somit die Stöchiometrie von 2 CN^--Liganden am Eisen erklären (Miki *et al*, 2020).

HypD ist das einzige redox-aktive Protein während der Liganden-Biosynthese. Es ist strittig, welcher diatomare Ligand (CO oder CN^-) zuerst auf das zwischen HypC und HypD gebundene Eisen übertragen wird. Es wurde jedoch postuliert, dass HypC das CO_2 an Eisen gebunden in den Komplex liefert und dieses dort zu CO reduziert wird (Soboh *et al*, 2012). Der HypCD-Komplex besitzt außerdem eine ATPase Aktivität, die entweder Energie für die Reduktion bereitstellt oder den anschließenden Transfer erleichtert (Nutschan *et al*, 2019). Sowohl der Lieferant des Eisenatoms als auch die CO_2-Quelle bleiben weiter zu identifizieren. HypC hat zusätzlich die Funktion, den $Fe(CO)CN_2$-Teil des Kofaktors in die große Untereinheit HycE zu transferieren (**Abbildung 12/2.**). Für diesen Transfer in die großen Untereinheiten der Hyd-1 und Hyd-2 (HyaB und HybC Proteine) ist das HypC-homologe HybG Protein verantwortlich.

Anschließend wird das Nickel-Ion in die große Untereinheit inseriert (**Abbildung 12/3.**). Dieses wird durch HypB mit seiner intrinsischen GTPase Aktivität katalysiert, wobei das Ni^{2+} auf HypA übertragen wird, welches es spezifisch in HycE einbaut. Für den Einbau des Nickels in HyaB und HybC (Hyd-1 und Hyd-2) fungiert erneut ein homologes Protein, HybF aus dem Hyd-2 Operon. Der Transfer wird unterstützt von dem Faltungshelferproteine SlyD, wobei SlyD in der exponentiellen Phase nicht essentiell benötigt wird (Pinske *et al*, 2015b).

Erst die Insertion von Ni^{2+} erlaubt die proteolytische Prozessierung des *C*-terminalen Peptides durch eine Protein-spezifische Endoprotease (**Abbildung 12/4.**). Die Endoproteasen werden mit Ausnahme vom *hyf*-Operon im jeweiligen Hyd-Operon

kodiert und spalten ein *C*-terminales Peptid von 15 Aminosäuren ab (32 Aminosäuren bei HycE). Die Spaltstelle ist zwischen den Hyd-Enzymen mit *C*-terminalen His und Arg-Resten relativ hoch konserviert (Theodoratou *et al*, 2000). Unsere Mutagenesestudien mit Austausch der *C*-terminalen Peptide von HyaB und HybC bewiesen, dass dieses Peptid nicht der bestimmende Faktor für die Protease-Spezifität ist (Pinske *et al*, 2019) (**Kapitel IV**). Anders als das Paradigma der Serinproteasen (Schechter & Berger, 1967), kann auch zusätzlich die Erkennungsstelle *N*-terminal von der proteolytischen Spaltstelle gegen Reste einer anderen Hyd ausgetauscht werden, ohne die Spezifität für die ursprüngliche Protease zu verlieren (**Kapitel IV**).

Es ist deshalb anzunehmen, dass das *C*-terminale Peptid vielmehr eine offene Konformation der katalytischen Apo-Untereinheit während des Kofaktoreinbaus stabilisiert. Durch die Prozessierung kommt es zu einer konformationellen Änderung in deren Folge das aktive Zentrum im Protein eingeschlossen wird. Das Ni^{2+}-Ion ist aufgrund seines Lewissäure-Charakters in den Proteolysemechanismus involviert, wodurch es gemeinsam mit der konformationellen Änderung der *N*-terminalen Domäne (Kwon *et al*, 2018) die Prozessierung kontrolliert. Die prozessierten großen Untereinheiten sind relativ stabil in Abwesenheit ihrer kleinen Untereinheiten, deren Assoziation den nächsten Schritt bei der Assemblierung der jeweiligen Hyd darstellt. Die Interaktion mit der kleinen Untereinheit ermöglicht es, die Aktivität mit Redoxfarbstoffen wie Benzylviologen nachzuweisen. Diese Redoxfarbstoffe können die Elektronen nicht direkt vom $Ni\text{-}Fe(CO)CN_2$-Kofaktor erhalten, sondern müssen sich in der Nähe der [FeS]-Cluster der kleinen Untereinheiten befinden (Pinske *et al*, 2011). Ob die sich anschließenden Schritte der Assemblierung des Komplexes spontan ablaufen, wie *in vitro* Studien nahelegen (Caserta *et al*, 2020), oder bei einigen Komplexen durch weitere Proteine kontrolliert werden, ist nicht abschließend geklärt. Für Hyd-Komplexe, welche auf der periplasmatischen Seite der Membran lokalisieren, wird die katalytische Untereinheit gemeinsam mit der kleinen Untereinheit, die das Signalpeptid für den Transport trägt, transloziert. Diese Kontrolle des Transportes wird durch Chaperone wie HyaE und HybE, die an den Signalpeptiden binden, durchgeführt (Dubini & Sargent, 2003).

13.   Das HycE Protein

Es ist unverstanden, warum während der HycE-Prozessierung ein „langes" Peptid von 32 Aminosäuren proteolytisch abgespalten wird, während von den meisten Hyd nur ein „kurzes" Peptid mit 15 Aminosäuren abgespalten wird (Sawers & Pinske, 2017). Eine von einer japanischen Gruppe generierte Kristallstruktur der großen Untereinheit in ihrer apo-Form in Interaktion mit einem ihrer Reifungsfaktoren gibt weitere Hinweise auf die Funktion des Peptides. So interagiert das "kurze" *C*-terminale Peptid eng mit dem Reifungsprotein HypA, dessen Position nach der Prozessierung durch den *N*-Terminus der großen Untereinheit ersetzt wird (Kwon *et al*, 2018).
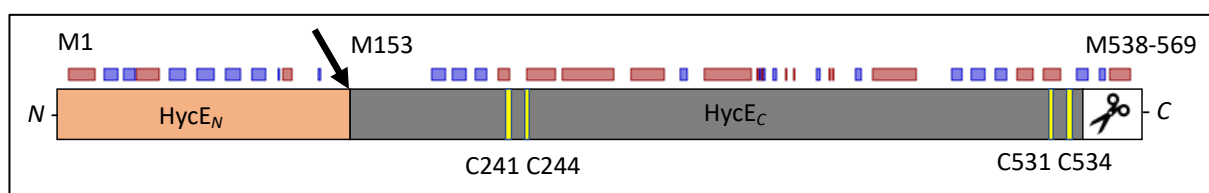
Abbildung 13: Domänenstruktur des HycE-Proteins. Die *N*-terminale Domäne reicht von Aminosäure 1-152, die *C*-terminale Domäne von 153-537, das prozessierte *C*-terminale Peptid von 538-569. Die Sekundärstrukturvorhersage (rot = alpha-Helix, blau = beta-Faltblatt) zeigt einen ungeordneten Bereich im Übergang der zwei Domänen an (Pfeil). Die gelben Balken markieren die Cysteine, die den [NiFe]-Kofaktor koordinieren. Modifiziert von (Skorupa *et al*, 2020)

In HycE scheint die *N*-terminale Domäne, eine weitere Funktion zu haben. Es liegt im Moment keine Struktur des FHL-Komplexes oder des unprozessierten HycE Proteins vor. Das HycE-Protein ist jedoch phylogenetisch verwandt mit dem Fusionsprotein NuoCD vom Komplex I der Atmungskette (**Abbildung 13**). Auch bei Komplex I gibt es Varianten mit fusioniertem NuoCD Protein (*E. coli*) oder separaten Proteinen. Aus der Strukturvorhersage des gesamten FHL-Komplexes (**Abbildung 9**) wird deutlich, dass die *N*-terminale Domäne aufgelagert ist und keine weiteren signifikanten Interaktionsflächen mit anderen Untereinheiten des FHL-Komplexes existieren. Unsere Studien mit *N*-terminal verkürztem HycE haben gezeigt, dass der FHL-Komplex ohne diese Domäne nicht assembliert (**Kapitel V**, (Skorupa *et al*, 2020)). Aus der phylogenetischen Beziehung zu Komplex I und in Kombination mit weiteren Experimenten lässt sich schlussfolgern, dass diese *N*-terminale Domäne die Assemblierung des Komplexes initiieren könnte. Die Elektronentransfer-Untereinheiten HycB, HycF und HycG werden anschließend assoziiert, gefolgt vom lose gebundenen Fdh-H-Protein. Final assoziiert diese lösliche Domäne an die Membranuntereinheiten HycC und HycD.

14.   **Funktion des HycH Proteins**

Eine weitere Besonderheit der FHL-Komplexe im Vergleich zu anderen Hyd ist das Vorhandensein eines spezifischen Chaperons HycH. Mein DFG-Projekt "Raumzeitliche Assemblierung und Funktion des modularen Formiat Hydrogenlyase (FHL) -Komplexes" fokussierte auf die Rolle des HycH Proteins, welches vom achten Gen des *hyc*-Operons kodiert wird. Es wird üblicherweise als Assemblierungs-Chaperon der großen Hyd-Untereinheit HycE bezeichnet. Das Gen selbst ist zwar in den FHL-Operons konserviert, aber es ist einzigartig für die Typ 4a Hyd (**Tabelle 1**). Die anfängliche Charakterisierung durch (Sauter *et al*, 1992) legte nahe, dass es die Funktion der spezifischen Endoprotease erfüllen könnte, welche die große Untereinheit nach der Kofaktorinsertion endoproteolytisch prozessiert. Die nachfolgende Analyse ergab jedoch, dass dies tatsächlich die Aufgabe des ursprünglich übersehenen *hycI*-Genprodukts war, wodurch die wahre Funktion von HycH unbekannt blieb (Rossmann *et al*, 1995) .

Eine erste Charakterisierung zeigte (**Kapitel VI**), dass HycH nur solange mit der katalytischen Hyd-Untereinheit HycE interagierte, bis HycE endoproteolytisch prozessiert wurde (Lindenstrauß *et al*, 2017). Die Studien fanden dabei mit Zellextrakten aus unterschiedlichen Stammhintergründen statt. So hatte der Phänotyp einer *hycH*-Deletion nur geringen Einfluss und reduzierte die FHL-Aktivität in allen Wachstumsphasen auf etwa 50% (Lindenstrauß *et al*, 2017). Eine Kombination mit der Deletion des Gens für das homologe HyfJ-Protein aus dem FHL-2$_{Ec}$-Komplex führte zu einem verstärkten Phänotyp mit einer Reduktion der FHL-Aktivität auf 20%. Eine Interaktion der HycE-Untereinheit mit diesem HyfJ Chaperon war ebenfalls nachweisbar. Daneben konnten in dieser Studie Aminosäurereste in HycH identifiziert werden, welche an der Interaktion mit HycE beteiligt sind. Diese HycH-Varianten waren jedoch weiterhin in der Lage, die FHL Aktivität eines Δ*hycH*-Stammes zu komplementieren. Interessanterweise wurden daneben Aminosäurereste identifiziert, welche die Interaktion mit HycE beibehielten, welche aber die Aktivität des FHL-Komplexes in einer Δ*hycH*-Mutante nicht wiederherstellen konnten. Dies lässt den Schluss zu, dass eine weitere Funktion von HycH über die Wechselwirkung mit HycE hinaus zu erwarten ist (Lindenstrauß *et al,* 2017). So finden im Zeitfenster um die Prozessierung der großen Untereinheit HycE eine Reihe von Schritten statt, die gut koordiniert sein müssen. Systematisch wurden die nachfolgenden Thesen zur Funktion von HycH während der Reifung und Assemblierung untersucht.

15.   Die Rolle von HycH bei der Rekrutierung der Reifungsproteine

Bei den Schritten vor der proteolytischen Prozessierung der großen Untereinheit HycE könnte das HycH-Protein durch seine starke Interaktion mit HycE möglicherweise weitere Reifungsproteine rekrutieren, um die zweistufige Insertion der Metalle zu erleichtern. Dafür müsste HycH entweder mit HypC ($Fe(CO)CN_2$-Einbau) oder HypA (Nickeleinbau) interagieren. Eine Verifikation dieser Protein-Protein-Wechselwirkungen mittels *bacterial two*-Hybrid-Assays ist bisher nicht gelungen. Die Metallbestimmung des HycEH-Komplexes wies außerdem kein Metall des [NiFe]-Kofaktors auf, sondern lediglich 1 Mol Zink (ICP-MS in Zusammenarbeit mit Arbeitsgruppe um Prof. Nies, MLU Halle-Wittenberg).
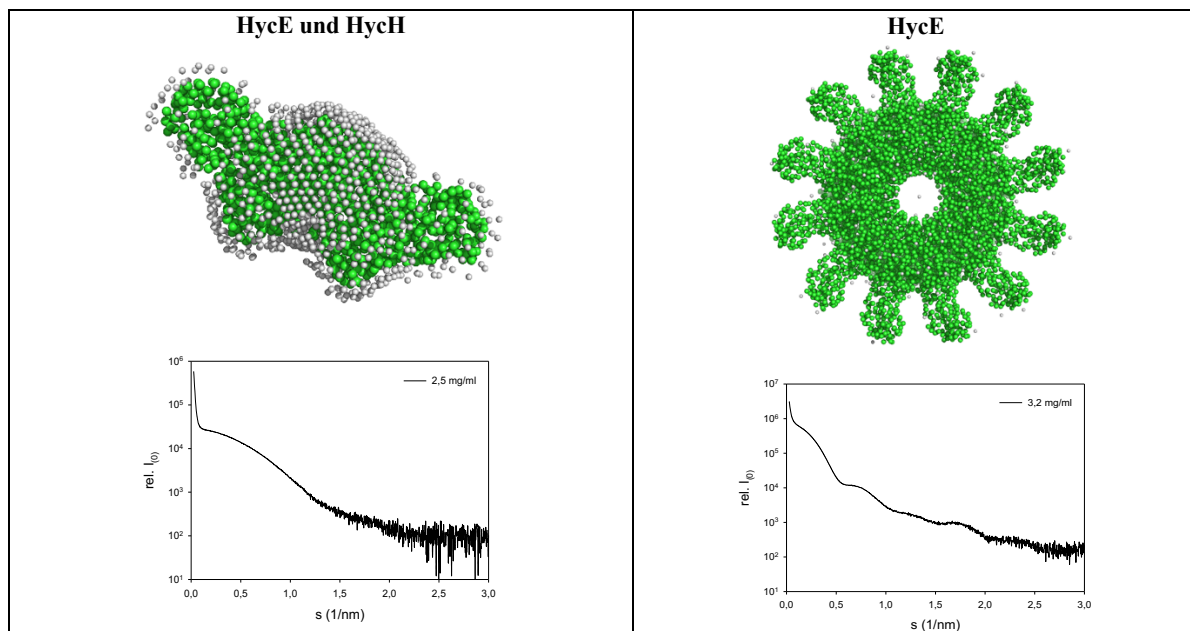
Abbildung 14: Strukturelle Informationen der HycEH und HycE Proteine (Modelle und SAXS Kurven; Daten aus der Arbeit von Philipp Skorupa in Kollaboration mit PD Dr. König).

Eine weitere Aufgabe HycHs könnte sein, dass es als typisches Chaperon die Multimerisierung des HycE-Proteins in höhere oligomere Zustände verhindert. Während der Anreicherung des HycE-Proteins fiel dieses häufig direkt nach der Elution von der Affinitätssäule aus. Das gleiche geschah bei der Reinigung des HycH-Proteins alleine. Beide ko-überexprimierten und gereinigten Proteine erwiesen sich hingegen als besonders stabil. Wir analysierten diesen Komplex in Kollaboration mit PD Stefan König (MLU Halle-Wittenberg) durch Röntgenkleinwinkelstreuung (SAXS), die bestätigte, dass sich HycE oder HycH allein bis zu decameren Strukturen zusammenlagerten. Diese Interpretation wurde durch analytische Ultrazentrifugation und analytische Größenausschlusschromatographie ebenfalls gestützt (PD Hauke Lilie, MLU Halle). Möglicherweise ist diese Multimerisierung auch ein Artefakt weil die

Multimerisierung von HycE stark von seiner Konzentration und des pH-Wertes abhängig war. Die berechnete SAXS-Struktur des HycEH-Komplexes ließ sich als ein HycE-Protein mit zwei an den distalen Enden von HycE gebunden HycH-Proteinen interpretierten **(Abbildung 14)**. Proteinkristalle des HycE x HycH-Komplexes konnten ebenfalls erfolgreich generiert werden, sie zeigten aber leider keine Reflexionen. In einer Kollaboration mit der Arbeitsgruppe um Petra Wendler (Universität Potsdam) werden aktuell Cryo-EM Strukturen des FHL-Komplexes durchgeführt.

16.   Das HycH Protein bei der Vermittlung der Proteasespezifität

Eine weitere mögliche HycH-Funktion könnte darin bestehen, die Spezifität der Protease zu bestimmen. Wie oben erwähnt, kodiert das FHL-2$_{Ec}$-*hyf*-Operon keine Protease für die notwendige Prozessierung der großen Untereinheit HyfG während im FHL-2$_{Tg}$-*hyf*-Operon ein Gen *hyfK* für die Protease vorhanden ist. Dieses Gen war bei der heterologen Überexpression des gesamten *T. guamensis hyf*-Operons in *E. coli* funktionsfähig für die HyfG$_{Tg}$ Prozessierung.

Während der Studien zur Untersuchung der Spezifität der Proteasen wurde die große Untereinheit HycE jeweils mit der eigenen Protease HycI oder mit der heterologen Protease HyfK kombiniert und in einem Stamm ohne weitere FHL-Gene exprimiert **(Abbildung 15)**. Beide Konstrukte wurden zusätzlich mit einem der beiden Chaperone HycH oder seinem homologen Protein HyfJ aus dem FHL-2$_{Tg}$ Operon kombiniert. Dabei zeigte sich, dass HycE nur dann prozessiert wurde, wenn HycI vorhanden war, unabhängig von der Anwesenheit eines Chaperon-Proteins, was ausschließt, dass das jeweilige Chaperon die Spezifität der Protease bestimmt.
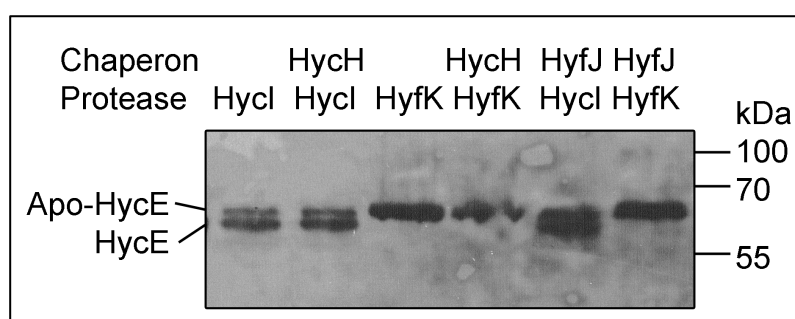
Abbildung 15: Prozessierung von HycE als Indiz für die Kofaktorinsertion. HycE wurde mit dem HA-Epitop-Fusionspeptid versehen und das Gen im Plasmid-kodierten Kontext auf einem pACYC-Duet1-Vektor mit den Genen für die Protease HycI$_{Ec}$ oder HyfK$_{Tg}$ sowie mit den Chaperonen HycH$_{Ec}$ oder HyfJ$_{Tg}$ kombiniert und in Abwesenheit aller weiteren *hyc* und *hyf*-Gene exprimiert. Im Western Blot gegen das HA-Fusionspeptid zeigte sich die Prozessierung von HycE als Erscheinen einer Doppelbande nur in Anwesenheit von HycI$_{Ec}$ unabhängig von der Anwesenheit der Chaperone (Experiment von Ute Lindenstrauß).

17. Das HycH Protein zur Rekrutierung von Elektronentransfer-Untereinheiten
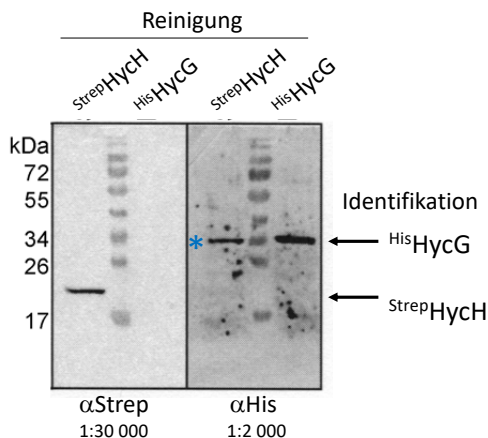
Abbildung 16: Ko-Reinigung von StrepHycG und HisHycH. Die Proteine wurden entsprechend ihrer Fusionspeptide aufgereinigt und anschließend durch Antikörper gegen die Epitoptags des Proteins bzw. seines Interaktionspartner identifiziert. Der Stern zeigt, dass HisHycG durch StrepHycH ko-gereinigt wird. HycE war in diesen Proben nicht nachweisbar (Experiment von Philipp Skorupa).

Im Anschluss an die Prozessierung von HycE erfolgt die Assemblierung des FHL-Komplexes. Die notwendigen Schritte der Rekrutierung der Elektronentransfer-Untereinheiten sind weitestgehend unverstanden und bieten dem HycH-Protein eine Vielzahl weiterer Handlungsmöglichkeiten. So könnte es HycE direkt nach Prozessierung an die kleine Untereinheit HycG übergeben. Die HycE-Prozessierung ist zwar unabhängig von HycG (Sauter *et al*, 1992) und **Abbildung 15**, aber die Assoziation stellt wahrscheinlich den ersten Schritt Assemblierung dar. Mit einem Plasmid, das sowohl His-fusioniertes HycG als auch Strep-fusioniertes HycH-Protein kodierte, konnte Philipp Skorupa zeigen, dass in *Pull-down*-Experimenten Strep-markiertes HycH-Protein das His-markierte HycG-Protein ko-reinigte (**Abbildung 16**, blauer Stern). Diese Interaktion war unabhängig von der Anwesenheit der anderen Hyc-Proteine und eine mögliche Kontamination mit HycE, die zur Verunreinigung mit HycG führen könnte, konnte ausgeschlossen werden. Da die Wechselwirkung jedoch nur in einer Richtung sichtbar war, bedeutet es auch, dass die Fusionspeptide die Eigenschaften der Proteine unterschiedlich beeinflussen. Das Experiment deutet darauf hin, dass HycH eine Rolle bei der Rekrutierung der restlichen Untereinheiten des FHL-Komplexes spielen könnte. Weitere Experimente zur Funktion von HycH sind in Planung.

Fazit

Der FHL-Komplex ist das wichtigste wasserstoffproduzierende Enzym *E. coli*s und seine zukünftige biotechnologische Nutzung eröffnet die Möglichkeit einer verantwortungsvollen Energieversorgung aus erneuerbaren Ressourcen. In erster Linie ist es dafür zunächst erforderlich, den Aufbau und die Reaktionen der beteiligten Enzymkomplexe zu verstehen. Die Funktion eines Chaperons mit unbekannter Rolle bei der Biosynthese des Komplexes gilt es zu klären. Es ist weiterhin unklar, ob die H_2-Produktion des FHL-Komplexes das Wachstum der Bakterien lediglich durch den Verbrauch von Protonen im Cytoplasma oder zusätzlich auch durch eine aktive Translokation von Ionen über die Membran unterstützt. Insbesondere die Duplikation der Antiporter-Membranuntereinheiten und die unterschiedliche Reaktion auf Protonophore suggeriert eine bioenergetische Bedeutung des FHL-Komplexes als Protonenpumpe während der Fermentation, die es zukünftig nachzuweisen gilt und die damit fundamentale Prinzipien der Bioenergetik verändern könnte.

Letztendlich könnte zwar die Notwendigkeit der Biosynthese verschiedener Metallkomplexe eine *in vitro* Nutzung für den FHL-Komplex erschweren, andererseits könnte die robuste *in vivo* H_2-Produktion eine gezielte Anwendung von Zellsystemen in Bioreaktoren bei der Abfallbeseitigung möglich machen. Unsere Forschung steckt trotz der langen Historie um die H_2-Produktion der Bakterien erst in den Anfängen. Es gibt noch zahlreiche offene Fragen bezüglich der Bioenergetik der H_2-Produktion, des Zusammenbaus großer Redoxenzymkomplexe und der biotechnologischen Verbesserungsmöglichkeiten der Reaktion, die ich in Zukunft beantworten will.

Kapitel I – Bioenergetik der Hyd-2 Reaktion

Aminosäure-Varianten der HybB Membranuntereinheit der *Escherichia coli* [NiFe]-Hydrogenase 2 unterstützen eine Funktion im Protonentransfer

Dorothea Lubek[a], Andreas H. Simon[b] und Constanze Pinske[a,*]

[a] Institut für Biologie/Mikrobiologie, Martin-Luther-Universität Halle-Wittenberg, 06108 Halle, Deutschland
[b] Institut für Naturstoffbiochemie, Charles-Tanford-Protein Zentrum, Martin-Luther-Universität Halle-Wittenberg, Kurt-Mothes-Str. 3a, 06120 Halle/Saale, Deutschland

*Korrespondierende Autorin: Constanze Pinske

Zusammenfassung:

Die [NiFe]-Hydrogenase (Hyd) 2 von *Escherichia coli* erzeugt während der H_2-Oxidation eine protonenmotorische Kraft, die in der Rückreaktion, bei der anaeroben Inkubation mit Glycerin, für die H_2-Produktion genutzt werden kann.

Die integrale Membranuntereinheit HybB wird für den Protonentransfer (PT) durch Hyd-2 benötigt, besitzt jedoch keinen eigenen Kofaktor. Um den PT durch HybB nachzuweisen, wurde die Rolle konservierter Aminosäurereste in einem vorhergesagten Protonenkanal analysiert. Durch gezielten Austausch konservierter Aminosäuren wurden Y99, E133, H184 und E228 als obligatorisch für den PT aus dem Zytoplasma und die Chinoloxidation identifiziert. Im Gegensatz dazu führte der Austausch von W54, D58 oder R89 zu Unidirektionalität der Reaktion durch Beeinflussung des Reaktionsgleichgewichtes. Unsere Ergebnisse zeigen, dass HybB die Schlüsseluntereinheit für PT ist.
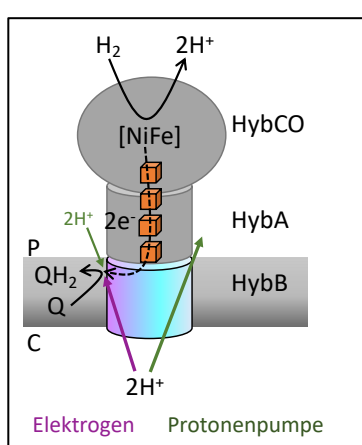
Abbildung 17: Mechanistisches und strukturelles Modell von HybB im Hyd-2 Komplex. Schema der Protonen- und Elektronenwege innerhalb einer heterotetrameren Einheit von Hyd-2 (Proteine HybCOAB). Orange Würfel repräsentieren vereinfacht die sieben Eisen-Schwefel-Cluster für den Elektronentransfer, [NiFe] steht für das aktive Zentrum, Q / QH$_2$ repräsentiert das Chinon/Chinol, P und C kennzeichnen die periplasmatische bzw. cytoplasmatische Seite der Membran. Die Pfeile zeigen alternative Wege für die Protonen gemäß des elektrogenen (lila) oder protonenpumpenden (grün) Mechanismus.

Amino acid variants of the HybB membrane subunit of *Escherichia coli* [NiFe]-hydrogenase-2 support a role in proton transfer

Dorothea Lubek[1], Andreas H. Simon[2] and Constanze Pinske[1]

1 Department of Microbiology, Martin-Luther University Halle-Wittenberg, Germany
2 Department Naturstoffbiochemie, Charles Tanford Protein Centre, Martin-Luther University Halle-Wittenberg, Germany

Correspondence

C. Pinske, Department of Microbiology, Martin-Luther University Halle-Wittenberg, Kurt-Mothes-Str. 3, 06120 Halle/Saale, Germany
Tel: +49 (0)345 55 26353
E-mail: constanze.pinske@mikrobiologie.uni-halle.de

[NiFe]-hydrogenase (Hyd) 2 of *Escherichia coli* has been proposed to generate proton motive force during H_2-oxidation, which it is dependent on if cells are incubated anaerobically with glycerol to drive reverse H_2-production. The integral membrane subunit HybB is required for proton transfer (PT) by Hyd-2 but has no cofactor. To provide evidence for PT by HybB, we analyzed the roles of conserved amino acid residues in a predicted proton channel. Exchange of conserved residues identified residues Y99, E133, H184, and E228 as mandatory for PT from the cytoplasm and quinol oxidation. In contrast, exchange of W54, D58, or R89 rendered Hyd-2 uni-directional and influenced the equilibrium. Our findings show that HybB is the key subunit in PT.

Keywords: conformational proton pump; electrogenic proton pumping; energy-conservation; HybB; hydrogen metabolism; hydrogenase-2

Hydrogenases (Hyd) 1 and 2 of *Escherichia coli* are membrane-associated H_2-oxidizing enzymes that face the periplasmic side of the membrane [1]. Hyd-1 represents one half of a classical redox-loop with two heme groups in the membrane subunit, which transfer electrons against the membrane potential towards the cytoplasmic side for quinone reduction and concomitant uptake of protons [2]. Hyd-2 also couples H_2-oxidation to quinone reduction, but the membrane anchor subunit HybB has no cofactor [3]. When the genes for Hyd-2 were first described, it appeared to have a similar architecture to Hyd-1 with a catalytic subunit, HybC, harboring the [NiFe]-cofactor, an electron-transfer subunit, HybA, with four iron–sulfur [FeS]-clusters and a membrane anchor subunit, HybB [4]. However, an additional gene was discovered at the beginning of the operon, which encodes a classical Hyd small subunit, HybO, including a Tat-signal

sequence, which made clear that the architecture of the Hyd-2 enzyme was different from that of Hyd-1 [5]. Subsequent studies revealed that the large and small subunits are tightly bound in a $(HybOC)_2$ dimer-of-dimers stoichiometry [6] and also translocated across the membrane as such, albeit independently from the other subunits HybA and HybB [3,7]. Furthermore, the HybA and HybB subunits function to anchor the HybOC-heterotetramer to the membrane and link them with the quinone pool [8].

In the structures of the homologous polysulfide reductase complex (Psr) from *Thermus thermophilus* and the alternative complex III (Act) from *Flavobacterium johnsoniae*, the quinone-binding sites are located close to the iron–sulfur-cluster (FeS-cluster) most distal to the active site [9–11]. The same position was predicted for the cofactor-less HybB subunit of Hyd-2 [9,12]. Initially, the homologous PsrC subunit

Abbreviations

CCCP, carbonyl cyanide *m*-chlorophenyl hydrazone; FeS-cluster, iron–sulfur-cluster; Hyd, hydrogenase; *Pmf*, proton motive force; PT, proton transfer.

was proposed to be a proton-pump [9]. But the homologous menaquinone reductase (Qrc) subunit QrcD from *Desulfovibrio* was recently demonstrated to reduce the quinone electrogenically using protons from the cytoplasm [13].

The proton transfer (PT) capability of Hyd-2 was demonstrated indirectly by its dependence on the proton motive force (*pmf*) during the reverse H_2-evolving reaction [8]. Hyd-2 is able to produce H_2 from an over-reduced quinone pool, for example, when cells are grown, or incubated fermentatively, in the presence of glycerol without addition of exogenous electron acceptors [8,14]. A particularly high level of Hyd-2 is synthesized when cells are grown in the presence of glycerol and fumarate, showing that cells favor these conditions for Hyd-2 activity [15]. Although our current evidence supports that Hyd-2 contributes to *pmf* generation during H_2-oxidation, we currently do not understand the underlying mechanism, nor do we know the fate of the proton that is drawn from the cytoplasm (Fig. 1A). If this proton is released on the periplasmic side, the HybB protein would represent a proton pump similar to Complex I of the respiratory chain (Fig. 1A, green arrows) [16]. If, however, the proton is used for reducing the quinone, this would imply an electrogenic mechanism analogous to that recently identified in the homologous subunit QrcD of the Qrc complex in sulfate respiration (Fig. 1A, purple arrow) [13]. In an attempt to distinguish between these two modes of PT, we performed *in silico* structural analysis to identify conserved amino acid residues within HybB and then experimentally validated their importance for Hyd-2 function. Our findings identify amino acid residues required for PT and that convert the Hyd-2 enzyme to an uni-directional H_2-oxidizing or H_2-evolving enzyme.

Materials and methods

Growth conditions

Escherichia coli cultures were routinely grown at 37 °C in LB medium or on LB-agar plates as described [17]. For plasmid maintenance and selection, the antibiotics ampicillin (100 $\mu g \cdot mL^{-1}$) and chloramphenicol (34 $\mu g \cdot mL^{-1}$) were added to the medium. For Hyd characterization the cells were either grown fermentatively in TGYEP medium (1% w/v tryptone; 0.5% w/v yeast extract; 0.8% w/v glucose; 0.1 M potassium phosphate buffer pH 6.5) according to [18] or anaerobically in M9-minimal medium (47.6 mM Na_2HPO_4, 22 mM KH_2PO_4, 8.4 mM NaCl, 19 mM NH_4Cl, 2 mM $MgSO_4$, 0.1 mM $CaCl_2$, 0.3 μM thiamine dichloride, 0.2% w/v casamino acids, 0.1% w/v trace element solution

[20]) [20]. The carbon source glycerol (0.4% w/v) and the electron acceptor fumarate (15 mM) were added to the M9 medium where indicated. Cells were grown for 16h as standing-liquid cultures at 30 °C. If the protonophore carbonyl cyanide *m*-chlorophenyl hydrazone (CCCP) was used, the final concentration was 100 μM.

Strains and plasmids

The *E. coli* K-12 strain MC4100 was used as the parental strain throughout this study [21]. Plasmid pJET-hybOABC was constructed by inserting the 4976 bp PCR product obtained by amplification from chromosomal DNA of MC4100 with the oligonucleotides HybO_NdeI 5′-GCGCATATGACTGGAGATAACACCCTCATC-3′ and HybC_BamHI 5′-GCGGGATCCTTACAGAACCTTCACTGAAAC-3′ as blunt end product into the pJET1.2 vector (Thermo Fisher Scientific, Waltham, MA, USA). Expression of the cloned genes was under the control of the T7 promoter. This vector was used for site-directed mutagenesis to generate variants of HybB using the oligonucleotides listed in Table S1 and the 'NEBase changer' method (NEB, Ipswich, MA, USA). The insert was also excised as a NdeI/BamHI fragment from the pJET-hybOABC vector and ligated into NdeI/BglII-digested pACYCDuet-1 vector to give pDuet-hybOABC. To generate the chromosomal deletion of the genes *hybO-C* coding for the Hyd-2 structural subunits in strain CPH28 [MC4100 (DE3) Δ*hycA-I* Δ*hybO-C*], the upstream and downstream 500 bp regions were amplified with oligonucleotides hybOC1_BamHI 5′-GCGGGATCCGACAATATATAGCGAATGAG-3′ with hybOC2_EcoRI 5′-GCGGAATTCCGCAACGGAATAACTATAA-3′ and hybOC3_EcoRI 5′-GCGGAATTCATGCGTATTTTAGTCTTAGG-3′ with hybOC4_HindIII 5′-GCGAAGCTTCTGCTATCTCTTCAGTCATG-3′, digested with BamHI/EcoRI and EcoRI/HindIII, respectively, and ligated simultaneously into BamHI/HindIII-digested pMAK705.

The strain CPH28 [MC4100 (DE3) Δ*hycA-I* Δ*hybO-C*] was constructed by following the pMAK705 protocol [22] with plasmid pMAK-hybO-C in strain MC4100 (DE3) that was obtained as a kind gift from Johann Heider (Marburg University) and previously transduced using P1$_{vir}$ with the deletion of *hycA-I* (described in [23]). The strain was further modified by deleting the *hyaB* allele by transducing the deletion mutation from strain JW0955 as described [17,24], resulting in strain DLH04 [MC4100 (DE3) Δ*hycA-I* Δ*hybO-C* Δ*hyaB*]. Strain HDK103 (Δ*hycA-I* Δ*hya*) was previously described [25] as well as strain DHP-F2 (Δ*hypF*) [26].

Native-PAGE and activity staining

Anaerobically or fermentatively grown cells were harvested by centrifugation, resuspended in MOPS buffer, pH 7.0 and briefly sonicated (15 W power for 10 s with 0.5 s pulses). Between 25 and 50 μg protein was loaded on a 7.0% (w/v
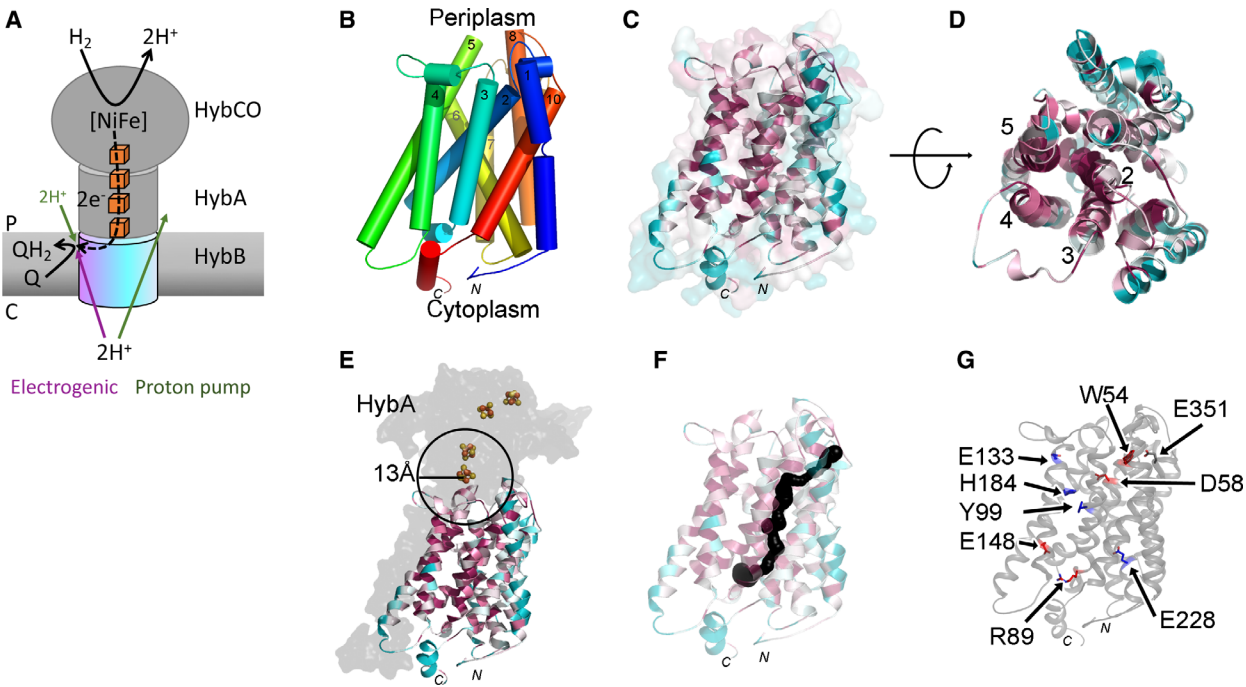
Fig. 1. Mechanistic and structural model of HybB. (A) Scheme of the proton and electron pathways within one heterotetrameric unit of Hyd-2 (proteins HybCOAB). Orange cubes represent the seven iron–sulfur clusters for electron transfer, [NiFe] stands for the active site, Q/QH$_2$ represent the quinone/quinol, P and C show the periplasmic and cytoplasmic side of the membrane, respectively. The arrows depict alternative routes for the protons according to the electrogenic (purple) or proton pumping (green) mechanisms. Further details see text. (B) In the HybB model, helices are shown as cylinders and are numbered from *N*-terminus to *C*-terminus. (C) Helices in cartoon representation are colored according to ConSurf: red highly conserved, cyan not conserved. (D) Tilted 90°, view from top/periplasmic side. (E) Predicted location of the HybA protein and its iron–sulfur clusters (yellow and brown spheres). The circle shows the electron transfer distance of 13 Å around the FeS-cluster closest to HybB. (F) Predicted tunnel from Caver. (G) Location of the identified amino acids W54, D58, R89, E148 (red), Y99, E133, H184, E228 (blue), and E351 (black).

acrylamide) native-PAGE as described [27]. The Hyd activity staining was done in 50 m\textsc{m} MOPS buffer, pH 7.0 with 0.5 m\textsc{m} benzyl viologen (BV) and 1 m\textsc{m} 2,3,5-triphenyltetra-zolium chloride under a 5% H$_2$/95% N$_2$ atmosphere.

Hydrogen oxidation and hydrogen production from glycerol

H$_2$ oxidation with fumarate was analyzed in nongrowing cell suspensions using a Clark-type electrode filled with 2 mL anaerobic MOPS buffer, pH 7.0 as described [8]. For analysis of small amounts of hydrogen production from glycerol, the cell suspensions were filled in 5 mL Hungate tubes, stoppered and flushed with N$_2$ before glycerol was added to a final concentration of 0.8% (w/v) and incubated at 37 °C for 16 h. The headspace was then analyzed by gas chromatography using a Shimadzu GC-2010 system as described [28].

In silico analysis and predictions

The amino acid sequence of HybB (Uniprot accession P37180; HybB_Ecoli) was submitted to the Phyre2

structure prediction server in the intensive mode (PDB.org) [29]. The resulting structural model was subsequently submitted to the ConSurf server resulting in the prediction of conserved and functionally relevant residues based on alignments [30]. Additionally, the structural model was used in the PyMOL plugin Caver to predict cavities within the protein [31]. Figures were prepared using the PyMOL Molecular Graphics System (DeLano Scientific LLC, Schrödinger).

Results

Structure prediction of the HybB membrane subunit

A recent crystal structure of the HybCO heterodimer of Hyd-2 was completed *in silico* with the structural prediction of the electron transfer subunit, HybA, and the membrane integral subunit, HybB, delivering the proposed architecture for the entire hetero-quaternary [HybOABC]$_2$ complex [12]. Our own prediction of HybB's tertiary structure was based on the cryo-EM

structure from the recently published membrane subunit ActC of the alternative respiratory complex III (PDB structure 6BTM) [10,29], which oxidizes quinol but has not yet been experimentally validated to contribute to *pmf* generation [10]. Similar to ActC, the modeled structure predicts 10 helices with an especially long, diagonal helix 6 within HybB (Fig. 1B).

Prediction of conservation, cavity, and cavity-forming residues

The generated structure was further submitted to the ConSurf server in order to calculate the sequence conservation scores from which functional residues can be reliably predicted [30]. The generated alignment is shown in Fig. S1. The conservation from ConSurf was then transferred to the structure model and elegantly showed that helices 2–5 within the core of the protein are highly conserved and form a bundle (Fig. 1C,D). In addition, the long, somewhat tilted, transmembrane helix 6 revealed that the residues on one interface of the helix are highly conserved.

When aligning the model of HybB and the model of the adjacent HybA protein with both the structures of Act (PDB: 6BTM) and of *E. coli* formate dehydrogenase *N* (PDB: 1KQF), because FdnH is structurally related to HybA, then it becomes clear that the FeS cluster proximal to HybB is located at the top of the conserved helix bundle 2–5 (Fig. 1E). In order to limit the maximal electron transfer distance of 13 Å to the distal FeS-cluster within HybA, the quinone reduction site must be located close to the periplasmic face (Circle in Fig. 1E), similar to the previously proposed site for Hyd-2 and those observed for Psr and Act [9,10,12].

Finally, analysis with the Caver plugin of PyMOL, which predicts cavities within a given structure [31], identified two half-channels within HybB that could form a continuous channel through the protein (Fig. 1F). Importantly, this channel does not point towards the putative quinone-binding site. The residues within 4 Å adjacent to the predicted channel and which are most highly conserved, include R34, V42, W54, D58, A66, A91, L93, G98, V225, and E228. Residues R34, W54, D58, and E228 were chosen to be individually exchanged to alanines due to the bulky/basic, bulky/hydrophobic and acidic/polar properties of the original residues (Fig. S2 shows all channel residues). In addition, the residues W51, P201, and W203 are conserved in structurally related proteins (Fig. S3) and further residues were manually chosen based on their conservation score in ConSurf and on their chemical properties.

Mutagenesis system and *hybB* mutant complementation

Perturbation of the stoichiometry of multi-subunit complexes, by separating the corresponding genes in polycistronic operons, often results in inactive gene products [32]. Therefore, strain CPH28 lacking the four structural genes (Δ*hybOABC*) was constructed, but expression of the downstream *hybDEFG* genes, encoding maturation enzymes for both Hyd-1 and Hyd-2, was retained. The strain has an additional deletion of the *hycA-I* genes, coding for the H_2-evolving Hyd-3, and, moreover, encodes the T7 RNA polymerase whose gene was placed in the lambda attachment site. Analysis of crude extracts of the mutant after anaerobic growth showed that the activity bands corresponding to Hyd-2 were absent, while the faster migrating Hyd-1 activity was retained (Fig. 2A, lane 1). This confirmed the successful retention of the maturation genes for Hyd-1 and Hyd-2 in the *hyb* operon [6]. The accompanying pJET-plasmid encoding the *hybOABC* genes restored Hyd-2 activity to the mutant (Fig. 2A, lane 2), while placing *hybOABC* on a pACYC-Duet low-copy vector failed to restore Hyd-2 activity to CPH28 (Fig. 2A, lane 3). Thus, the pJET-vector was chosen as a template for site-directed mutagenesis of *hybB*.

Interestingly, the activity of Hyd-1 was strongly reduced when the Hyd-2 plasmid was introduced into these cells, suggesting that the multiple copies of *hybOABC* overburdened the maturation machinery. The increase in unprocessed HybC protein content compared to parental strain MC4100, which has only one chromosomal copy of the structural genes, and the similar migration pattern to strain DHP-F2 (Δ*hypF*), that cannot insert the [NiFe]-cofactor and synthesizes only unprocessed, inactive protein, supports this hypothesis (Fig. 2B). The variant constructs W51A and D58A also have increased protein amounts but low amounts of processed, active HybC (Fig. 2B).

Initial Hyd-2 complex structure characterization by native-PAGE

After mutagenesis the region covering a minimum of 300 bp upstream and downstream of the mutation site was verified by DNA sequencing in order to ensure no secondary mutations in the *hybB* gene accumulated. Three of the planned amino acid exchanges (E155A, R308A, and R329A) could not be generated, as the plasmids either did not yield clones or they were only stable when secondary mutations within the plasmid accrued. We currently suspect that this is due to
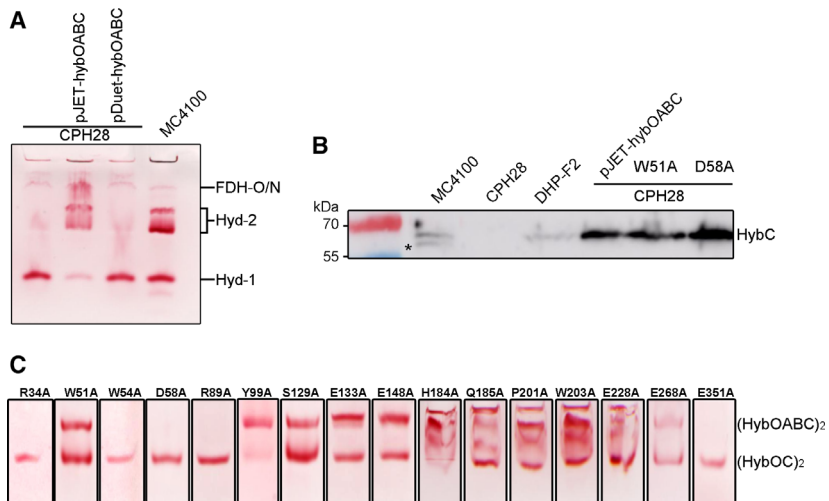
Fig. 2. Complementation of Hyd-2 activity by the *hybOABC* genes. Strain CPH28 (MC4100 (DE3) Δ*hycAI* Δ*hybOABC*) was transformed with plasmids carrying the *hybOABC* genes, cells were grown under fermentative conditions and extracts (50 μg protein), including that from the parental strain MC4100, were applied to a (A) native-PAGE and subsequently stained for Hyd activity. The activities of formate dehydrogenases O and N and the Hyd 1 and 2 are indicated on the right of panel A. (B) SDS-PAGE of extracts from the strains MC4100, CPH28, DHP-F2 (Δ*hypF*), and CPH28 complemented with pJET-hybOABC and the two variant versions W51A and D58A were blotted and challenged with antibodies raised against HybC, the catalytic subunit of Hyd-2. The asterisk indicates the processed, active HybC polypeptide, which is labelled on the right and the mass ladder sizes are given on the left side of panel B. (C) Strain CPH28 (MC4100 (DE3) Δ*hycAI* Δ*hybOABC*) was transformed with a pJET-hybOABC variant plasmid carrying the indicated amino acid exchange in HybB (indicated above the panel). The strains were grown anaerobically in TGYEP and extracts (50 μg protein) were applied to native-PAGE and stained for Hyd activity. The panels were aligned according to the internal control and cropped. The complexes in the upper and lower band are labeled.

toxicity of the product, because we also observed that cells frequently became cured of the plasmid when maintained on plates for longer than 7 days.

The characteristic doublet of Hyd-2 activity bands in activity staining after native-PAGE represents complexes with different subunit compositions (Fig. 2A,C). The faster migrating band consists of the $(HybOC)_2$ heterodimer [3] and occurs in the absence of *hybB* [8]. The slower migrating activity band represents the activity of $(HybOC)_2$ bound to the electron transfer subunit HybA and the membrane subunit HybB [3]. The $(HybOC)_2$ catalytic and small subunit are sufficient to transfer electrons to the artificial electron acceptor BV [33].

The amino acid exchanges in HybB had a number of different effects on the Hyd-2 activity bands. The majority of variants remained unaltered in their Hyd-2 activity-staining pattern, showing the upper band for the $(HybOABC)_2$ heterotetramer and the faster migrating $(HybOC)_2$ heterodimer (residues W51, Y99, S129, E133, E148, H184, Q185, P201, W203, E228, E268) (Fig. 2C). Slight variations in the resolution of the bands frequently occurred, but the internal controls of the parental strain MC4100 on each native-PAGE showed that these

effects were unlikely to be due to the respective amino acid exchange.

Another group of variants (R34A, W54A, D58A, R89A, E351A) only showed the active $(HybOC)_2$ heterodimer (Fig. 2C) although the following experiments indicate that the heterotetrameric complex might still be assembled in most of these variants, but rendered inactive in native-PAGE. The appearance of a further doublet for the upper band was frequently observed. This was especially obvious for the E133A variant, but was also observed occasionally for MC4100. We suspect this represents partial degradation of one of the subunits as has been previously observed during purification of Hyd-1 [34].

Variants unable to evolve H_2

In the next experiment, cells of strain CPH28 transformed with the plasmids encoding variants of HybB were harvested after anaerobic growth in minimal medium containing glycerol as carbon source and fumarate as electron acceptor, conditions that favor the expression of *hyb* genes [15]. After washing in medium, cell suspensions were incubated anaerobically with glycerol and the accumulated H_2 in the headspace

quantified after 16h. Strain CPH28 lacking the *hyc*-operon and parts of the *hyb*-operon, synthesizes only active Hyd-1, and the strain produced 0.18 μmol $H_2 \cdot mg$ protein^{-1} from glycerol (Table 1). The same amount of H_2 is produced from the parental strain MC4100 when the protonophore CCCP was added. This indicated that the residual H_2 production stems from Hyd-1 and production is not *pmf*-dependent. Table 1 further shows that the complemented strain DLH04 with the pJET-hybOABC parental plasmid produced more H_2 (2.90 ± 1.64 μmol $H_2 \cdot mg$ protein^{-1}) than the Hyd-2 only strain HDK103 (0.99 ± 0.73 μmol $H_2 \cdot mg$ protein^{-1}) but less than MC4100 (4.66 ± 2.45 μmol $H_2 \cdot mg$ protein^{-1}). Most of the tested variants produced H_2 in the range of HDK103 and were not further analyzed (Table S2). The variants W54A, Y99A, E133A, H184A, E228A, and E351A, when introduced in strain CPH28, produced less or equal amounts of H_2 from glycerol than the Hyd-1-only strain CPH28. These variants with a clear phenotype lacking H_2-production activity and furthermore the variants R34A, W51A, D58A, R89A, and E148A were investigated in the forward H_2-oxidation reaction (Table 2).

W54A is unidirectional in H_2-oxidation

A whole-cell assay for the ability to oxidize H_2 and concomitantly reduce quinone in the presence of the electron acceptor fumarate was used to assay the forward reaction. Strain DLH04 (Δ*hycA-I* Δ*hybO-C* Δ*hyaB*) was devoid of the corresponding structural genes of Hyd-2 and Hyd-1, that can also oxidize H_2 in the presence of fumarate. Of the tested variants R34A and W51A had no influence neither on H_2-production nor on H_2-oxidation (Table 2). Surprisingly, when

Table 1. Hyd activities of control strains and constructs. All measurements were performed using three biological replicates. Values in parentheses were obtained in the presence of CCCP.

Strain/ construct	H_2- production from glycerol (μmol $H_2 \cdot mg$ protein^{-1})	H_2-oxidation (nmol $H_2 \cdot min^{-1} \cdot mg$ protein^{-1})	Comments
MC4100	4.66 ± 2.45 (0.18 ± 0.14)	131 ± 19 (145 ± 25)	Parental, Hyd-1,2,3
HDK103	0.99 ± 0.73	158 ± 26 (186 ± 16)	Only Hyd-2
CPH28	0.18 ± 0.08	13 ± 2	Only Hyd-1
DLH04	0.01 ± 0.01	< 1	No Hyd-1,2,3
pJET-hybOABC	2.90 ± 1.64 (0.27 ± 0.47)[a]	78 ± 12[a]	*In trans* complementation

[a] Strain DLH04 (MC4100 DE3 Δ*hycA-I* Δ*hybO-C* Δ*hyaB*) was used.

transformed with the plasmids encoding the HybB variants, the W54A variant, that lacked H_2-production from glycerol, showed normal H_2-oxidation activity in the range of DLH04/pJET-hybOABC with 78 nmol $H_2 \cdot min^{-1} \cdot mg$ protein^{-1}, respectively (Tables 1 and 2).

Variants D58A, R89A, and E148 are unidirectional in H_2-production

The opposite behavior was seen in the variants D58A, R89A, and E148A, which, with the exception of E148A, showed only one activity band in native-PAGE but exhibited high H_2-production from glycerol. However, these variants were unable to couple H_2-oxidation to quinone reduction (Table 2). This could either be interpreted as that they appear to be unable to overcome the backpressure when moving protons against the *pmf* or that they are unable to draw protons from the cytoplasm. Interestingly, the effect could not be overcome by addition of CCCP, which lowers the cytoplasmic pH [35]. Therefore, these amino acid residues are suggested to be important in gating PT through the HybB protein.

Amino acid residues crucial for proton transfer

The four other variants Y99A, E133A, H184A, and E228A that could not perform the H_2-production reaction, also exhibited only a very low H_2-oxidation activity, which was in the range of 5–9 nmol H_2 min$^{-1} \cdot mg$ protein^{-1}. These variants also shared a similar activity band profile with the characteristic doublet (Fig. 2C). Upon addition of the protonophore CCCP, the H_2-oxidizing activity increased immediately to between 52% (E133A) and 100% (E228A) of the control DLH04/pJET-hybOABC (Table 2/Fig. 3). This result indicates that PT within the protein was impeded in these HybB variants. The protonophore released this pressure either by uncoupling proton from electron transfer, allowing electron flow to the quinone or by providing better access of protons on the cytoplasmic side.

E351 is essential for Hyd-2 protein stability

Finally, the E351A variant, which also showed only the lower (HybOC)$_2$ band in activity staining, was strongly reduced in whole-cell H_2-production from glycerol and deficient in fumarate-dependent H_2-oxidation, suggesting that the Hyd-2 complex is probably unstable. Notably, H_2-oxidizing activity could not be recovered by addition of CCCP (Table 2). This residue is located in the poorly conserved helix bundle of HybB (Fig. 1G), which is neither part of the predicted

Table 2. Summary of properties of the targeted amino acid residues and controls. Values in parentheses were obtained in the presence of CCCP.

Residue	Predicted location	H_2- production from glycerol (µmol $H_2 \cdot$mg protein^{-1}) in strain CPH28[a]	H_2-oxidation (nmol $H_2 \cdot$min$^{-1} \cdot$mg protein^{-1}) in strain DLH04[b]	Comments
R34	Transmembrane helix (TMH) 1, channel residue	2.33 ± 0.99	78 ± 15	Lower band only
W51	periplasmic loop (PPL) 1	1.69 ± 0.69	40 ± 6 (57 ± 8)	Conserved in structurally related proteins[c]
W54	TMH2, channel residue	0.02 ± 0.04	71 ± 36 (83 ± 46)	Lower band only
D58	TMH2, channel residue	3.76 ± 2.81 (0.09 ± 0.06)	2 ± 0.4 (3 ± 2)	Lower band only
R89	TMH3	1.53 ± 1.27 (0.11 ± 0.15)	4 ± 1 (7 ± 2)	Lower band only
Y99	TMH3	0.01 ± 0.02 (0.03 ± 0.03)	11 ± 3 (40 ± 8)	
E133	TMH4	0.12 ± 0.01 (0.04 ± 0.04)	9 ± 3 (41 ± 14)	
E148	TMH4	0.97 ± 0.84	3 ± 0.4 (6 ± 2)	
H184	TMH5	0.09 ± 0.02	7 ± 2 (37 ± 2)	
E228	TMH6, channel residue	0.08 ± 0.07 (0.02 ± 0.03)	5 ± 1 (79 ± 20)	
E351	TMH10	0.25 ± 0.11	2 ± 1 (2 ± 1)	Lower band only

[a] The exchanges were analyzed in strain CPH28 (MC4100 DE3 Δ*hycA-I* Δ*hybO-C*) on the *in trans* complementing plasmid pJET-hybOABC; all measurements were performed using three biological replicates; [b] The exchanges were analyzed in strain DLH04 (MC4100 DE3 Δ*hycA-I* Δ*hybO-C* Δ*hyaB*) on the *in trans* complementing plasmid pJET-hybOABC; all measurements were performed using three biological replicates; [c] By alignment of Phyre2 identified within structurally related proteins.
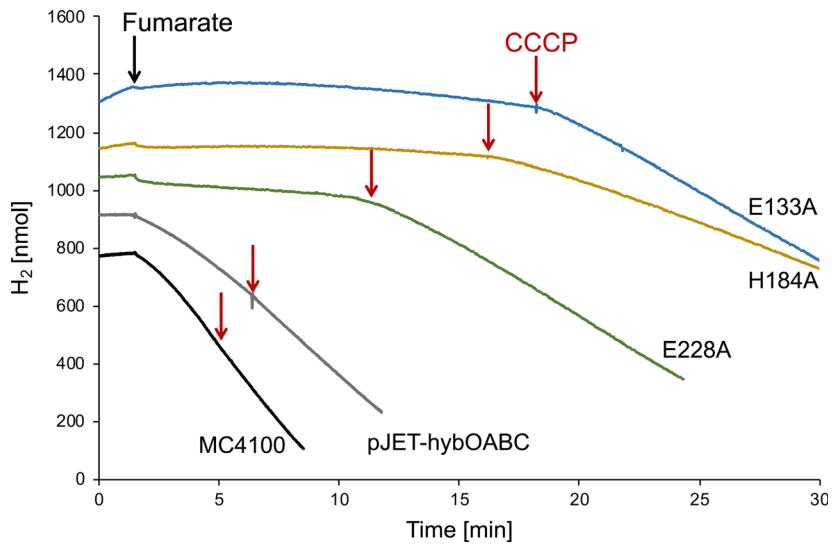
proton channel nor close enough to the surface to interfere directly with HybB's interaction with HybA. However, this residue is close to a periplasmic exit-site of the putative proton channel (Fig. 1G).

Discussion

The work presented in this study has identified six amino acid residues (W54, Y99, E133, H184, E228, E351) in the membrane subunit HybB that, when exchanged for alanine residues, render Hyd-2 unable to use the *pmf* or the more basic cytoplasm to drive

H_2-production with concomitant proton release in the cytoplasm. This is the reverse reaction of the physiologically more relevant H_2-oxidizing role of the enzyme, and these variants were considered devoid of H_2 production. Moreover, four of these amino acid variants (Y99, E133, H184, E228) appeared less efficient in the uptake of protons from the cytoplasm when working in the H_2-oxidation direction, which could be relieved by inclusion of the protonophore CCCP. Addition of CCCP decreases the cytoplasmic pH [35] and thus increases the availability of protons to Hyd-2. This finding suggests that the proton path

Fig. 3. H_2-oxidation by whole cells in the presence of fumarate and CCCP. The Clark-type electrode was filled with H_2-saturated anaerobic 50 mM MOPS buffer, pH 7.0, before 50 µL of cell suspension (see Materials and methods) of either MC4100 or of strain DLH04 complemented with plasmids carrying the *hybOABC* genes and the respective amino acid exchanges E133A, H184A, and E228A in HybB were added. The reaction was started by the addition of 15 mM fumarate (black arrows) and CCCP was added where indicated (red arrows). The electrode was calibrated with known amounts of H_2-saturated buffer.

through HybB was blocked by altering these residues. Of these five amino acid variants, only W54A retained the ability to oxidize H_2 and to reduce quinone without CCCP addition. Based on *in silico* modeling, W54 lies within the predicted proton channel near the periplasmic exit (Fig. 1G) suggesting that it plays a role in access of protons required to drive the thermodynamically demanding H_2-evolution reaction.

Notably, our predicted proton channel within HybB is not in the proximity of the quinone-binding site. If this predicted channel is indeed the pathway for protons, then a conformational change would be necessary to permit electrogenic quinone reduction in analogy to that recently observed in a homologous subunit of Qrc [13]. The driving force for the conformational change would either be quinone binding and reduction or quinol release. It is unclear how this motion could be achieved, but the highly conserved helix bundle (helices 2–5; Fig. 1D) directly beneath the quinone-binding site is a possible candidate. The transmembrane helix of HybA is predicted to be directly adjacent to this bundle and residue E133, the third amino acid identified to influence PT, points outwards and faces the transmembrane helix of HybA (Fig. 1G). Furthermore, E133 is in the vicinity of the quinone-binding site and is within 15 Å of the FeS-cluster in HybA. Respiratory enzymes usually contain a conserved glutamate residue next to the quinone-binding site, which is thought to be the primary proton acceptor/donor [36]. The $E133_{HybB}$ corresponds to the identified quinone binding $E87_{DmsC}$ residue [37] and the proposed quinone binding $E142_{QrcD}$ [13]. The fact that the E133A variant could only recover 50% activity with CCCP supports this additional role of E133 in quinone protonation.

The H184 and Y99 residues are approximately in the middle of the membrane face and also reside within the conserved helix bundle, but face inwards towards each other. Exchanges of H184 and Y99 resulted in similar phenotype to the E133A exchange and thus they might also function in proton-gating or in modulation of the conformational change. These residues have been proposed to be part of the predicted proton channel of QrcD [13]. The other residue that had a similar phenotype to H184 and E133 when exchanged for alanine, was E228; however, this residue is located at the cytoplasmic exit of HybB's predicted proton channel (Fig. 1G). It could be involved in gating proton access to, or release from, the channel at the cytoplasmic face of HybB.

Another set of variants (D58A, R89A, E148A) retained parental-like activity in the H_2-production direction and retained CCCP-dependence, but they lacked activity in the forward H_2-oxidizing direction. Moreover, this could not be restored upon CCCP addition and rendered these Hyd-2 enzyme variants truly unidirectional. The R89 residue is close to the cytoplasmic interface and due to its bulky nature could stabilize the helix orientation. D58, like H148, is located in the conserved helix bundle but is also part of the predicted channel and is also close to W54 (Fig. 1G). The shift of the equilibrium indicates that D58, R89 and E148 are essential for delivering protons to the reduced quinone, but not for expulsion of protons into the cytoplasm during H_2-production.

The final variant that exhibited a defect in both H_2 oxidation and evolution was E351. This residue is located adjacent to W54 (near the periplasmic exit of the proton channel) and has a similar activity-staining profile to the W54A, D58A, and R89A variants, with only the lower band visible. But in contrast to the activity of these variants, the strongly reduced H_2-production and deficient H_2-oxidizing activities suggest that assembly or activity of the $(HybOABC)_2$ complex might be somehow impaired in the E351 variant.

Clearly, our data indicate that protons are transferred through the HybB protein either directly as protons *via* protonable residues or by holding water molecules in a channel in the correct position to serve as hydride ions during PT in a Grotthus mechanism; or most likely by a combination of both mechanisms [38]. Our data identified key amino acid residues for PT from the quinone to the cytoplasm (D58, R89, E148), for uptake of protons from the cytoplasm (Y99, E133, H184, E228), for release of protons from the quinol (W54) and for the possible stability of the heterotetrameric complex (E351). Future work will be required to detect the transferred protons and provide crystal structures comparing bound and unbound quinone states to validate these results.

Acknowledgements

Author contributions

DL performed the experiments. AHS conducted the in silico analysis. CP conceived the study and wrote the manuscript.

References

1 Ballantine S and Boxer D (1986) Isolation and characterisation of a soluble active fragment of hydrogenase isoenzyme 2 from the membranes of anaerobically grown *Escherichia coli*. *Eur J Biochem* **156**, 277–284.

2 Pinske C (2019) Bioenergetic aspects of archaeal and bacterial hydrogen metabolism. *Adv Microb Physiol* **74**, 487–541.

3 Dubini A, Pye R, Jack R, Palmer T and Sargent F (2002) How bacteria get energy from hydrogen: a genetic analysis of periplasmic hydrogen oxidation in *Escherichia coli*. *Int J Hydrogen Energy* **27**, 1413–1420.

4 Menon NK, Chatelus CY, Dervartanian M, Wendt JC, Shanmugam KT, Peck HD and Przybyla AE (1994) Cloning, sequencing, and mutational analysis of the *hyb* operon encoding *Escherichia coli* hydrogenase 2. *J Bacteriol* **176**, 4416–4423.

5 Sargent F, Ballantine S, Rugman P, Palmer T and Boxer D (1998) Reassignment of the gene encoding the *Escherichia coli* hydrogenase 2 small subunit-identification of a soluble precursor of the small subunit in a *hypB* mutant. *Eur J Biochem* **255**, 746–754.

6 Pinske C and Sawers RG (2016) Anaerobic formate and hydrogen metabolism. *EcoSal Plus* **7**, 0011–2016.

7 Rodrigue A, Chanal A, Beck K, Müller M and Wu LF (1999) Co-translocation of a periplasmic enzyme complex by a hitchhiker mechanism through the bacterial tat pathway. *J Biol Chem* **274**, 13223–13228.

8 Pinske C, Jaroschinsky M, Linek S, Kelly CL, Sargent F and Sawers RG (2015) Physiology and bioenergetics of [NiFe]-hydrogenase 2-catalyzed H_2-consuming and H_2-producing reactions in *Escherichia coli*. *J Bacteriol* **197**, 296–306.

9 Jormakka M, Yokoyama K, Yano T, Tamakoshi M, Akimoto S, Shimamura T, Curmi P and Iwata S (2008) Molecular mechanism of energy conservation in polysulfide respiration. *Nat Struct Mol Biol* **15**, 730–737.

10 Sun C, Benlekbir S, Venkatakrishnan P, Wang Y, Hong S, Hosler J, Tajkhorshid E, Rubinstein JL and Gennis RB (2018) Structure of the alternative complex III in a supercomplex with cytochrome oxidase. *Nature* **557**, 123–126.

11 Venceslau SS, Lino RR and Pereira IAC (2010) The Qrc membrane complex, related to the alternative complex III, is a menaquinone reductase involved in sulfate respiration. *J Biol Chem* **285**, 22774–22783.

12 Beaton SE, Evans RM, Finney AJ, Lamont CM, Armstrong FA, Sargent F and Carr SB (2018) The structure of hydrogenase-2 from *Escherichia coli*: implications for H_2-driven proton pumping. *Biochem J* **475**, 1353–1370.

13 Duarte AG, Catarino T, White GF, Lousa D, Neukirchen S, Soares CM, Sousa FL, Clarke TA and Pereira IAC (2018) An electrogenic redox loop in sulfate reduction reveals a likely widespread mechanism of energy conservation. *Nat Commun* **9**, 5448.

14 Trchounian K, Sanchez-Torres V, Wood TK and Trchounian A (2011) *Escherichia coli* hydrogenase activity and H_2 production under glycerol fermentation at a low pH. *Int J Hydrogen Energy* **36**, 4323–4331.

15 Sawers RG, Ballantine S and Boxer D (1985) Differential expression of hydrogenase isoenzymes in *Escherichia coli* K-12: evidence for a third isoenzyme. *J Bacteriol* **164**, 1324–1331.

16 Friedrich T (2001) Complex I: a chimaera of a redox and conformation-driven proton pump? *J Bioenerg Biomembr* **33**, 169–177.

17 Miller J (1972) Experiments in Molecular Genetics. Cold Spring Harbor Laboratory, Cold Spring Harbor, NY.

18 Begg Y, Whyte J and Haddock B (1977) The identification of mutants of *Escherichia coli* deficient in formate dehydrogenase and nitrate reductase activities using dye indicator plates. *FEMS Microbiol Lett* **2**, 47–50.

19 Hormann K and Andreesen J (1989) Reductive cleavage of sarcosine and betaine by *Eubacterium acidaminophilum* via enzyme systems different from glycine reductase. *Arch Microbiol* **153**, 50–59.

20 Sambrook J and Russell D (2001) Molecular Cloning: A Laboratory Manual, 3rd edn. Cold Spring Harbor Laboratory Press, Cold Spring Harbor, NY.

21 Casadaban MJ (1976) Transposition and fusion of the *lac* genes to selected promoters in *Escherichia coli* using bacteriophage lambda and Mu. *J Mol Biol* **104**, 541–555.

22 Hamilton CM, Aldea M, Washburn BK, Babitzke P and Kushner SR (1989) New method for generating deletions and gene replacements in *Escherichia coli*. *J Bacteriol* **171**, 4617–4622.

23 Pinske C, Bönn M, Krüger S, Lindenstrauß U and Sawers RG (2011) Metabolic deficiences revealed in the biotechnologically important model bacterium *Escherichia coli* BL21(DE3). *PLoS ONE* **6**, e22830.

24 Baba T, Ara T, Hasegawa M, Takai Y, Okumura Y, Baba M, Datsenko K and Tomita M (2006) Wanner B & Mori H (2006) Construction of *Escherichia coli* K-12 in-frame, single-gene knockout mutants: the Keio collection. *Mol Syst Biol* **2**, 0008.

25 Jacobi A, Rossmann R and Böck A (1992) The *hyp* operon gene products are required for the maturation of catalytically active hydrogenase isoenzymes in *Escherichia coli*. *Arch Microbiol* **158**, 444–451.

26 Paschos A, Bauer A, Zimmermann A, Zehelein E and Böck A (2002) HypF, a carbamoyl phosphate-converting enzyme involved in [NiFe] hydrogenase maturation. *J Biol Chem* **277**, 49945–49951.

27 Pinske C, Jaroschinsky M, Sargent F and Sawers RG (2012) Zymographic differentiation of [NiFe]-hydrogenases 1, 2 and 3 of *Escherichia coli* K-12. *BMC Microbiol* **12**, 134.

28 Pinske C (2018) The ferredoxin-like proteins HydN and YsaA enhance redox dye-linked activity of the formate dehydrogenase H component of the formate hydrogenlyase complex. *Front Microbiol* **9**, 1238.

29 Kelley LA and Sternberg MJE (2009) Protein structure prediction on the Web: a case study using the Phyre server. *Nat Protoc* **4**, 363–371.

30 Ashkenazy H, Erez E, Martz E, Pupko T and Ben-Tal N (2010) ConSurf 2010: calculating evolutionary conservation in sequence and structure of proteins and nucleic acids. *Nucleic Acids Res* **38**, W529–W533.

31 Jurcik A, Bednar D, Byska J, Marques SM, Furmanova K, Daniel L, Kokkonen P, Brezovsky J, Strnad O, Stourac J *et al.* (2018) CAVER Analyst 2.0: analysis and visualization of channels and tunnels in protein structures and molecular dynamics trajectories. *Bioinformatics* **34**, 3586–3588.

32 Evans RM and Beaton SE (2018) A novel overproduction system for the structural determination of a proton-pumping hydrogen-producing [NiFe]-hydrogenase. *Meth Enzymol* **613**, 91–116.

33 Pinske C, Krüger S, Soboh B, Ihling C, Kuhns M, Braussemann M, Jaroschinsky M, Sauer C, Sargent F, Sinz A *et al.* (2011) Efficient electron transfer from hydrogen to benzyl viologen by the [NiFe]-hydrogenases of *Escherichia coli* is dependent on the coexpression of the iron-sulfur cluster-containing small subunit. *Arch Microbiol* **193**, 893–903.

34 Sawers RG and Boxer D (1986) Purification and properties of membrane-bound hydrogenase isoenzyme 1 from anaerobically grown *Escherichia coli* K12. *Eur J Biochem* **156**, 265–275.

35 Diez-Gonzalez F and Russell JB (1997) Effects of carbonylcyanide-*m*-chlorophenylhydrazone (CCCP) and acetate on *Escherichia coli* O157:H7 and K-12: uncoupling versus anion accumulation. *FEMS Microbiol Lett* **151**, 71–76.

36 Iverson TM, Luna-Chávez C, Croal LR, Cecchini G and Rees DC (2002) Crystallographic studies of the *Escherichia coli* quinol-fumarate reductase with inhibitors bound to the quinol-binding site. *J Biol Chem* **277**, 16124–16130.

37 Geijer P and Weiner JH (2004) Glutamate 87 is important for menaquinol binding in DmsC of the DMSO reductase (DmsABC) from *Escherichia coli*. *Biochim Biophys Acta* **1660**, 66–74.

38 Wraight CA (2006) Chance and design–proton transfer in water, channels and bioenergetic proteins. *Biochim Biophys Acta* **1757**, 886–912.

Supporting information

Additional supporting information may be found online in the Supporting Information section at the end of the article.

Fig. S1. Alignment of the 142 proteins chosen by Con-Surf [1].

Fig. S2. Protter representation of HybB [3].

Fig. S3. Sequence Logo [4] of HybB based on proteins collected from the Phyre2 server [5].

Table S1. Oligonucleotides used for site-directed mutagenesis.

Table S2. Variants with little effect in H_2-production.

Kapitel II – FHL-2 Aktivität in *Trabulsiella guamensis*

Untersuchung des Wasserstoffmetabolismus des Enterobakteriums *Trabulsiella guamensis*: Identifizierung eines formiatabhängigen und essentiellen Formiat Hydrogenlyase Komplexes mit phylogenetischer Ähnlichkeit zu Komplex I.

Ute Lindenstrauß und Constanze Pinske*

Institut für Biologie/Mikrobiologie, Martin-Luther-Universität Halle-Wittenberg, 06108 Halle, Deutschland, Kurt-Mothes-Str. 3, 06120 Halle/Saale, Deutschland

* Korrespondierende Autorin: Constanze Pinske

Zusammenfassung:

Trabulsiella guamensis ist ein apathogenes Enterobakterium, welches aus einem Staubsauger auf der Insel Guam isoliert wurde. Es hat eine H_2-oxidierende Hydrogenase (Hyd) vom Hyd-2-Typ und codiert eine H_2-bildende Hyd, die dem uncharakterisierten *Escherichia coli*-Formiat-Hydrogenlyase (FHL-2$_{Ec}$) -Komplex am ähnlichsten ist. Der *T. guamensis* FHL-2 (FHL-2$_{Tg}$) -Komplex besitzt voraussichtlich fünf membranintegrale und zwischen vier und fünf cytoplasmatische Untereinheiten aufweist. Es konnte gezeigt werden, dass der FHL-2$_{Tg}$-Komplex die Disproportionierung von Formiat zu CO_2 und H_2 katalysiert und der FHL-2$_{Tg}$ damit eine ähnliche Aktivität wie der *E. coli*-FHL-1$_{Ec}$-Komplex bei der H_2-Produktion aus Formiat aufweist. Der Komplex scheint jedoch bei Zelllyse labil zu sein. Durch Klonierung des gesamten 13-kbp FHL-2$_{Tg}$-Operons im heterologen *E. coli*-Wirt konnten die FHL-2$_{Tg}$-Aktivität eindeutig nachwiesen und der FHL-2$_{Tg}$-Komplex biochemisch charakterisiert werden. Obwohl das Formiatdehydrogenase (Fdh-H)-Gen *fdhF* nicht im Operon kodiert ist, ist das Fdh-H Protein Teil des Komplexes und die FHL-2$_{Tg}$-Aktivität abhängig von der Anwesenheit der *E. coli* Fdh-H. Im Gegensatz zu *E. coli* kann *T. guamensis* auch die alternative Kohlenstoffquelle Cellobiose fermentieren, und daher wurden die Beteiligung sowohl der H_2-oxidierenden Hyd-2$_{Tg}$ als auch des H_2-bildenden FHL-2$_{Tg}$ unter diesen Bedingungen untersucht.

Die biologische H_2-Produktion ist eine attraktive Alternative für fossile Brennstoffe. Um mit herkömmlichen H_2-Produktionsmethoden konkurrieren zu können, erfordert der Prozess Verständnis auf molekularer Ebene. FHL-Komplexe sind effiziente H_2-Produzenten, und der Prototyp des FHL-1$_{Ec}$-Komplexes in *E. coli* ist gut untersucht. Hier wird die erste biochemische Charakterisierung eines Komplexes vom FHL-2-Typ vorgestellt. Die hier präsentierten Daten ermöglichen es, den FHL-2$_{Ec}$-Komplex näher zu untersuchen, eine erste biochemische Charakterisierung des fermentativen Metabolismus von *T. guamensis* durchzuführen und dieses Enterobakterium als Modellorganismus für die FHL-abhängige Energiekonservierung zu etablieren.

RESEARCH ARTICLE

Dissection of the Hydrogen Metabolism of the Enterobacterium *Trabulsiella guamensis*: Identification of a Formate-Dependent and Essential Formate Hydrogenlyase Complex Exhibiting Phylogenetic Similarity to Complex I

Ute Lindenstrauß,[a] Constanze Pinske[a]

[a]Department of Microbiology, Martin Luther University Halle-Wittenberg, Halle (Saale), Germany

ABSTRACT *Trabulsiella guamensis* is a nonpathogenic enterobacterium that was isolated from a vacuum cleaner on the island of Guam. It has one H_2-oxidizing Hyd-2-type hydrogenase (Hyd) and encodes an H_2-evolving Hyd that is most similar to the uncharacterized *Escherichia coli* formate hydrogenlyase (FHL-2$_{Ec}$) complex. The *T. guamensis* FHL-2 (FHL-2$_{Tg}$) complex is predicted to have 5 membrane-integral and between 4 and 5 cytoplasmic subunits. We showed that the FHL-2$_{Tg}$ complex catalyzes the disproportionation of formate to CO_2 and H_2. FHL-2$_{Tg}$ has activity similar to that of the *E. coli* FHL-1$_{Ec}$ complex in H_2 evolution from formate, but the complex appears to be more labile upon cell lysis. Cloning of the entire 13-kbp FHL-2$_{Tg}$ operon in the heterologous *E. coli* host has now enabled us to unambiguously prove FHL-2$_{Tg}$ activity, and it allowed us to characterize the FHL-2$_{Tg}$ complex biochemically. Although the formate dehydrogenase (FdhH) gene *fdhF* is not contained in the operon, the FdhH is part of the complex, and FHL-2$_{Tg}$ activity was dependent on the presence of *E. coli* FdhH. Also, in contrast to *E. coli*, *T. guamensis* can ferment the alternative carbon source cellobiose, and we further investigated the participation of both the H_2-oxidizing Hyd-2$_{Tg}$ and the H_2-forming FHL-2$_{Tg}$ under these conditions.

IMPORTANCE Biological H_2 production presents an attractive alternative for fossil fuels. However, in order to compete with conventional H_2 production methods, the process requires our understanding on a molecular level. FHL complexes are efficient H_2 producers, and the prototype FHL-1$_{Ec}$ complex in *E. coli* is well studied. This paper presents the first biochemical characterization of an FHL-2-type complex. The data presented here will enable us to solve the long-standing mystery of the FHL-2$_{Ec}$ complex, allow a first biochemical characterization of *T. guamensis*'s fermentative metabolism, and establish this enterobacterium as a model organism for FHL-dependent energy conservation.

KEYWORDS FHL, formate, formate hydrogenlyase, hydrogen, hydrogenase

Die Publikation kann unter https://journals.asm.org/doi/full/10.1128/JB.00160-19 aufgerufen werden. Sie nimmt die Seiten 42-52 der Druckversion der Habilitationsschrift ein.

Kapitel III – Protonophoreinfluss auf FHL

Die Empfindlichkeit der Formiat Hydrogenlyase-Reaktion gegenüber des Protonophors CCCP hängt von der Hydrogenase Zusammensetzung ab

Janik Telleria Marloth und Constanze Pinske*

Institut für Biologie/Mikrobiologie, Martin-Luther-Universität Halle-Wittenberg, 06108 Halle, Deutschland, Kurt-Mothes-Str. 3, 06120 Halle/Saale, Deutschland

* Korrespondierende Autorin: Constanze Pinske

Zusammenfassung:

Die fermentative Wasserstoffproduktion durch Enterobakterien beruht auf der Aktivität des Formiathydrogenlyase (FHL)-Komplexes, welcher die Formiatoxidation mit der H_2-Produktion koppelt. Die Molybdän-haltige Formiatdehydrogenase und Typ-4 [NiFe]-Hydrogenase bilden zusammen mit drei weiteren Eisen-Schwefel-Proteinen die lösliche Domäne, die über zwei integrale Membranuntereinheiten an die Membran gebunden ist. Der FHL-Komplex ist phylogenetisch mit dem Komplex I der Atmungskette verwandt, so dass er eine ähnliche Rolle bei der Energiekonservierung wie die Protonenpumpaktivität von Komplex I spielen könnte. Wir haben die H_2-produzierende Aktivität von FHL in Gegenwart verschiedener Konzentrationen des Protonophors CCCP untersucht. Eine Hemmung mit einem apparenten EC_{50} von 31 µM CCCP in Gegenwart von Glucose wurde beobachtet. Eine höhere Toleranz gegenüber CCCP gab es, wenn nur die oxidierende Hydrogenase Hyd-1 vorhanden war, aber eine höhere Empfindlichkeit gab es, wenn nur Hyd-2 vorhanden war. Die Anwesenheit von 200 mM einwertigen Kationen verringerte die FHL-Aktivität um mehr als 20%. Der Na^+/H^+-Antiporterinhibitor 5-(N-Ethyl-N-isopropyl)-amilorid (EIPA) in Kombination mit CCCP inhibierte die H_2-Produktion vollständig. Diese Ergebnisse zeigen eine Kopplung nicht nur zwischen der Na^+-Transportaktivität und der H_2-Produktionsaktivität, sondern auch zwischen der FHL-Reaktion, dem Protonenimport und dem Kationenexport.

Susceptibility of the Formate Hydrogenlyase Reaction to the Protonophore CCCP Depends on the Total Hydrogenase Composition

Janik Telleria Marloth and Constanze Pinske *

Institute for Biology/Microbiology, Martin-Luther-University Halle-Wittenberg, 06108 Halle, Germany; constanze.pinske@mikrobiologie.uni-halle.de

* Correspondence: constanze.pinske@mikrobiologie.uni-halle.de; Tel.: +49-(0)-345-5526-353

Abstract: Fermentative hydrogen production by enterobacteria derives from the activity of the formate hydrogenlyase (FHL) complex, which couples formate oxidation to H_2 production. The molybdenum-containing formate dehydrogenase and type-4 [NiFe]-hydrogenase together with three iron-sulfur proteins form the soluble domain, which is attached to the membrane by two integral membrane subunits. The FHL complex is phylogenetically related to respiratory complex I, and it is suspected that it has a role in energy conservation similar to the proton-pumping activity of complex I. We monitored the H_2-producing activity of FHL in the presence of different concentrations of the protonophore CCCP. We found an inhibition with an apparent EC_{50} of 31 µM CCCP in the presence of glucose, a higher tolerance towards CCCP when only the oxidizing hydrogenase Hyd-1 was present, but a higher sensitivity when only Hyd-2 was present. The presence of 200 mM monovalent cations reduced the FHL activity by more than 20%. The Na^+/H^+ antiporter inhibitor 5-(N-ethyl-N-isopropyl)-amiloride (EIPA) combined with CCCP completely inhibited H_2 production. These results indicate a coupling not only between Na^+ transport activity and H_2 production activity, but also between the FHL reaction, proton import and cation export.

Keywords: formate hydrogenlyase; hydrogen metabolism; energy conservation; MRP (multiple resistance and pH)-type Na^+/H^+ antiporter; CCCP—carbonyl cyanide m-chlorophenyl-hydrazone; EIPA—5-(N-ethyl-N-isopropyl)-amiloride

1. Introduction

Anaerobic or fermentative growth in the absence of oxygen requires that conservation of energy is at its utmost efficiency. The reaction of the formate hydrogenlyase (FHL) complex contributes indirectly to the generation of a proton gradient at the cytoplasmic membrane by consumption of protons (H^+) from the cytoplasm, diffusion of H_2-gas across the membrane and subsequent oxidation by the two periplasmic H_2-oxidizing hydrogenases (Hyd-1 and Hyd-2) [1] (Figure 1). Hyd-1 forms a redox loop, and Hyd-2 contributes directly to proton transfer from the cytoplasm to the quinone during oxidation of H_2 [1,2]. The *hyaB* and *hybC* genes encode the catalytic subunits of Hyd-1 and Hyd-2, respectively [3]. This kind of intracellular syntrophy was initially described for *Desulfovibrio* species [4] and more recently for *Acetobacterium woodii* [5]. The FHL complex of *Escherichia coli* is active during mixed acid fermentation to disproportionate formate, which, when accumulated intracellularly, has cytotoxic effects [6]. The two active sites of the FHL complex comprise the [NiFe]-hydrogenase 3 (HycE protein) and the molybdenum- and selenium-containing formate dehydrogenase H (FdhH protein), which function together with three electron-transferring iron-sulfur carrying subunits located in the cytoplasm. Membrane attachment to the membrane-integral

HycC and HycD subunits is required for coupling of these half-reactions [7,8]. Our previous studies have shown that the FHL complex can work in reverse in resting cells, a reaction of great biotechnological interest for H_2 and CO_2 storage as formate [8,9]. A second FHL complex with a predicted five instead of two membrane subunits is encoded in the *hyf*-operon on the *E. coli* chromosome, but, presumably due to its low level of gene expression, the activity of this enzyme complex is not detectable under our growth conditions [10,11].
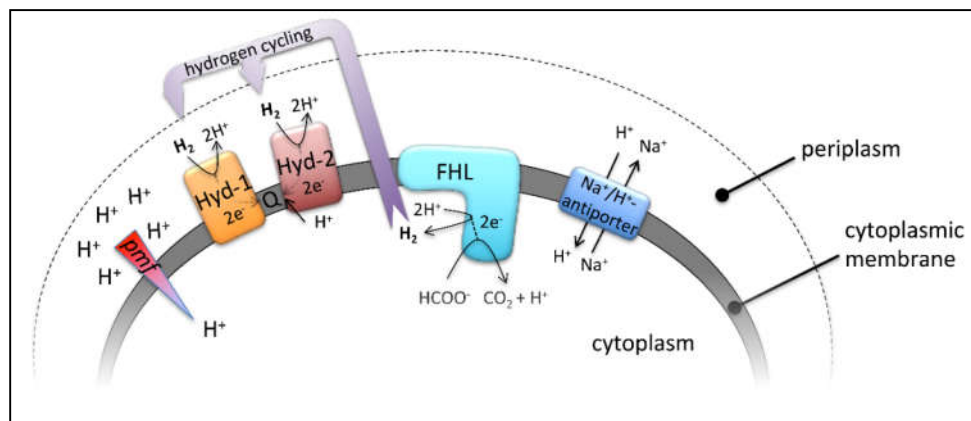
Figure 1. Relevant enzyme complexes of this study, their reactions and their membrane localization. Hyd-1 and Hyd-2 indicate the periplasmic H_2-oxidizing hydrogenases, which channel electrons into the quinone pool (Q), FHL—the cytoplasmic formate hydrogenlyase—and the membrane bound Na^+/H^+ antiporters. Further details are highlighted in the main text.

When the phylogenetic relationship between the FHL complex and complex I was discovered, energy conservation by proton-pumping of the complex was also assumed [12,13]. The hydrogenase 3 (HycE protein) belongs to the class 4 hydrogenases and is similar to the Ech (Energy-converting hydrogenase) hydrogenases, which were shown to generate proton gradients during catalysis [14]. However, while studying FHL bidirectionality as the basis for analyzing the influence of ionophores, we unexpectedly found that the protonophore carbonyl cyanide *m*-chlorophenyl-hydrazone (CCCP) showed only a 40% inhibition of the H_2 production activity and a 30% increase of the reverse formate production reaction from H_2 and CO_2 [8].

It was speculated that due to the small difference in standard redox potentials of formate ($E_0' = -432$ mV, pH 7.0) and H_2 ($E_0' = -414$ mV, pH 7.0), redox energy for proton translocation becomes available only when the physiological conditions shift to a more acidic pH [15]. However, the reversibility of an artificially coupled hydrogenase and formate dehydrogenase reaction from *Desulfovibrio* via an electrode was able to mimic the FHL reaction in both directions *in vitro* without dependence of the reaction on energy provision [16]. Instead, a controversially discussed model of a multienzyme transport supercomplex comprising F_1F_0-ATPase, the K^+-transporting TrkA symporter and the FHL(-2) complex was suggested for energetic coupling [17,18]; however, its existence still requires verification (reviewed in [19]). Therefore, both the necessity for and the role of the FHL complex's membrane attachment in energy conservation remains to be resolved.

In the present work we have systematically re-examined the CCCP effect on FHL activity, whereby we combined different CCCP concentrations with use of different carbon sources to initiate FHL activity in strains either bearing or lacking the H_2-oxidising Hyds. We found that ultimately all strains could be inhibited by CCCP, but strains lacking Hyd-1 required lower, and those lacking Hyd-2 required higher, concentrations of CCCP for inhibition. Based on the relationship of the membrane subunit HycC to Na^+/H^+ (MRP)-type antiporters, we further addressed the question of whether the FHL reaction is driven by or is contributing to the *pmf* and if it might be linked to the sodium motive force. We present strong evidence for a dependence of the FHL reaction on proton influx and sodium export.

2. Results and Discussion

2.1. CCCP Inhibits H₂ Production to Different Degrees Depending on the Hydrogenase Composition

Cell suspensions initiate H_2 production after the anaerobic addition of either formate or glucose, the latter requires metabolizing by the cells to formate prior to H_2 production. Consequently, the mixed-acid fermentation yields 2 mol formate per mol glucose (reviewed in [3]). Formate is the direct substrate for the FHL complex, but its import via the formate channel FocA could mask the effects seen. FocA behaves as a pH-dependent channel *in vitro*, while its activity is mostly determined by its interaction with the pyruvate formate lyase protein PflB *in vivo* [20]. It is feasible that formate export across the membrane contributes to *pmf* generation by proton symport, but the import mechanism is unresolved, except that it only occurs when formate-consuming reactions in the cytoplasm can take place [21]. Therefore, the apparent 1.3 mol H^+ that are translocated across the membrane per mole of formate oxidized during the FHL reaction could be indirect [22]. On the other hand, the transport of glucose across the membrane is PTS (phosphotransferase system)-dependent, where phosphoenolpyruvate provides the phosphoryl group for the incoming glucose in a *pmf*-independent manner [23]. Our parallel experimental design circumvents the fact that indirect effects through the transport of the carbon source into the cells are observed.

The parental strain MC4100, the isogenic *hyaB* deletion strain CP630, which lacks Hyd-1 activity, the isogenic *hybC* deletion strain CP631, which lacks Hyd-2 activity, or the *hyaB hybC* double deletion strain CP734 were grown under the optimal conditions for FHL activity. Subsequently, cells were harvested and suspensions used on a modified Clark-type electrode to monitor H_2 production. The strains showed initial activities very similar to each other in the presence of the same carbon source, but generally higher activity was observed in the presence of formate than glucose (Table 1). A strain lacking the genes for the FHL complex (HDK103) did not produce H_2 under these conditions, supporting the observation that the second FHL is inactive under the conditions tested here [10].

Table 1. H_2 production rates in nmol $H_2 \cdot min^{-1} \cdot mg^{-1}$ ± standard deviation from at least three independent biological samples.

Strain [1]	Glucose	Formate
MC4100	69 ± 12	160 ± 47
CP630 (Δ*hyaB*)	74 ± 23	173 ± 13
CP631 (Δ*hybC*)	101 ± 15	145 ± 20
CP734 (Δ*hyaB* Δ*hybC*)	114 ± 24	121 ± 13

[1] Strains were grown in TGYEP, pH 6.5 medium for 16 h at 30 °C, cells harvested and suspended in 50 mM Tris/HCl, pH 7.0, prepared and assayed on the Clark-type electrode.

When CCCP concentrations of 100 μM were employed, the effect this had on the H_2 production was strain dependent. A previous study from our lab had shown that 100 μM CCCP caused a slight inhibition of the H_2 production rate in a strain with a similar Hyd composition to CP734 [8]. If indeed proton translocation is directly performed by the FHL complex, then CCCP would be expected to cause an increase of the activity, not a decrease. Nevertheless, 100 μM CCCP caused complete inhibition of H_2 production by the parental strain MC4100 independent of the employed carbon source. The slope of the H_2 production even inverted (i.e., H_2 oxidation) after CCCP addition (Figure 2), which indicates consumption of the produced H_2 within the electrode system and indicates the activity of H_2-oxidation reactions, which are usually not performed by the FHL complex, but by the H_2-oxidizing Hyd-1 and Hyd-2 enzymes, indicating they are responsible for the difference.

In the next step, strains lacking the genes encoding the large subunit of either Hyd-1 (Δ*hyaB*, strain CP630) or Hyd-2 (Δ*hybC*, strain CP631) were used in the same experimental setup. While the Hyd-2-deficient strain CP631 (purple curves) mimics the H_2 production curves of the double deletion strain CP734 (Δ*hyaB* Δ*hybC*) after CCCP addition, the Hyd-1 deficient strain CP630 (blue curves) looks very similar to the parental curves and negative slopes after CCCP addition is observed. It can be further observed that the effect of CCCP addition is not immediate, but H_2 production rates shift

rather gradually. For the direct dependence of an activity on *pmf*, we have previously observed immediate and complete effects of CCCP addition on the activity [2], suggesting an indirect effect of CCCP occurs here. Notably, the addition of other protonophores like 2,4-dinitrophenol (DNP) up to 1 mM had no effect on the H_2 production activity of the cells, similar to what was observed before at lower concentrations [8]. Taken together, this indicates that the effect of CCCP on FHL activity is indirect.
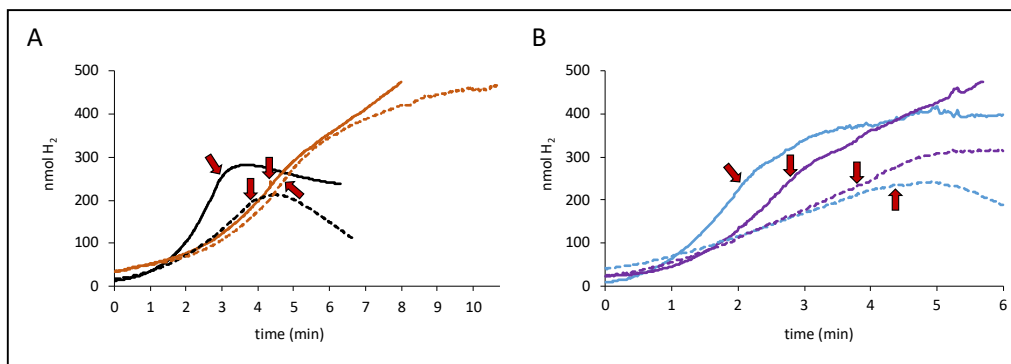
Figure 2. Different degrees of inhibition by protonophore carbonyl cyanide *m*-chlorophenyl-hydrazone (CCCP). Panel A shows H_2 production from the strains MC4100 (parental, black curves) and CP734 (Δ*hyaB* Δ*hybC*, orange curves) while panel B shows the strains CP630 (Δ*hyaB*, blue curves) and CP631 (Δ*hybC*, purple curves) after addition of either 14 mM glucose (dashed lines) or 50 mM formate (solid lines). When H_2 production was linear, a final concentration of 100 μM CCCP was added to the reaction vessel, as indicated by the red arrows.

2.2. Hyd-1 Confers Resistance and Hyd-2 Sensitivity of H_2 Production to CCCP

In order to quantify the effect of CCCP on the FHL activity, we calculated the apparent EC_{50} (half maximal effective concentration) values (Table 2). For that purpose, we analyzed the H_2 production on the electrode, and at about 100 nmol H_2, different concentrations of CCCP were added to the reaction. Figure 3A shows an example of the effect of the CCCP addition on strain CP630 (Δ*hyaB*). A concentration of 1 and 10 μM did not significantly alter the slope of H_2 production, while 50 and 100 μM CCCP clearly slowed down the reaction, and 200 μM led to complete stagnation of H_2 production. A further increase to 400 μM CCCP revealed negative slopes, indicating re-oxidation of H_2 by Hyd-2. Due to slight variations in the initial FHL activities, the reduction of activity after CCCP addition was calculated as the ratio of the activity after CCCP addition to the activity before its addition (Figure 3B). In the case of a negative slope, the ratio after CCCP addition was calculated as zero.
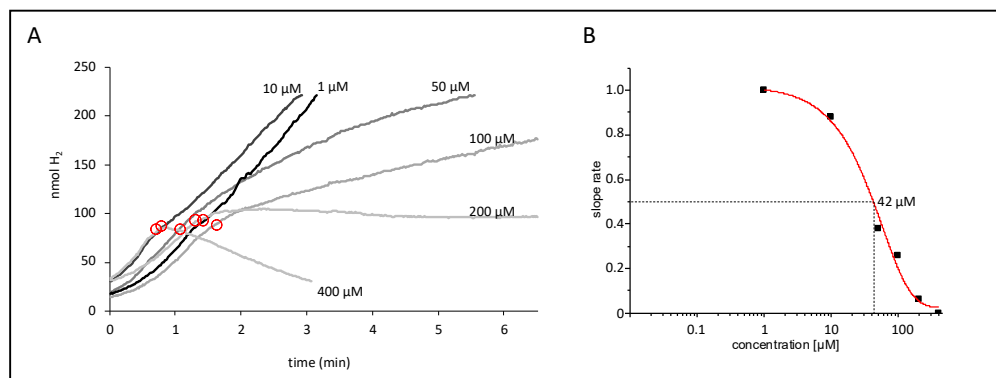
Figure 3. Dose-dependent effect of CCCP. **(A)** Strain CP630 (Δ*hyaB*) was used as a representative strain for CCCP inhibition after initiation of the reaction with 50 mM formate and linear slope; the designated concentrations of CCCP were added at the time points encircled in red. (**B**) The apparent

EC$_{50}$ values of this set of activities were calculated from the ratio of slopes after and before CCCP addition and subsequent fitting with the EC$_{50}$ function in SigmaPlot.

An apparent half-maximal inhibition (EC$_{50}$) of H$_2$ production can be observed at 31 μM CCCP with glucose or 81 μM CCCP with formate as substrate in strain MC4100 (Table 2). These higher concentrations of CCCP, which are required in the presence of formate compared to glucose, reflect the higher initial activities in the presence of formate (Table 1). The double deletion strain CP734 (Δ*hyaB* Δ*hybC*) only showed reduction of H$_2$ production at elevated CCCP concentrations, which is reflected in the increased apparent EC$_{50}$ values. For example, we observed complete inhibition of MC4100 (glucose initiated) at 50 μM CCCP but in strain CP734 only at 500 μM CCCP. Looking at the effect of single deletions of the two H$_2$-oxidizing Hyd in strains CP630 and CP631, respectively, then the Hyd-1 deletion (Δ*hyaB*, strain CP630) caused increased sensitivity to CCCP compared to the parental MC4100, while the Hyd-2 deletion (Δ*hybC*, strain CP631) increased resistance to CCCP similar to the double deletion strain CP734 (Table 2).

Table 2. Apparent EC$_{50}$ values of CCCP inhibition.

Strain [1]	Glucose	Formate
MC4100	31 μM	81 μM
CP630 (Δ*hyaB*)	0.13 μM	42 μM
CP631(Δ*hybC*)	125 μM	223 μM
CP734 (Δ*hyaB* Δ*hybC*)	98 μM	348 μM

[1] The same cell suspensions were used for the glucose and formate experiments. The same amount of total cell protein (1 mg) was used for the different strains. All values were calculated from at least five different CCCP concentrations.

Hyd-1 has a lower catalytic activity than Hyd-2 [24,25], while at the same time it has a similar abundance in the membrane under the conditions used to grow the cells here [26]. It is possible that the inactivation of Hyd-1 in strain CP630 results in elevated amounts of Hyd-2 because more maturation enzymes for cofactor construction and more membrane space are available. Hyd-2 is the enzyme that contributes to *pmf* generation [27], and the data show that Hyd-2 but not Hyd-1 catalyzes the oxidation of H$_2$ at high CCCP concentrations. CCCP enhances Hyd-2 activity by removing the back-pressure of the *pmf* on the enzyme. When assayed directly, the effect is not very prominent because the enzyme works at its catalytic optimum, but in variants that exhibit difficulties in transferring electrons across the membrane, the effect is more pronounced [2]. Electrons from Hyd-2 are concomitantly channeled into the quinone pool for reduction of electron acceptors like fumarate, which can be internally produced during mixed-acid fermentation when glucose is provided to the cells [28]. Therefore, negative slopes occur mostly when Hyd-2 is present and glucose is provided. This does not account for H$_2$ oxidation in the presence of formate; however, we cannot currently explain this effect (Figure 3A). The higher amounts of Hyd-2 enzyme in combination with its CCCP-elevated activity account for the apparent higher CCCP sensitivity in the absence of Hyd-1. Therefore, the absence of Hyd-2 confers resistance, and the absence of Hyd-1, resulting in a concomitant increase in Hyd-2 levels, causes sensitivity to CCCP.

CCCP is, however, also effective at stalling the H$_2$ production when Hyd-1 and Hyd-2 are both absent, albeit only at higher concentrations, but independent of the given carbon source. Hence, a secondary effect, exclusively based on FHL activity, must occur. When, in an unrelated study, a proteorhodopsin was expressed in *E. coli* cells, the H$_2$ production from FHL was increased upon light exposure, which initiates proton-pumping activity of the proteorhodopsin [29] and supports the observed *pmf*-consumption during H$_2$-evolution observed here. We can exclude a direct inhibition of either the hydrogenase or formate dehydrogenase half-reaction of the FHL complex. When assayed independently of one another with benzyl viologen redox dye, crude extracts from strain CP734 showed a hydrogenase activity of 2.43 ± 0.48 U mg^{-1} in the absence and 2.36 ± 0.42 U mg^{-1} in the

presence of CCCP. The formate dehydrogenase activity was similarly unaltered with an activity of 0.26 ± 0.09 U mg^{-1} without and 0.27 ± 0.07 U mg^{-1} with CCCP present.

2.3. CCCP Promotes the Reverse FHL Reaction

Due to the inhibitory effect of CCCP addition on the H$_2$ production of FHL, we investigated its effect on the reverse FHL reaction, which can be initiated if resting cells are incubated under elevated pressure of H$_2$ and CO$_2$ gas mix, as exploited before [8,9]. The reverse reaction was tested in the presence of different concentrations of CCCP, and the resulting formate concentration secreted by the cell suspensions at the equilibrium state was subsequently analyzed using HPLC (Figure 4). While cells produced 23 mM formate in the absence of CCCP in a strain that lacked Hyd-1 and Hyd-2, no formate formation was observed in the parental strain MC4100 under these conditions. The amount of formate initially decreased in the presence of 1, 10 and 50 μM CCCP, was then similar to no addition in the presence of 75 μM CCCP and finally increased to 180 mM formate when 500 μM CCCP was added. The parental strain MC4100 only showed formate production when 200 μM CCCP or more was present but eventually produced 157 mM formate in the presence of 500 μM CCCP (Figure 4). This difference between the two strains clearly showed that when Hyd-1 and Hyd-2 are present (strain MC4100), H$_2$ oxidation by these enzymes is the preferred route for H$_2$ oxidation to the FHL reverse reaction. Generally, an increase of the CCCP concentration resulted in an increase of formate production. If the CCCP effect was *pmf*-mediated, then this could be interpreted as CCCP-mediated relief of the *pmf* counter-pressure during the reverse FHL reaction. An alternative explanation is provided by the proton symport of the formate channel FocA during export, which would be enhanced in the presence of CCCP, thus removing cytoplasmic formate from the reaction and, therefore, shifting the equilibrium of the FHL reaction towards formate production.
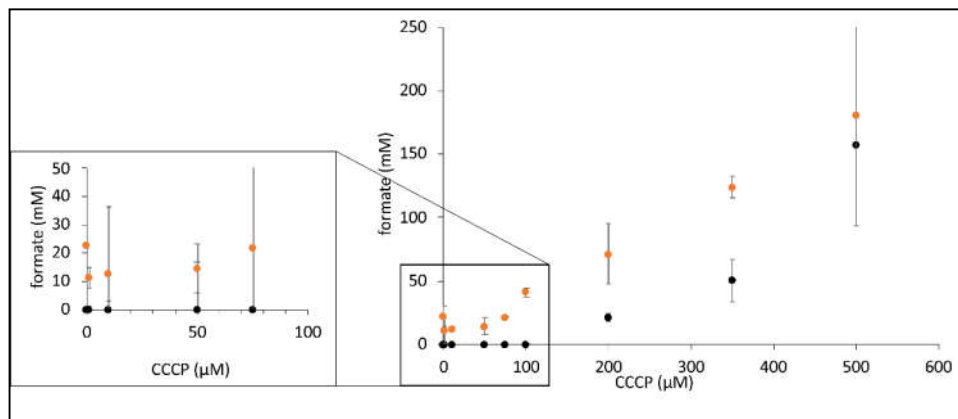
Figure 4. CCCP-dependent increase in formate synthesis by FHL. Strains MC4100 (parental, black dots) and CP734 (Δ*hyaB* Δ*hybC*, orange dots) were triggered for formate production in the presence of different concentration of CCCP as indicated (described in the Materials and Methods section). Each dot represents the average of three biological replicates with standard deviation.

2.4. The DTT Reversal of the CCCP Effect is not Mediated by Hyd-2 Activity

It has been observed that the effects of CCCP can be generally relieved by addition of dithiothreitol (DTT) [30] and also specifically restore the activity of FHL with DTT after CCCP inhibition [17]. Initially, it was verified that the addition of DTT on its own had no effect on the H$_2$ production rate of MC4100 (Figure 5A). Once the H$_2$ production was CCCP-inhibited, the addition of DTT was able to gradually restore H$_2$ production up to the rate it had been before CCCP addition (Figure 5A). We also observed that the DTT relief of CCCP inhibition is independent of the strain used, indicating that the presence of Hyd-2 or Hyd-1 is not essential for the reversibility. Furthermore, CCCP was unable to inhibit H$_2$ production when it was already pre-incubated with DTT (red curve in Figure 5A).

We were recently able to show that Hyd-2 contributes to *pmf* generation in an electrogenic fashion that is susceptible to CCCP addition [2,27]. If CCCP addition substantially increased Hyd-2 activity to the amount where it outcompeted the H_2 production of the FHL complex and thus reduced the overall H_2 production, then the DTT addition would inhibit Hyd-2 H_2-oxidizing activity and consequently restore overall H_2 production. Strain HDK103 (Δ*hyaB* Δ*hycA-I*), which only synthesizes active Hyd-2 enzymes, was used to investigate whether DTT addition influenced the H_2-oxidizing activity of Hyd-2. H_2-saturated buffer was applied to the electrode, and cell suspension was added before the reaction was initiated with 15 mM fumarate as electron acceptor and the H_2 trace recorded (Figure 5B). The addition of 5 mM DTT is indicated but did not inhibit H_2 oxidation. Hence, DTT did not inhibit the H_2-oxidizing activity of Hyd-2, and restoration of overall H_2 production is caused otherwise.

It is noteworthy that a redshift of the CCCP spectrum in the presence of DTT was observed, where the absorbance maximum shifts from 381 nm to 405 nm (Figure 5C). The reaction of CCCP derivatives with thiols has been characterized [31] and showed that they are inactivated in the reaction in the presence of DTT. Taken together, this supports the observation made above that the observed effects of CCCP are not merely due to its protonophore activity but rather could be attributed to its interaction with thiols from cysteine residues, possibly those within the FHL complex. Cysteine residues are essential for electron transfer within the FHL complex by coordinating the metal cofactors. Recently, the number of free thiols was determined and was reduced in strains unable to synthesize a functional FHL complex [32]. However, an inactivation of CCCP by DTT and re-formation of the *pmf* by the cell can also not be excluded.
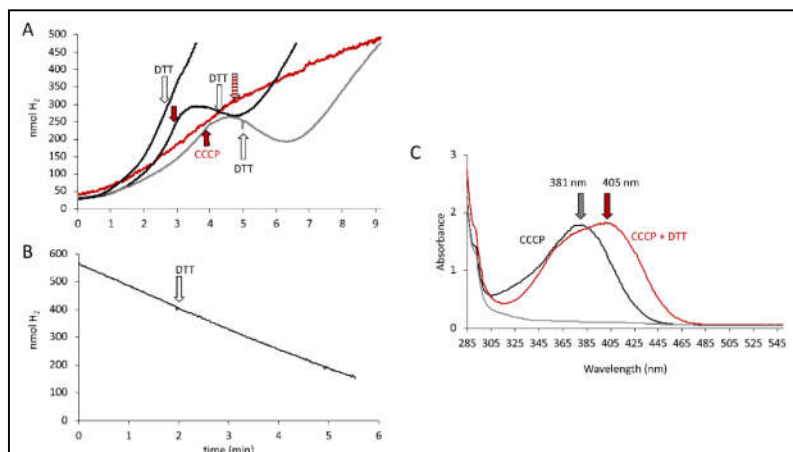
Figure 5. DTT effect. (**A**) Electrode traces of MC4100 cells producing H_2 from either glucose (grey curves) or formate (black curves). CCCP addition (red arrow, 100 μM) and DTT addition (white arrow, 5 mM) are indicated. The red trace shows the combined addition of DTT and CCCP (striped red arrow). (**B**) Electrode trace of strain HDK103 (Δ*hyaB* Δ*hycA-I*) showing the activity of Hyd-2 as H_2 oxidation of H_2-saturated buffer after the addition of 15 mM fumarate. The white arrow indicates the addition of 5 mM DTT. (**C**) Absorption spectra of CCCP solution (black), CCCP solution after DTT addition (red) and DTT alone (grey). The arrows indicate the respective maxima.

2.5. Effect of Monovalent Cations on FHL Reactions

CCCP has been described to collapse both the ΔpH and the transmembrane electrical gradient (ΔΨ) component of the *pmf* [33]. It has been observed that FHL is more active and the *hyc*-genes more strongly expressed under acidic conditions [34,35]. While a ΔpH collapse would increase the availability of protons to the hydrogenase active site in the cytoplasm, and hence increase substrate availability, the ΔΨ collapse represents reduction of the outer positive charge and inner negative charge of the membrane. In order to investigate the possibility that the apparent *pmf* dependence could be due to the ΔΨ collapse mediated by CCCP, we analyzed the effects of cation addition on H_2 production.

Kinetic experiments on the electrode showed reduction of the H_2 production rate when increasing concentrations of Na^+ ions were present. The rates were reduced by 27% in strain CP734 in the presence of 200 mM sodium compared to in its absence (Figure 6A). When 100 μM CCCP was added to any of the reactions, the reduction was between 40%–50%, regardless of the sodium ion concentration present (Figure 6A, grey dots). Therefore, the presence of NaCl did not enhance the effect of CCCP in this strain.

The net charge of the ions remains unaltered through the addition of NaCl or KCl, because the chloride counterion is present. However, the cation/H^+ antiporters counteract the increased salt concentrations that challenge the cell and concomitantly excrete excess cations, which is accompanied by an increased H^+ influx. It was observed that ΔΨ decreased over the first 15–20 min after addition of KCl or NaCl [36], hence within the time-frame where H_2 production was monitored. Apparently, it is this disturbance of the electrical gradient that is detrimental to H_2 production by FHL.

Similarly, when cells were already grown in the presence of different concentrations of Na^+ or K^+ ions and subsequently the H_2 content in the headspace sampled by gas chromatography (GC), which indirectly reflects the activity of the FHL complex, a reduction in the presence of increasing concentrations of Na^+ ions could be observed (Figure 6B). Strain CP734 (Δ*hyaB* Δ*hybC*) showed an increased H_2 accumulation by 30%–70% compared to its parent MC4100 under all conditions. This effect is due to the absence of Hyd-1 and Hyd-2 enzymes, which oxidize part of the produced H_2. The H_2 content of strain MC4100 was reduced by 36% and 48% in the presence of 200 mM and 500 mM NaCl, respectively, while strain CP734 showed a similar reduction of 26% and 42% in the presence of 200 and 500 mM NaCl, respectively. This further supports the notion that H_2 oxidation, and hence the activity of the H_2-oxidizing enzymes, was not increased in response to NaCl. To verify whether the effect of Na^+ ions was specific, 200 mM K^+ ions were used instead and showed an identical reduction of the H_2 content by 35% and 22% for MC4100 and CP734, respectively. Therefore, the reduction was not specific for a particular cation. However, Na^+-transport was shown to be K^+ dependent in *E. coli*, albeit not by direct exchange but rather is H^+-antiport coupled [37]. This interconnection of the two cation transport systems could explain the similar effect of both cations.

Headspace H_2 derives from supplemented glucose given to the cells during growth, which is converted to formate as one of the products of mixed-acid fermentation. Elevated concentrations of 500 mM Na^+-ions reduced the amount of produced H_2 (Figure 6B). In order to identify the fate of the carbon, the formate concentration was determined. The cultures had reduced formate amounts by 35% and 29% for MC4100 and CP734, respectively (Figure 6C). Other key metabolites of the mixed acid fermentation like succinate and acetate were similarly reduced under high salt conditions (data not shown). At the same time, the growth of the cultures was reduced by only 15% and was therefore not the main reason for the reduced formate production. This result indicates that under high salt conditions formate is not accumulated because of FHL inhibition, but rather, more generally, the entire mixed-acid fermentation was reduced.
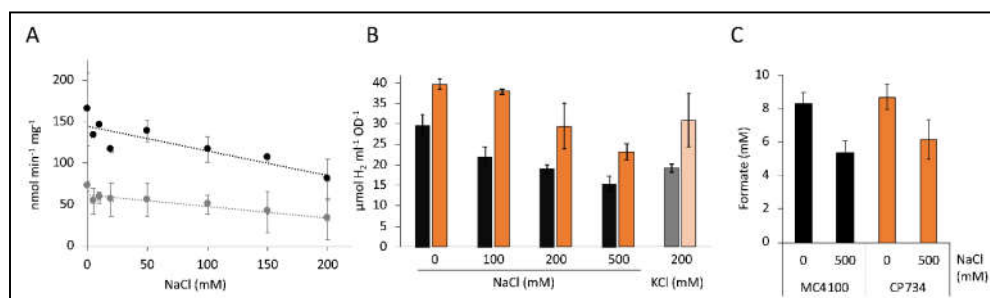
Figure 6. Effect of cations on H_2 production. Panel (**A**) shows the kinetic H_2 production rates of CP734 cells in the presence of different concentrations of NaCl (black dots) and in combination with 100 μM CCCP (gray dots). Reactions were initiated with 50 mM formate. Each point represents the average of two independent biological experiments with the respective standard deviation. The trend lines were calculated using linear regression. Panel (**B**) shows the H_2 content in the headspace of a 7 mL culture tube of MC4100 (black graphs) or CP734 (Δ*hyaB* Δ*hybC*, orange graphs) after anaerobic

overnight growth in M9-minimal medium with 0.8% (*w/v*) glucose in the presence of NaCl or KCl as indicated. (**C**) The formate concentration of cultures from panel B was quantified using HPLC, as described in the Materials and Methods section. All values represent the average of three independent biological replicates and their standard deviations.

2.6. The Na⁺ Ionophore EIPA Enhances CCCP Inhibition

The sodium concentration of the cell is maintained by Na^+/H^+ antiporters that reside in the cell membrane and also function in regulation of the intracellular pH. *E. coli* synthesizes three MRP-type antiporter proteins (NhaA, NhaB and ChaA), which are responsible for Na^+/H^+ exchange [38]. Intriguingly, this class of Na^+/H^+ antiporters is homologous to the HycC protein of the FHL membrane domain and to the NuoLMN (*E. coli* nomenclature) proteins, the proton-pumping subunits of the NADH-oxidizing complex I [39]. Some of these antiporters, especially those homologous subunits within the membrane domain of respiratory complex I, can be inhibited by EIPA (5-(*N*-ethyl-*N*-isopropyl)-amiloride) [40]. *Klebsiella pneumoniae* complex I was shown to translocate Na^+ ions instead of protons and some evidence for Na^+ translocation of *E. coli* complex I exists, but this might merely be a secondary effect [41,42]. In addition, in thermophilic organisms like *Thermococcus onnurineus*, energy conservation functions in an intricate mechanism that couples formate oxidation with concomitant H_2 production for the generation of a proton gradient. This proton gradient is subsequently converted into a Na^+ gradient by a Na^+/H^+-antiporter and then employed by a Na^+ ATPase for ATP synthesis [43].

Due to the observed reduction of H_2 production by NaCl, we tested the effect EIPA had on the H_2 production of FHL and found that, on its own or combined with 200 mM NaCl, the effects were negligible as described before [8]. Surprisingly, however, when EIPA and CCCP were given shortly after each other, they were able to inhibit H_2 production completely (Figure 7A). A similar effect was also determined for strain CP734 (Δ*hyaB* Δ*hybC*, Figure 7B); however, inhibition of H_2 production was not as complete as for MC4100. EIPA on its own also had no effect (Figure 7B). Notably, inhibition was also not complete for MC4100 when the reaction was started with formate instead of glucose (Figure 7C), and no effect was seen in strain CP734 (Δ*hyaB* Δ*hybC*) when formate was used to initiate the H_2 production (Figure 7D). This indicates that the activity of the Na^+/H^+ antiporter plays a crucial role during H_2 production from glucose. However, the MRP-type membrane subunit HycC of the FHL complex, which is essential for the reaction, is not inhibited by EIPA. Taken together, this could imply that a H^+ gradient is converted into a Na^+ gradient at the cell membrane during catalysis and that the FHL reaction couples both. Further experiments will be necessary to find the target of the ionophores.
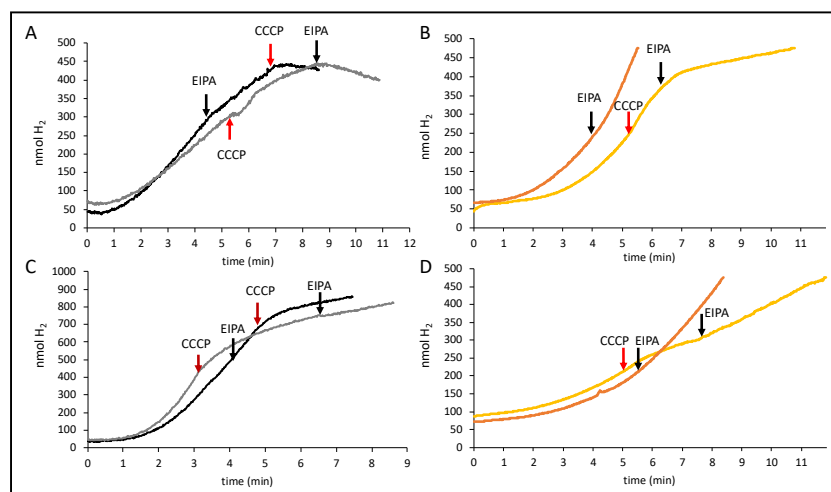
Figure 7. Effect of EIPA combination with CCCP. Cells of MC4100 (black, panels (**A**) and (**C**)) or CP734 (orange, panels (**B**) and (**D**)) were grown anaerobically in TGYEP, pH 6.5, and applied to the electrode

as described in the Materials and Methods section. The reaction was initiated with glucose (top panels (**A**) and (**B**)) or formate (bottom panels (**C**) and (**D**)). Where indicated, 50 μM CCCP (red arrows) or 50 μM EIPA (black arrows) were added to the reaction.

3. Materials and Methods

3.1. Strains and Growth Conditions

Strains are listed in Table 3. Strains CP630 and CP631 were constructed using P1*kc*-mediated phage transduction of the Δ*hyaB* and Δ*hybC* alleles of the Keio-collection strains JW0955 and JW2962, respectively, as described [44]. Strains were routinely grown aerobically in LB medium or on LB agar plates at 37 °C. For analysis of FHL activity, the strains were grown anaerobically as standing liquid cultures for 16 h in 50 mL TGYEP medium, pH 6.5 (1% (*w/v*) tryptone, 0.5% (*w/v*) yeast extract, 0.1 M potassium phosphate buffer, pH 6.5, 0.8% (*w/v*) glucose) at 30 °C [45]. Cultures for H_2 headspace and HPLC analyses were grown in phosphate-buffered M9-minimal medium supplemented with 0.8% (*w/v*) glucose as described [46]. When indicated, sterile solutions of NaCl or KCl were added. CCCP was used at 100 μM unless otherwise indicated. Cultures were harvested by centrifugation at 4000 g for 15 min at 4 °C, resuspended in 800 μL 50 mM Tris/HCl, pH 7.0, and kept on ice until further use.

Table 3. Strain list.

Strain	Genotype	Reference
MC4100	F⁻ *araD139* Δ(*argF-lac*)*U169* λ *rpsL150 relA1 deoC1 flhD5301* Δ(*fruK-yeiR*)*725*(*fruA25*), *rbsR22*, Δ(*fimB-fimE*)*632*(::IS*1*)	[47]
CP630	Like MC4100, but Δ*hyaB*	This study
CP631	Like MC4100, but Δ*hybC*	This study
CP734	Like MC4100, but Δ*hyaB* Δ*hybC*	[24]
HDK103	Like MC4100, but Δ*hyaB* Δ*hycA-I*	[48]

3.2. Enzymatic Assays

The kinetic activity of the FHL complex was determined on a modified Clark-type electrode equipped with an OXY/ECU module (Oxytherm, Hansatech Instruments, Norfolk, UK) to reverse the polarizing voltage to −0.7 V. A volume of 2 mL degassed 50 mM Tris/HCl buffer, pH 7.0, at 30 °C was added to the chamber prior to adding 50 μL of cell suspension. The reaction was started either with 50 mM formate or with 14 mM glucose. When the effect of sodium ions was studied, the ammonium salt of formate was used to initiate the reaction, which increased the pH by 0.02 units. The amount of H_2 was calibrated as described [49]. EC_{50} values were calculated with Origin Pro 2017G software (OriginLab, Northampton, MA, USA). The protein content of the respective cell suspensions was determined using the method of Lowry in a micro-scale assay [50]. Optical densities and spectra were recorded with a Tecan plate reader.

The H_2 content of the gas headspace of a 15-mL Hungate tube filled with 7 mL of culture was determined using gas chromatography with a GC2010 Plus Gas Chromatograph (Shimadzu, Kyõto, Japan) as described [39].

For the reverse FHL reaction, the cells were initially grown anaerobically in TGYEP, pH 6.5, for 16 h at 30 °C, harvested and resuspended in 50 mM Tris/HCl, pH 7.5. Cell suspensions were further mixed with different concentrations of CCCP, as indicated, and incubated under 2 atm pressure of H_2 and CO_2 1:1 mixture for 16 h at 37 °C. Cells were then removed by filtration through a 0.2 μM filter and supernatants applied to an HPLC system equipped with an Aminex HPX-87H column (Bio-Rad, Hercules, CA, USA), and formate concentrations were determined as previously described [8]. The culture supernatant was centrifuged and subsequently passed through a 0.2 μM filter prior to loading onto the HPLC system.

Calorimetric assays of FdhH activity and hydrogenase activity were carried out with crude extracts from anaerobically grown cells. The cells were harvested, sonicated for 2 min at 20 W with 0.5 sec pulses and briefly centrifuged. Anaerobic cuvettes were prepared containing 0.8 mL 50 mM

Tris/HCl buffer, pH 7.0, and 4 mM benzyl viologen. The FdhH reaction was started with 15 mM formate, and the hydrogenase reaction was started by adding crude extract to the cuvettes after exchange of the N_2 headspace with H_2. The signal at 600 nm was recorded, and an E_M value of 7400 M^{-1} cm^{-1} was assumed for reduced benzyl viologen. Data were derived from three independent biological replicates. Protein concentration was determined using the Lowry method [50].

4. Conclusions

The data presented here confirm CCCP-dependent inhibition of FHL activity. Here, we quantified this effect for the first time and saw striking differences depending on the presence of active H_2-oxidizing Hyd enzymes. The CCCP-dependent inhibition showed clearly that FHL did not contribute to proton translocation across the membrane, and in contrast, the data suggest it is driven by proton influx. Nevertheless, the data further highlight that the effect of CCCP might not be due to its protonophore activity but might rather be indirect, either by interacting with thiol groups within the complex or by disturbing the charge distribution at the membrane. The absence of an effect of another protonophore on the H_2 production further supports this finding. The sodium/potassium inhibition of the H_2 production showed that in order for it to function most effectively, the FHL complex requires low external cation concentrations. Our data clearly suggests that H_2 production couples H^+ influx with Na^+ efflux. However, evidence shows that it is not the MRP antiporter subunit HycC of the FHL complex that is directly involved, but rather it is the cation/H^+ antiport of the membrane that influences H_2 production.

References

1. Pinske, C. Bioenergetic aspects of archaeal and bacterial hydrogen metabolism. *Adv. Microb. Physiol.* **2019**, *74*, 487–514.
2. Lubek, D.; Simon, A.H.; Pinske, C. Amino acid variants of the HybB membrane subunit of *Escherichia coli* [NiFe]-hydrogenase-2 support a role in proton transfer. *FEBS Lett.* **2019**, *156*, 2194–2203.
3. Pinske, C.; Sawers, R.G. Anaerobic formate and hydrogen metabolism. *EcoSal Plus* **2016**, *7*, ESP-0011-2016.
4. Odom, J.M.; Peck, H.D. Hydrogen cycling as a general mechanism for energy coupling in the sulfate-reducing bacteria, *Desulfovibrio* sp. *FEMS Microbiol. Lett.* **1981**, *12*, 47–50.
5. Wiechmann, A.; Ciurus, S.; Oswald, F.; Seiler, V.N.; Müller, V. It does not always take two to tango: "Syntrophy" via hydrogen cycling in one bacterial cell. *ISME J.* **2020**, *14*, 1561–1570.
6. Sawers, R.G. Formate and its role in hydrogen production in *Escherichia coli*. *Biochem. Soc. Trans.* **2005**, *33*, 42–46.
7. Sauter, M.; Böhm, R.; Böck, A. Mutational analysis of the operon (*hyc*) determining hydrogenase 3 formation in *Escherichia coli*. *Mol. Microbiol.* **1992**, *6*, 1523–1532.
8. Pinske, C.; Sargent, F. Exploring the directionality of *Escherichia coli* formate hydrogenlyase: A membrane-bound enzyme capable of fixing carbon dioxide to organic acid. *Microbiologyopen* **2016**, *5*, 721–737.
9. Roger, M.; Brown, F.; Gabrielli, W.; Sargent, F. Efficient hydrogen-dependent carbon dioxide reduction by *Escherichia coli*. *Curr. Biol.* **2018**, *28*, 140–145.
10. Redwood, M.D.; Mikheenko, I.P.; Sargent, F.; Macaskie, L.E. Dissecting the roles of *Escherichia coli* hydrogenases in biohydrogen production. *FEMS Microbiol. Lett.* **2008**, *278*, 48–55.

11. Andrews, S.C.; Berks, B.C.; McClay, J.; Ambler, A.; Quail, M.A.; Golby, P.; Guest, J.R. A 12-cistron *Escherichia coli* operon (*hyf*) encoding a putative proton-translocating formate hydrogenlyase system. *Microbiology* **1997**, *143*, 3633–3647.

12. Böhm, R.; Sauter, M.; Böck, A. Nucleotide sequence and expression of an operon in *Escherichia coli* coding for formate hydrogenlyase components. *Mol. Microbiol.* **1990**, *4*, 231–243.

13. Marreiros, B.C.; Batista, A.P.; Duarte, A.M.S.; Pereira, M.M. A missing link between complex I and group 4 membrane-bound [NiFe] hydrogenases. *Biochim. Biophys. Acta* **2012**, *1827*, 198–209.

14. Welte, C.; Krätzer, C.; Deppenmeier, U. Involvement of Ech hydrogenase in energy conservation of *Methanosarcina mazei*. *FEBS J.* **2010**, *277*, 3396–3403.

15. McDowall, J.S.; Murphy, B.J.; Haumann, M.; Palmer, T.; Armstrong, F.A.; Sargent, F. Bacterial formate hydrogenlyase complex. *Proc. Natl. Acad. Sci. USA* **2014**, *111*, E3948–E3956.

16. Sokol, K.P.; Robinson, W.E.; Oliveira, A.R.; Zacarias, S.; Lee, C.-Y.; Madden, C.; Bassegoda, A.; Hirst, J.; Pereira, I.A.C.; Reisner, E. Reversible and selective interconversion of hydrogen and carbon dioxide into formate by a semiartificial formate hydrogenlyase mimic. *J. Am. Chem. Soc.* **2019**, *141*, 17498–17502.

17. Bagramyan, K.A.; Martirosov, S.M. Formation of an ion transport supercomplex in *Escherichia coli*. An experimental model of direct transduction of energy. *FEBS Lett.* **1989**, *246*, 149–152.

18. Babu, M.; Bundalovic-Torma, C.; Calmettes, C.; Phanse, S.; Zhang, Q.; Jiang, Y.; Minic, Z.; Kim, S.; Mehla, J.; Gagarinova, A.; et al. Global landscape of cell envelope protein complexes in *Escherichia coli*. *Nat. Biotechnol.* **2018**, *36*, 103–112.

19. Trchounian, A.; Sawers, R.G. Novel insights into the bioenergetics of mixed-acid fermentation: Can hydrogen and proton cycles combine to help maintain a proton motive force? *IUBMB Life* **2014**, *66*, 1–7.

20. Doberenz, C.; Zorn, M.; Falke, D.; Nannemann, D.; Hunger, D.; Beyer, L.; Ihling, C.H.; Meiler, J.; Sinz, A.; Sawers, R.G. Pyruvate formate-lyase interacts directly with the formate channel FocA to regulate formate translocation. *J. Mol. Biol.* **2014**, *426*, 2827–2839.

21. Beyer, L.; Doberenz, C.; Falke, D.; Hunger, D.; Suppmann, B.; Sawers, R.G. Coordination of FocA and pyruvate formate-lyase synthesis in *Escherichia coli* demonstrates preferential translocation of formate over other mixed-acid fermentation products. *J. Bacteriol.* **2013**, *195*, 1428–1435.

22. Hakobyan, M.; Sargsyan, H.; Bagramyan, K. Proton translocation coupled to formate oxidation in anaerobically grown fermenting *Escherichia coli*. *Biophys. Chem.* **2005**, *115*, 55–61.

23. Mayer, C.; Boos, W. Hexose/Pentose and Hexitol/Pentitol Metabolism. *EcoSal Plus* **2005**, *1*, 1.

24. Pinske, C.; Krüger, S.; Soboh, B.; Ihling, C.; Kuhns, M.; Braussemann, M.; Jaroschinsky, M.; Sauer, C.; Sargent, F.; Sinz, A.; et al. Efficient electron transfer from hydrogen to benzyl viologen by the [NiFe]-hydrogenases of *Escherichia coli* is dependent on the coexpression of the iron-sulfur cluster-containing small subunit. *Arch. Microbiol.* **2011**, *193*, 893–903.

25. Laurinavichene, T.V.; Tsygankov, A.A. H_2 consumption by *Escherichia coli* coupled via hydrogenase 1 or hydrogenase 2 to different terminal electron acceptors. *FEMS Microbiol. Lett.* **2001**, *202*, 121–124.

26. Sawers, R.G.; Ballantine, S.; Boxer, D. Differential expression of hydrogenase isoenzymes in *Escherichia coli* K-12: Evidence for a third isoenzyme. *J. Bacteriol.* **1985**, *164*, 1324–1331.

27. Pinske, C.; Jaroschinsky, M.; Linek, S.; Kelly, C.L.; Sargent, F.; Sawers, R.G. Physiology and bioenergetics of [NiFe]-hydrogenase 2-catalyzed H_2-consuming and H_2-producing reactions in *Escherichia coli*. *J. Bacteriol.* **2015**, *197*, 296–306.

28. Laurinavichene, T.V.; Zorin, N.A.; Tsygankov, A.A. Effect of redox potential on activity of hydrogenase 1 and hydrogenase 2 in *Escherichia coli*. *Arch. Microbiol.* **2002**, *178*, 437–442.

29. Kuniyoshi, T.M.; Balan, A.; Schenberg, A.C.G.; Severino, D.; Hallenbeck, P.C. Heterologous expression of proteorhodopsin enhances H_2 production in *Escherichia coli* when endogenous Hyd-4 is overexpressed. *J. Biotechnol.* **2015**, *206*, 52–57.

30. Ridgway, H.F. Source of energy for gliding motility in *Flexibacter polymorphus*: Effects of metabolic and respiratory inhibitors on gliding movement. *J. Bacteriol.* **1977**, *131*, 544–556.

31. Šturdík, E.; Antalík, M.; Sulo, P.; Baláž, Š.; Ďurčová, E.; Drobnica, Ľ. Relationships among structure, reactivity towards thiols and basicity of phenylhydrazonopropanedinitriles. *Collect. Czechoslov. Chem. Commun.* **1985**, *50*, 2065–2076.

32. Gevorgyan, H.; Trchounian, A.; Trchounian, K. Formate and potassium ions affect *Escherichia coli* proton ATPase activity at low pH during mixed carbon fermentation. *IUBMB Life* **2020**, *72*, 915–921.

33. Akiyama, Y. Proton-motive force stimulates the proteolytic activity of FtsH, a membrane-bound ATP-dependent protease in Escherichia coli. *Proc. Natl. Acad. Sci. USA* **2002**, *99*, 8066–8071.

34. Rossmann, R.; Sawers, R.G.; Böck, A. Mechanism of regulation of the formate-hydrogenlyase pathway by oxygen, nitrate, and pH: Definition of the formate regulon. *Mol. Microbiol.* **1991**, *5*, 2807–2814.

35. Bagramyan, K.; Mnatsakanyan, N.; Poladian, A.; Vassilian, A.; Trchounian, A. The roles of hydrogenases 3 and 4, and the F_0F_1-ATPase, in H_2 production by *Escherichia coli* at alkaline and acidic pH. *FEBS Lett.* **2002**, *516*, 172–178.

36. Kashket, E.R. Effects of K^+ and Na^+ on the proton motive force of respiring *Escherichia coli* at alkaline pH. *J. Bacteriol.* **1985**, *163*, 423–429.

37. Verkhovskaya, M.L.; Verkhovsky, M.I.; Wikström, M. K^+-dependent Na^+ transport driven by respiration in *Escherichia coli* cells and membrane vesicles. *Biochim. Biophys. Acta* **1996**, *1273*, 207–216.

38. Padan, E.; Landau, M. Sodium-proton (Na^+/H^+) antiporters: Properties and roles in health and disease. *Met. Ions Life Sci.* **2016**, *16*, 391–458.

39. Friedrich, T.; Scheide, D. The respiratory complex I of bacteria, archaea and eukarya and its module common with membrane-bound multisubunit hydrogenases. *FEBS Lett.* **2000**, *479*, 1–5.

40. Steuber, J. The *C*-terminally truncated NuoL subunit (ND5 homologue) of the Na^+-dependent complex I from *Escherichia coli* transports Na^+. *J. Biol. Chem.* **2003**, *278*, 26817–26822.

41. Steuber, J.; Schmid, C.; Rufibach, M.; Dimroth, P. Na^+ translocation by complex I (NADH:quinone oxidoreductase) of *Escherichia coli. Mol. Microbiol.* **2000**, *35*, 428–434.

42. Stolpe, S.; Friedrich, T. The *Escherichia coli* NADH:ubiquinone oxidoreductase (complex I) is a primary proton pump but may be capable of secondary sodium antiport. *J. Biol. Chem.* **2004**, *279*, 18377–18383.

43. Kim, Y.J.; Lee, H.S.; Kim, E.S.; Bae, S.S.; Lim, J.K.; Matsumi, R.; Lebedinsky, A.V.; Sokolova, T.G.; Kozhevnikova, D.A.; Cha, S.-S.; et al. Formate-driven growth coupled with H_2 production. *Nature* **2010**, *467*, 352–355.

44. Baba, T.; Ara, T.; Hasegawa, M.; Takai, Y.; Okumura, Y.; Baba, M.; Datsenko, K.; Tomita, M.; Wanner, B.; Mori, H. Construction of *Escherichia coli* K-12 in-frame, single-gene knockout mutants: The Keio collection. *Mol. Syst. Biol.* **2006**, *2*, 2006.0008.

45. Begg, Y.A.; Whyte, J.N.; Haddock, B.A. The identification of mutants of *Escherichia coli* deficient in formate dehydrogenase and nitrate reductase activities using dye indicator plates. *FEMS Microbiol. Lett.* **1977**, *2*, 47–50.

46. Sambrook, J.; Russell, D. *Molecular Cloning: A Laboratory Manual*, 3rd ed.; Cold Spring Harbor Laboratory Press: Cold Spring Harbor, NY, USA, 2001.

47. Casadaban, M.J. Transposition and fusion of the *lac* genes to selected promoters in *Escherichia coli* using bacteriophage lambda and Mu. *J. Mol. Biol.* **1976**, *104*, 541–555.

48. Jacobi, A.; Rossmann, R.; Böck, A. The *hyp* operon gene products are required for the maturation of catalytically active hydrogenase isoenzymes in *Escherichia coli*. *Arch. Microbiol.* **1992**, *158*, 444–451.

49. Sargent, F.; Stanley, N.R.; Berks, B.C.; Palmer, T. Sec-independent protein translocation in *Escherichia coli*. A distinct and pivotal role for the TatB protein. *J. Biol. Chem.* **1999**, *274*, 36073–36082.

50. Lowry, O.; Rosebrough, N.; Farr, A.; Randall, R. Protein measurement with the Folin phenol reagent. *J. Biol. Chem.* **1951**, *193*, 265–275.

Kapitel IV – Funktion des *C*-terminalen Peptides

Eingrenzung der Funktion der *C*-terminalen Verlängerung des Vorläufers der *Escherichia coli* [NiFe]-Hydrogenase 2 großen Untereinheit

Constanze Pinske, Claudia Thomas, Kerstin Nutschan und R. Gary Sawers *

Institut für Biologie/Mikrobiologie, Martin-Luther-Universität Halle-Wittenberg, 06108 Halle, Deutschland, Kurt-Mothes-Str. 3, 06120 Halle/Saale, Deutschland

* Korrespondierender Autor: Gary Sawers

Zusammenfassung:

Das aktive Zentrum aller [NiFe]-Hydrogenasen (Hyd) hat einen Bimetall-NiFe(CN)$_2$CO-Cofaktor, welcher die gemeinsame Funktion mehrerer Reifungsproteine für seine Biosynthese und Insertion in die Vorläuferform der großen Untereinheit des Enzyms erfordert. Die Cofaktorinsertion ist ein komplizierter und kontrollierter Prozess. Die große Untereinheit fast aller Hyd-Enzyme weist hierbei eine *C*-terminale Oligopeptid-Verlängerung auf, die als letzter Reifungsschritt endoproteolytisch abgespalten wird. Dieses Peptid könnte entweder als eines der Erkennungsmotive für die Endoprotease dienen, als Interaktionsfläche für die Reifungsproteine fungieren oder eine strukturelle Rolle spielen, um sicherzustellen, dass die Kavität des aktiven Zentrums offenbleibt bis der [NiFe]-Kofaktor inseriert wird. Um zwischen diesen Hypothesen zu unterscheiden, tauschten wir das vollständige *C*-terminale Peptid des Vorläufers der *Escherichia coli*-Hydrogenase 2 (Hyd-2) gegen die *C*-terminale Verlängerung des Hyd-1-Enzyms aus. Mittels Gel-Aktivitätsfärbung wurde deutlich, dass dieser Vorläufer einer großen Untereinheit trotz des *C*-terminalen Austauschs seine Spezifität für das HybG-Reifungs-Chaperon sowie für die Pro-HybC-spezifische Endoprotease HybD beibehält. *Bacterial-two-hybrid* Interaktions-Studien bestätigten diese Wechselwirkung zwischen HybD und der Pro-HybC-Variante mit ausgetauschtem *C*-Terminus. Limitierte Proteolysestudien des gereinigten Vorläufers und des reifen HybC-Proteins zeigten, dass das reife Protein im Gegensatz zum Vorläufer Proteolysestabil (Trypsin) war, was auf eine wesentliche Konformationsänderung des Proteins hinweist. Zusammengenommen unterstützen die Ergebnisse ein Modell, bei dem die Funktion des *C*-terminalen Peptides während der Reifung der Untereinheit strukturell ist.

Delimiting the Function of the C-Terminal Extension of the *Escherichia coli* [NiFe]-Hydrogenase 2 Large Subunit Precursor

Constanze Pinske, Claudia Thomas†, Kerstin Nutschan and R. Gary Sawers*

Institute of Microbiology, Martin-Luther University Halle-Wittenberg, Halle (Saale), Germany

The active site of all [NiFe]-hydrogenases (Hyd) has a bimetallic $NiFe(CN)_2CO$ cofactor that requires the combined action of several maturation proteins for its biosynthesis and insertion into the precursor form of the large subunit of the enzyme. Cofactor insertion is an intricately controlled process, and the large subunit of almost all Hyd enzymes has a C-terminal oligopeptide extension that is endoproteolytically removed as the final maturation step. This extension might serve either as one of the recognition motifs for the endoprotease, as well as an interaction platform for the maturation proteins, or it could have a structural role to ensure the active site cavity remains open until the cofactor is inserted. To distinguish between these alternatives, we exchanged the complete C-terminal extension of the precursor of *Escherichia coli* hydrogenase 2 (Hyd-2) for the C-terminal extension of the Hyd-1 enzyme. Using in-gel activity staining, we demonstrate clearly that this large subunit precursor retains its specificity for the HybG maturation chaperone, as well as for the pro-HybC-specific endoprotease HybD, despite the C-terminal exchange. Bacterial two-hybrid studies confirmed interaction between HybD and the pro-HybC variant carrying the exchanged C-terminus. Limited proteolysis studies of purified precursor and mature HybC protein revealed that, in contrast to the precursor, the mature protein was protected against trypsin attack, signifying a major conformational change in the protein. Together, our results support a model whereby the function of the C-terminal extension during subunit maturation is structural.

Keywords: hydrogenase, Hyp proteins, large-subunit precursor, protein interaction, protease, maturation

INTRODUCTION

A still unresolved issue on the maturation pathway of the catalytic, or large, subunit of [NiFe]-hydrogenases (Hyd) is what role the C-terminal oligopeptide extension plays during the maturation process: Does it act as a recognition motif allowing interaction with maturation proteins, or does it function as a form of "intra-molecular" chaperone that constrains the large subunit precursor in a conformation allowing access of the maturation machinery, which then interacts elsewhere on the protein? Or does it do both?

With the exception of the large subunit of sensory and Ech hydrogenases (Theodoratou et al., 2005), the final step in the maturation process of the large subunit involves endoproteolytic cleavage of an approximately 15-amino acid-long oligopeptide from the C-terminus of the protein (Gollin et al., 1992; Menon et al., 1993; Rossmann et al., 1994; Böck et al., 2006). Proteolytic cleavage of the precursor of the large subunit is an exquisitely controlled process and only occurs after insertion of the bimetallic NiFe-cofactor has been completed (Böck et al., 2006; Sawers and Pinske, 2017). The NiFe-cofactor is coordinated within the active site by four conserved cysteinyl thiolates (henceforth referred to as Cys1–4), two of which are located N-terminally (Cys1–2) and the other two (Cys3–4) are close to the ultimate C-terminus of the protein (see **Figure 1**; Magalon and Böck, 2000).

Having been constructed on the HypCDEF protein scaffold complex (Böck et al., 2006; Sawers and Pinske, 2017), the Fe(CN)$_2$CO moiety of the cofactor is the first component to be delivered to the precursor, probably by the HypC protein. In bacteria synthesizing more than one Hyd, paralogues of HypC exist, e.g., HybG in *Escherichia coli*, and these paralogues deliver the Fe(CN)$_2$CO moiety to a specific Hyd enzyme (Blokesch et al., 2001). Only after the Fe group has been delivered and coordinated by the Cys residues 1 and 2, can nickel be delivered by the combined actions of the HypAB and SlyD proteins (Lacasse and Zamble, 2016). The nickel is initially coordinated by Cys-3 (**Figure 1A**). Nickel is the template recognized by the specific endoprotease (Theodoratou et al., 2000a) and cleavage occurs between the conserved His and Val residues, which are located three and four amino acid residues, respectively, C-terminal to the Cys-4 residue that

coordinates the cofactor (**Figure 1A**). Based on the concept of Schechter and Berger (1967) and Hedstrom (2002), these two positions of a peptide (P1 and P1′) determine the specificity of the protease. Notably, however, the Hyb endoprotease cannot be classified either as a metallo- or as a serine-protease (Rossmann et al., 1995; Sawers, 2012). Proteolytic removal of the C-terminal oligopeptide causes a conformational switch in the complete protein bringing the Cys-4 residue (**Figures 1A,C**) into coordination distance to bridge both metals and "fix" the cofactor firmly within the active site (Magalon and Böck, 2000; Böck et al., 2006; Kwon et al., 2018).

The recently determined crystal structure of the HyhL large subunit precursor of the Hyd enzyme from the hyperthermophilic archaeon *Thermococcus kodakarensis* in complex with the nickel delivery protein HypA provided an initial indication that the presence of the C-terminal extension causes significant displacement of Cys-4 from the other three coordinating Cys residues, leaving the active site accessible for cofactor delivery (Kwon et al., 2018). Moreover, HypA was shown to bind at a flexible region of the large subunit near the N-terminus, suggesting that the C-terminus is not involved in binding maturation proteins.

Our model system to study the role of the C-terminal extension in maturation is the large subunit, HybC, of *E. coli* Hyd-2. Hyd-2 enzyme activity is readily detectable and an array of available mutants makes this system highly amenable to analysis of the maturation process (Pinske et al., 2015; Thomas et al., 2015). Moreover, the recently determined crystal structure of the enzyme reveals that the mature HybC subunit has a compact and characteristic oxidoreductase fold common to many hydrogenases (Beaton et al., 2018).
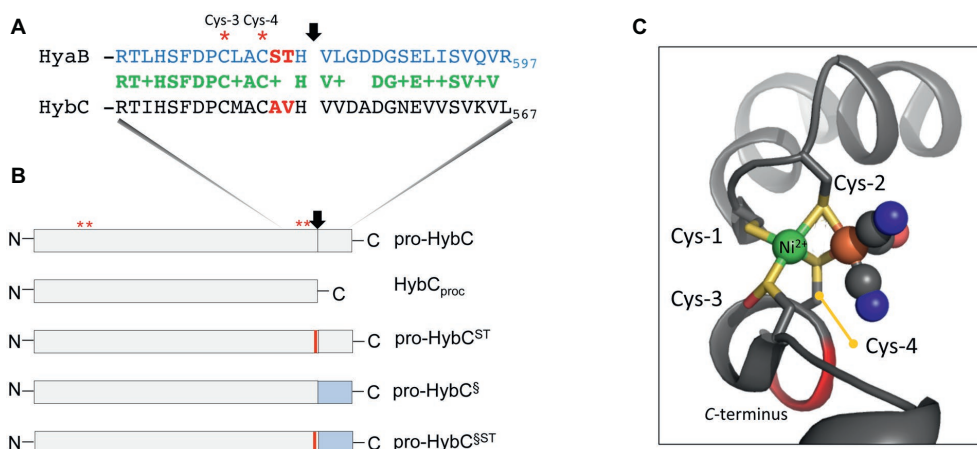
FIGURE 1 | Schematic representation of the HybC large subunit variants. **(A)** The amino acid sequences in single-letter code of the C-terminal 30 residues of the large subunit pro-HybC and pro-HyaB precursors are shown. Identical amino acids are shown in green, the + indicates similar amino acids and the residues depicted in red signify those exchanged in this study. The vertical arrow indicates the site of endoproteolytic cleavage and the red asterisks signify the conserved Cys-3 and Cys-4 residues involved in coordinating the Ni-Fe-cofactor. **(B)** The HybC variants used in this study (not drawn to scale) are shown, as is the location of the sequence represented in part **(A)**. N and C represent N- and C-terminus of the polypeptides, respectively. The thin red bar indicates that A and V were changed to S and T, and the blue rectangle signifies that the 15-amino acid extension (after the cleavage site) from pro-HyaB replaced the native oligopeptide. The red asterisks depict the approximate locations of the four conserved Cys residues (1–4) that coordinate the NiFe-cofactor. **(C)** The structural organization of the Cys-1 through Cys-4 and how they coordinate the NiFe(CN)$_2$CO group in HybC (Beaton et al., 2018) is shown for the reduced enzyme (6EHS). The representation was generated using PyMOL. The green sphere represents the nickel and the large brown sphere the iron ion, where the cyanyl (black and blue spheres) and carbonyl (black and red spheres) ligands are coordinated.

HybG, a HypC paralogue, is specifically required for maturation of pro-HybC (Blokesch et al., 2001), the precursor, or proprotein, form of HybC and interacts with this polypeptide, but not with the processed form of the protein HybC$_{proc}$ (Thomas et al., 2015; Senger et al., 2017). HybC$_{proc}$ is a genetically generated variant of pro-HybC (**Figure 1B**) that lacks the 15-amino acid C-terminal extension normally removed by the HybC-specific endoprotease HybD *in vivo* (Fritsche et al., 1999; Theodoratou et al., 2005; Sawers, 2012). Preliminary studies carried out by our group have indicated that when the terminal 15 amino acids present on pro-HybC are exchanged for those of the *E. coli* Hyd-1 large subunit precursor, pro-HyaB (see **Figure 1B**), cleavage of the hybrid proprotein retains its specificity for the HybD endoprotease and does not become dependent on HyaD, the pro-HyaB-specific endoprotease (Thomas et al., 2015). An alignment of the C-terminal regions of pro-HybC and pro-HyaB reveals that the 15-amino acid extension of both proteins shares 7 conserved and 5 similar amino acid residues (**Figure 1A**). Overlooked in the initial study by Thomas et al. (2015) were the two amino acid residues immediately adjacent to Cys-4, which are AV in HybC and ST in HyaB (**Figure 1A**). These residues locate to the P2 and P3 positions that still have a significant impact on protease recognition (Schechter and Berger, 1967; Hedstrom, 2002). Because of the important role played by Cys-4 in coordinating the NiFe-cofactor (Magalon and Böck, 2000) and the significant displacement of this residue revealed by the crystal structure of immature HyhL (Kwon et al., 2018), this suggests a potentially significant role for residues A-550 and V-551 in the recognition of the precursor by hydrogenase maturation proteins. We therefore decided to analyze whether these two amino acid residues act as determinants in the recognition of pro-HybC by either HybG or HybD. Our findings indicate that, in contrast to the latter suggestion, the complete C-terminal extension behind the final cysteinyl residue coordinating the cofactor functions solely to constrain pro-HybC in a conformation appropriate for interaction with the maturation machinery.

MATERIALS AND METHODS

Strains and Growth Conditions

The strains listed in **Table 1** were used in this study. All growth experiments involving the analysis of in-gel hydrogenase enzyme activity were performed anaerobically in M9 minimal medium (Sambrook et al., 1989) supplemented with 0.1 mM CaCl$_2$, 0.1 mM thiamin dichloride, and trace element solution SLA (Hormann and Andreesen, 1989) at 37°C in Hungate tubes under a nitrogen gas atmosphere as described (Thomas et al., 2015). The carbon source was glucose (0.8% w/v). For routine cloning experiments, strains were grown on LB-agar plates or in LB-broth at 37°C (Miller, 1972). When required, the antibiotics ampicillin, kanamycin, or chloramphenicol were added to a final concentration of 100, 50, or 25 μg ml^{-1}, respectively. Cells were harvested by centrifugation at 5,000 *g* for 15 min at 4°C when cultures had reached an OD$_{600\,nm}$ of between 0.8 and 1.2. Cell pellets were either used immediately or stored at −20°C until use.

TABLE 1 | Strains and plasmids used in this study.

Strain or plasmid	Relevant genotype or characteristic(s)	Reference or source
Strain		
BTH101	F$^-$, *cya*-99, *araD*139, *galE*15, *galK*16, *rpsL*1(Str^R), *hsdR*2, *mcrA*1, *mcrB*1	Karimova et al., 1998
MC4100	F$^-$ *araD*139 (*argF-lac*)U169 *ptsF*25 *deoC*1 *relA*1 *flbB*5301 *rspL*150	Casadaban, 1976
FTD150	As MC4100, but Δ*hyaB* Δ*hybC* Δ*hycE* Δ*hyfB-R*	Redwood et al., 2008
CB16	As FTD150, but *hyaB*$^+$ Δ*hyaD*::Kan^R	Thomas et al., 2015
CB17	As FTD150, but *hybC*$^+$ Δ*hybD*::Kan^R	This study
CB18	As FTD150, but *hybC*$^+$ Δ*hybG*::Kan^R	This study
CB19	As FTD150, but *hycE*$^+$ Δ*hypC*::Kan^R	This study
Plasmids		
pASK-hybC	*hybC* in pASK-IBA5$^+$, Amp^R	Pinske et al., 2011
pASK-hybC$_{proc}$	pASK-hybC, V553 Stop (codon 553 converted to TAA), Amp^R	Thomas et al., 2015
pASK-hybC^{hyaB}	*hybC* with *hyaB* C-Terminus in pASK-IBA5$^+$, Amp^R; product designated pro-HybC§	Thomas et al., 2015
pASK-hybCST	*hybC* with AV changed to ST in pASK-IBA5$^+$, Amp^R; product designated pro-HybCST	This study
pASK-hybC^{hyaBST}	*hybC* with *hyaB* C-Terminus and AV changed to ST in pASK-IBA5$^+$, Amp^R; product designated pro-HybC^{§ST}	This study
pASK-hybG	*hybG* in pASK-IBA3, carries a C-terminal Strep-tag; Amp^R	Soboh et al., 2013
pCB-hybC	pCAN-hybC (Kitagawa et al., 2005) with a TAA at codon 568 in *hybC*, producing His-pro-HybC; Cm^R	This study
pCB-hybC$_{proc}$	pCAN-hybC with a TAA at codon 553 (GTA → TAA) in *hybC*, producing His-HybC$_{proc}$; Cm^R	This study
pUT18	Bacterial two hybrid plasmid expressing the T18 fragment and a MCS at the 5′ end of T18, Amp^R	Karimova et al., 1998
pKT25	Bacterial two hybrid plasmid expressing the T25 fragment and a MCS at the 3′ end of T25, Cm^R	Karimova et al., 1998
pT18-zip	pUT18, Leucine zipper fused to T18 fragment (225-399 amino acids of CyaA)	Karimova et al., 1998
pT25-zip	pKT25, Leucine zipper fused to T25 fragment (1-224 amino acids of CyaA)	Karimova et al., 1998

(Continued)

TABLE 1 | Continued

Strain or plasmid	Relevant genotype or characteristic(s)	Reference or source
pT18-hybD	pUT18, hybD⁺, Amp^R	This study
pT25-hybC	pKT25, hybC⁺, Cm^R	This study
pT25-hybC§	pKT25, hybC with hyaB C-terminus, Cm^R	This study
pT25-hybC^ST	pKT25, hybC⁺ including the AV550ST exchange, Cm^R	This study
pT25-hybC§ST	pKT25, hybC with hyaB C-terminus and including the AV550ST exchange, Cm^R	This study
pT25-hyaB	pKT25, hyaB⁺, Cm^R	This study
pT25-hyaB§	pKT25, hyaB with hybC C-terminus, Cm^R	This study
pT-hypC	pT7–7 hypC⁺, HypC carries a Cterminal Strep-tag, Amp^R	Soboh et al., 2013

Plasmid and Strain Construction

Amino acid exchanges of the A550S and V551 T (numbers are based on untagged protein) were introduced simultaneously in *hybC* using the NEBase changer method (NEB, USA). The templates used were the plasmids pASK-hybC (Pinske et al., 2011) and pASK-hybC^hyaB (Thomas et al., 2015). The oligonucleotides used were wtHybC_AV>ST_FW with HybC_AV>ST_RW for the pASK-hybC plasmid and HybC/HyaB_AV>ST_FW with HybC_AV>ST_RW for the pASK-hybC^hyaB plasmid (**Table 2**). The stop codons introduced into *hybC* in pCAN-hybC (**Table 1**; Kitagawa et al., 2005) to generate pCB-hybC and pCB-hybC_proc (see **Table 1**) were done using PCR mutagenesis with pCAN-hybC as DNA template and the oligonucleotides described previously (Thomas et al., 2015).

Plasmids for the bacterial-two-hybrid analysis were constructed by using either the large subunit variants as template or, for the *hybD* gene, chromosomal DNA as template. The genes were amplified with Q5 polymerase (NEB, USA) using the appropriate combination of oligonucleotides (**Table 2**), and PCR fragments were subsequently digested with PstI and BamHI for the large subunits or with HindIII and EcoRI for *hybD* and ligated into the bacterial two hybrid vectors pKT25 or pUT18 (Karimova et al., 1998), which had been previously digested with the same respective enzyme combinations. The authenticity of all constructs was verified by DNA sequencing.

E. coli strains were constructed using P1*kc*-mediated phage transduction (Miller, 1972) to introduce the respective defined deletion mutation in *hypC* or *hybG* from the appropriate donor strain of the Keio collection (Baba et al., 2006).

Preparation of Crude Cell Extracts, Non-denaturing Polyacrylamide Gel Electrophoresis, and Hydrogenase Activity-Staining

Crude cell extracts were prepared anaerobically as described (Pinske et al., 2012). Determination of protein concentration was done as described (Lowry et al., 1951). Non-denaturing

TABLE 2 | Oligonucleotides used in this study.

Oligonucleotide	Sequence 5′ → 3′
wtHybC_AV>ST_FW	CATGGCCTGTTCAACACACGTAGTGGATG
HybC/HyaB_AV>ST_FW	CATGGCCTGTTCAACACACGTGCTGG
HybC_AV>ST_RW	CACGGGTCAAAGGAGTGA
HyaB_FW_PstI	GCGCTGCAGGGAGCACTCAGTACGAAACTC
HyaB_RW_BamHI	GCGGGATCCTTAACGCACCTGCACGGAGATC
HybC_FW_PstI	GCGCTGCAGGGAGCCAGAGAATTACTATTG
HybC_RW_BamHI	GCGGGATCCTTACAGAACCTTCACTGAAAC
HybD_FW_HindIII	GCGAAGCTTATGCGTATTTTAGTCTTAGG
HybD_RW_EcoRI	GCGGAATTCGAGTCATGAATCGCCTCCCGTG
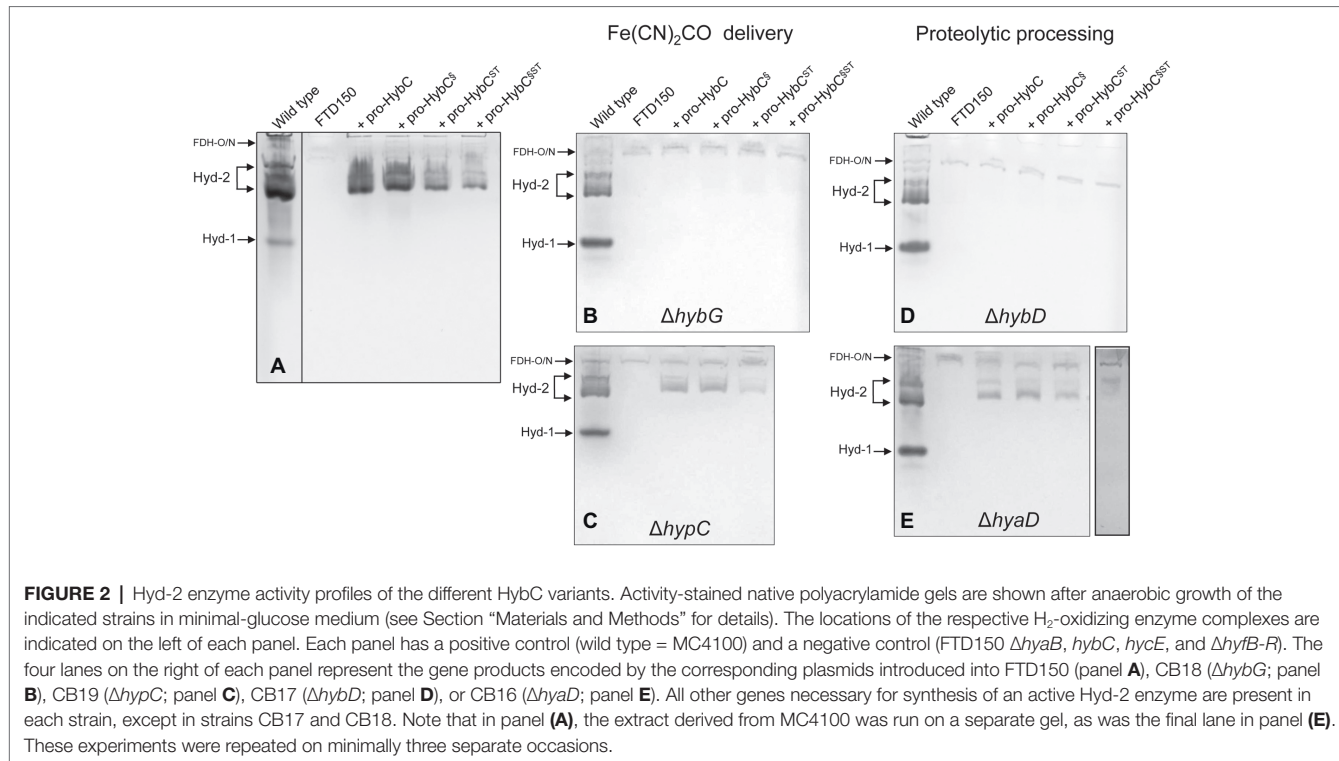
polyacrylamide gel electrophoresis (PAGE) was performed anaerobically. Separating gels included 0.1% (w/v) Triton X-100 as described (Ballantine and Boxer, 1985). Crude extracts were incubated with a final concentration of 4% (w/v) Triton X-100 prior to application (usually 50 μg of protein) to the gel, which included 6% (w/v) polyacrylamide. Hydrogenase activity-staining was done in 50 mM MOPS buffer pH 7.0, as described (Pinske et al., 2012) and included 0.5 mM BV and 1 mM 2,3,5-triphenyltetrazolium chloride (TTC). Gels were incubated under an atmosphere of 100% hydrogen gas.

Purification and Limited Proteolysis of Pro-HybC and HybC_proc

N-terminally His-tagged HybC variants were purified after overproduction in strain CB17 (**Table 1**) by metal-affinity chromatography using cobalt-charged TALON® superflow resin (Clontech Laboratories Inc., USA). A column containing 1 ml bed-volume of resin was pre-equilibrated with 10 ml of anaerobic buffer A (50 mM Tris–HCl, pH 8, 300 mM NaCl) followed by application of filtered (0.45 μm sterile filter, Sartorius), anaerobically prepared crude extract (typically 5 ml, 10 mg ml⁻¹ protein) containing the His-tagged protein at a flow rate of 1 ml min⁻¹. Unbound proteins were washed from the column with 10–15 column volumes of buffer A, followed by a washing step (3 column volumes) using buffer A containing 30 mM imidazole. Bound, His-tagged proteins were eluted with buffer A containing 300 mM imidazole. After elution, pooled eluate containing the purified protein(s) of interest was buffer-exchanged into buffer C (25 mM Tris-HCl, pH 8, 150 mM NaCl) using a Sephadex PD-10 column (GE Healthcare, Germany).

Aliquots (100 μg) of pro-HybC or HybC_proc (both N-terminally His-tagged) in a 100 μl reaction volume of 200 mM HEPES pH 7.8 containing 200 mM NaCl and 40 mM CaCl₂ were incubated with 1 μg of trypsin or chymotrypsin and 10 μl aliquots were removed at the indicated times and immediately added to boiling SDS buffer to terminate the reaction. Polypeptides were separated in denaturing SDS-PAGE (Laemmli, 1970) containing 12.5% (w/v) polyacrylamide. Gels were subsequently stained with Coomassie Brilliant Blue.

C-terminally Strep-tagged HypC and HybG were purified as described in Soboh et al. (2011, 2013). Aliquots of 50 μg were used in limited proteolysis experiments.

- 71 -

FIGURE 2 | Hyd-2 enzyme activity profiles of the different HybC variants. Activity-stained native polyacrylamide gels are shown after anaerobic growth of the indicated strains in minimal-glucose medium (see Section "Materials and Methods" for details). The locations of the respective H_2-oxidizing enzyme complexes are indicated on the left of each panel. Each panel has a positive control (wild type = MC4100) and a negative control (FTD150 $\Delta hyaB$, $hybC$, $hycE$, and $\Delta hyfB$-R). The four lanes on the right of each panel represent the gene products encoded by the corresponding plasmids introduced into FTD150 (panel **A**), CB18 ($\Delta hybG$; panel **B**), CB19 ($\Delta hypC$; panel **C**), CB17 ($\Delta hybD$; panel **D**), or CB16 ($\Delta hyaD$; panel **E**). All other genes necessary for synthesis of an active Hyd-2 enzyme are present in each strain, except in strains CB17 and CB18. Note that in panel **(A)**, the extract derived from MC4100 was run on a separate gel, as was the final lane in panel **(E)**. These experiments were repeated on minimally three separate occasions.

Analysis of Protein Interactions Using the Bacterial Two-Hybrid System

These experiments were performed as described by Pinske (2018). Briefly, growth of strain BTH101 (Karimova et al., 1998) transformed with two compatible BTH plasmids was performed under anaerobic conditions in TGYEP medium (1% w/v tryptone, 0.5% w/v yeast extract, 0.8% w/v glucose, 0.1 M potassium phosphate buffer pH 6.5; Begg et al., 1977) at 30°C for 16 h in the presence of ampicillin and chloramphenicol. Determination and calculation of β-galactosidase enzyme activity was done using a 0.5 ml culture grown according to Miller (1972). Each experiment was performed in biological, as well as technical, triplicates. In a qualitative test, 5 μl aliquots of culture were dropped on MacConkey plates containing 0.5% (w/v) maltose, ampicillin, and chloramphenicol. The plates were incubated aerobically at 30°C for 16 h and strains lacking β-galactosidase enzyme activity remained white, while those exhibiting activity ranged from pink to deep red (data not shown).

RESULTS AND DISCUSSION

Exchange of the Amino Acids Ala-550 and Val-551 on Pro-HybC for Those in Pro-HyaB Does Not Prevent Processing

The C-terminal peptide on pro-HybC, the large subunit precursor of Hyd-2, functions either as a recognition motif for the Hyp cofactor-insertion machinery or it maintains the empty active site in an open conformation, facilitating insertion of the nickel and $Fe(CN)_2CO$ moieties of the cofactor. Current evidence

strongly suggests the latter role (Thomas et al., 2015; Kwon et al., 2018). To demonstrate this conclusively, however, we decided to generate a HybC variant carrying a complete swap of all 18 amino acids after Cys-4 (**Figure 1A**), for the corresponding C-terminal 18-amino acid oligopeptide from the Hyd-1 large subunit precursor pro-HyaB (**Figure 1B**). A variant in which the final 15-amino acid residues of the pro-HybC protein were exchanged for those of pro-HyaB was constructed previously (Thomas et al., 2015). This construct, referred to in this study as pro-HybC§ (**Figure 1B**), was used as the basis to introduce further changes at codons 550 and 551 in the $hybC$ gene, resulting in a protein product (pro-HybC^{§ST}) carrying the Hyd-1-specific ST instead of the Hyd-2-specific AV amino acid residues at these positions (**Figure 1A**). These exchanges were also made in the native $hybC$ gene, delivering pro-HybCST (**Figure 1B**). The plasmids delivering the gene products pro-HybC, pro-HybC§, pro-HybCST, and pro-HybC^{§ST} (see **Table 1**) were introduced into the *E. coli* strain FTD150 (Redwood et al., 2008), which lacks the genes encoding the large subunits of all four hydrogenases, as well as into isogenic strains lacking $hybG$ (CB18), $hypC$ (CB19), $hyaD$ (CB16), or $hybD$ (CB17). After anaerobic growth in minimal medium with glucose as a carbon source, cell-free extracts were prepared, and the Hyd-2 enzyme activity profile of each strain was analyzed after separation of enzyme complexes in native-PAGE (**Figure 2**). The wild-type strain MC4100 acted as a positive control in each experiment and revealed three sets of signals (Ballantine and Boxer, 1985; Pinske et al., 2011) representing H_2-oxidizing enzyme activity (see **Figure 2A**), characteristic for the conditions used: Hyd-1 had the fastest

mobility in the gel; Hyd-2 migrated as a double band, and occasionally a third band could be discerned; and near the origin of the gel a weakly staining activity band due to a secondary H_2-oxidizing activity of the formate dehydrogenases FDH-O and FDH-N was observed (Soboh et al., 2011). The activity due to FDH-O/N acted as a useful loading control in these experiments and was the only activity band visible in extracts of the negative control FTD150 lacking a plasmid (**Figure 2**). Introduction of the genes encoding pro-HybC and pro-HybC§ restored Hyd-2 activity to strain FTD150, indicating that both precursor proteins were efficiently recognized and processed to active subunits by the Hyp maturation machinery (Thomas et al., 2015). Exchange of amino acids AV for ST at amino acid positions 550-551, delivering pro-HybC^{§ST}, also resulted in an active Hyd-2 enzyme, albeit with a slightly weaker activity signal (**Figure 2A**). This result indicated that exchange of the AV for ST amino acid residues adjacent to the terminal Cys-549 residue only reduced the efficiency of maturation or processing of the large subunit precursor but did not prevent maturation of an active Hyd-2 enzyme. Exchange of the complete 18-amino acid C-terminal peptide on pro-HybC for that on pro-HyaB, delivering pro-HybC^{§ST}, reduced the level of Hyd-2 activity still further under the conditions used in this experiment (**Figure 2A**). Nevertheless, these data showed that the enzyme retained activity and indicated that NiFe-cofactor insertion had occurred and that the C-terminal extension was removed. Addition of 1 mM Ni^{2+} ions to the growth medium failed to increase enzyme activity of pro-HybCST or pro-HybC^{§ST} (data not shown).

The AV → ST Exchange in Pro-HybCST and Pro-HybC^{§ST} Did Not Affect Dependence on Either the HybG Chaperone or the HybD Protease

HybG is the chaperone protein specific for delivery of the $Fe(CN)_2CO$ group into pro-HybC during maturation of Hyd-2 (Blokesch et al., 2001; Sawers and Pinske, 2017). Pro-HyaB on the other hand can receive the $Fe(CN)_2CO$ group from either HybG or HypC (Blokesch et al., 2001). To determine whether the specificity of pro-HybCST for HybG was in any way altered by the exchange of the AV to ST residues, we introduced all four plasmids into the *hybG* mutant CB18 (**Figure 2B**). No clearly defined activity band corresponding to Hyd-2 could be observed in extracts of the *hybG* mutant (**Figure 2B**). When three of these constructs were introduced into strain CB19, which lacked HypC, the Hyd-2 activity profile of each was similar to that when the same plasmids were introduced into FTD150 (compare **Figures 2A,C**). This result indicates that all variants retained their dependence on HybG for maturation.

The final step in hydrogenase large subunit maturation after nickel-insertion involves the proteolytic cleavage of the C-terminal peptide. This cleavage event has been proposed to result in a conformational change in the protein resulting in closure of the active site (Drapal and Böck, 1998; Böck

et al., 2006; Senger et al., 2017). Each precursor polypeptide has a specific protease that recognizes, among other features, the presence of the nickel ion as a motif (Theodoratou et al., 2000a,b). Although exceptions exist (Albareda et al., 2017), generally, each [NiFe]-hydrogenase large subunit has a protease specific for that particular large-subunit precursor (Böck et al., 2006; Sawers, 2012). This fact implies recognition of not only the nickel ion but also particular amino acid motifs of the hydrogenase precursor polypeptide by the protease (see Kwon et al., 2018). In *E. coli*, HyaD is the maturation endoprotease that is specific for pro-HyaB, while HybD is specific for pro-HybC (Theodoratou et al., 2005). Consequently, testing endoprotease specificity provides a very clear means of asking the question whether, apart from the nickel ion, the C-terminal peptide is a key determinant for protease recognition. To answer this question, we introduced the plasmids encoding the four different pro-HybC derivatives into isogenic FTD150 strains lacking either the *hybD* (**Figure 2D**) or the *hyaD* (**Figure 2E**) genes and analyzed the Hyd-2 activity profiles of cell-free extracts derived from the strains after anaerobic growth in minimal-glucose medium. The results showed very clearly that neither exchange of the 15-amino acid C-terminal peptide of pro-HybC for that of pro-HyaB (pro-HybC§) nor introduction of the AV → ST exchanges (pro-HybCST) affected the protease specificity of the precursor; all four derivatives retained an absolute dependence on HybD (**Figure 2D**) and all four retained activity in the *hyaD* mutant background, although, however, the pro-HybC^{§ST} derivative had reduced activity (**Figure 2E**). Together, these data indicate that the specificity neither for the chaperone HybG nor for the protease HybD was affected by the amino acid substitutions in the C-terminal peptide of pro-HybC. Furthermore, they suggest that neither protein binds to the C-terminus of pro-HybC behind Cys-549 (Cys-4 in **Figures 1A,C**).

The Pro-HybC^{§ST} Variant Including a Complete Exchange of the 18-Amino Acid C-Terminus of HybC Interacts With HybD

The results clearly show that pro-HybC^{§ST} could be matured into an active hydrogenase large subunit (HybC$_{proc}$). Moreover, the results confirmed that this pro-HybC^{§ST} variant generated a lower Hyd-2 enzyme activity compared with pro-HybCST. In order to demonstrate the protease specificity for HybD of all four pro-HybC derivatives, we performed bacterial two-hybrid analysis, whereby peptide T25 of adenylate cyclase was fused to the N-terminus of the HybC derivatives, while the protease HybD was fused with peptide T18 of adenylate cyclase (Karimova et al., 1998). The β-galactosidase enzyme activities measured for the empty vectors (pKT25 and pUT18) in the reporter strain BTH101 (**Table 1**) without insert, or pT25-zip together with pT18-zip, provided the negative or positive control values for the experiment, respectively (**Figure 3**). A clear interaction could be shown for HybD and pro-HybC, as reflected by the β-galactosidase enzyme activity of approximately 340 units. Similar activities were observed for both pro-HybCST and

pro-HybC$^{\$ST}$, indicating both precursor proteins interacted with a similar affinity with HybD. Notably, pro-HybC$^{\$}$ had a significantly higher β-galactosidase activity (∼ 820 units; **Figure 3**) in its interaction with HybD, suggesting an improved interaction between HybD and this precursor variant. A possible explanation for this finding is that the improved interaction may signify that HybD processes this variant more poorly.

In contrast to what was observed for fusions with pro-HybC, a fusion of the Hyd-1 large subunit precursor, pro-HyaB, or of pro-HyaB$^{\$}$, the Hyd-1 precursor with its C-terminus exchanged with that from pro-HybC, with the T25 adenylate cyclase fragment did not reveal any interaction with HybD (∼95 units, similar to the negative control). This result indicates that the interaction between HybD and the HybC precursors was highly specific.
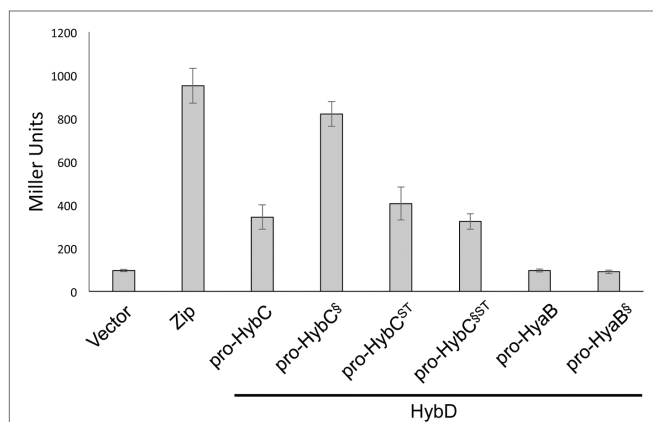
**FIGURE 3** | All four HybC variants interact with the endoprotease HybD. The histograms show the β-galactosidase enzyme activities of strain BTH101 carrying plasmids encoding T25 fusions of the indicated hydrogenase variants as well as T18 fused with HybD (see Section "Materials and Methods" for details). "Vector" shows the activity of the strain carrying empty vectors pUT18 and pKT25, while "Zip" shows the activity of the strain carrying the positive controls pT25-zip and pT18-zip (Karimova et al., 1998). Each histogram shows the mean plus standard deviation of the biological replicates, each performed in triplicate.

Limited Proteolysis Studies Reveal That HybC$_{proc}$ Has a More Compact Conformation Than Pro-HybC

The findings of a recent CD-spectroscopic analysis have suggested that pro-HybC and HybC$_{proc}$, the processed form of HybC lacking the 15-amino-acid long C-terminal peptide, have different conformations (Senger et al., 2017). To confirm and extend that observation, we undertook limited proteolysis experiments to gain insight into whether the genetic removal (HybC$_{proc}$ in **Figure 1B**; Thomas et al., 2015) of the C-terminal peptide of pro-HybC indeed resulted in a more compact, "closed" conformation of the protein. The pro-HybC protein was isolated from a genetic background that lacked the *hybD* gene to ensure that no *in vivo* processing could occur. Studies were performed using both trypsin (**Figure 4A**) and chymotrypsin (**Figure 4B**), as well as using GluC (data not shown), and all three experiments showed an enhanced resistance of the purified HybC$_{proc}$ species toward proteolysis compared with the unprocessed pro-HybC protein. After a 2 h incubation with trypsin, pro-HybC was almost completely cleaved (**Figure 4A**), while approximately 50% of HybC$_{proc}$ remained uncleaved during the same period of incubation (**Figure 4A**). Similar observations were made for chymotrypsin treatment of the purified proteins (**Figure 4B**). Moreover, there were clearly fewer peptides visible in the 25–35 kDa mass range for the HybC$_{proc}$ protein compared with pro-HybC (**Figure 4A**). Together, these findings indicated that HybC lacking the C-terminal peptide was more resistant toward proteolysis and therefore has a different, more "compact" conformation, compared with pro-HybC.

HybG Protects Pro-HybC Against Proteolysis by Trypsin

HybG is required for the delivery of the Fe(CN)$_2$CO group to pro-HybC (Blokesch et al., 2001) and HybG interacts with pro-HybC (Thomas et al., 2015; Senger et al., 2017). Our findings presented above also demonstrate that the pro-HybC variants with a C-terminal extension exchanged for that of pro-HyaB retained their dependence on HybG for maturation. These results
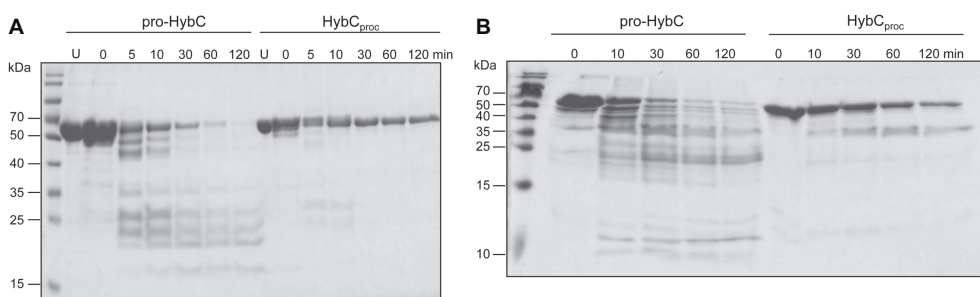
FIGURE 4 | Different conformations of immature pro-HybC and mature HybC$_{proc}$ revealed by limited proteolysis. Aliquots (100 µg protein) of purified His-tagged pro-HybC or HybC$_{proc}$ were incubated at 37°C with 1 µg of trypsin **(A)** or chymotrypsin **(B)** and samples were removed at the indicated time points and separated in 10% (w/v) SDS-PAGE for **(A)**, or 12.5% (w/v) SDS-PAGE for **(B)**. After electrophoresis, the gels were stained with Coomassie Brilliant Blue. U, untreated, purified polypeptide. Molecular mass standards are shown in kDa. Limited proteolysis experiments were performed three times for each protease.
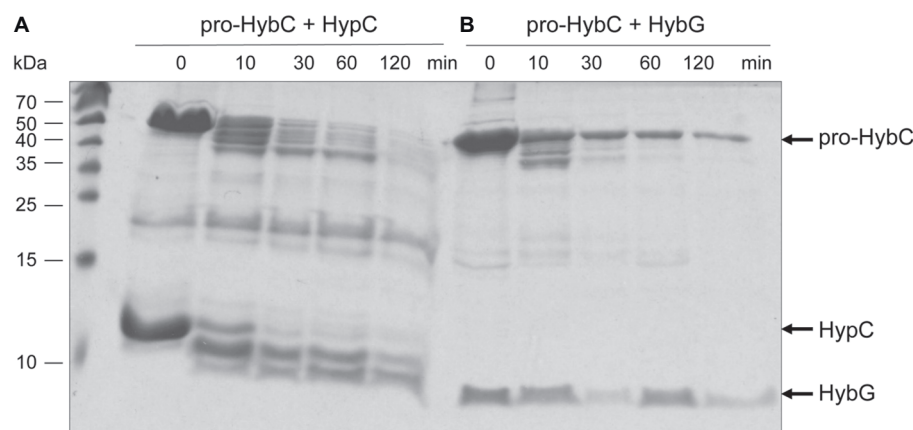
FIGURE 5 | HybG protects pro-HybC against proteolytic attack by trypsin. The experiment shown in part **(A)** of Figure 4 was repeated under the same conditions but pro-HybC was incubated with 50 µg of either HypC **(A)** or HybG **(B)** prior to addition of trypsin. The migration positions of pro-HybC, HypC, and HybG are indicated on the right of the figure. Limited proteolysis experiments were performed three times.

strongly suggest that HybG, like the protease HybD, binds to and recognizes motifs in pro-HybC that are distinct from the C-terminal peptide, as has also been suggested based on the results of mutagenesis (Magalon and Böck, 2000) and recent structural studies (Kwon et al., 2018). To provide further support for this suggestion, we examined whether HybG, through its interaction with pro-HybC could offer protection against attack by trypsin (**Figure 5**). As a control, we performed at the same time an experiment in which HypC was incubated with pro-HybC. HypC does not specifically interact with pro-HybC (Blokesch et al., 2001; Thomas et al., 2015) and indeed the gel shown in **Figure 5A** reveals that HypC failed to protect pro-HybC against proteolysis by trypsin, with the degradation pattern being similar to that shown for pro-HybC alone (see **Figure 4A**). Full-length HypC was also degraded during the 2 h incubation with trypsin. In contrast, HybG clearly reduced the rate of degradation of pro-HybC (**Figure 5B**), suggesting that it either sterically hindered access of trypsin to the vulnerable sites, or altered the conformation of pro-HybC such that it was no longer accessible to the protease. Unfortunately, attempts to isolate pro-HybCST or pro-HybC$^{\$ST}$ for similar interaction analyses failed due to inherent instability of both variants (data not shown).

CONCLUDING REMARKS

Our results support the conclusion that the C-terminal oligopeptide extension on the large subunit of Hyd-2 has a chaperone-like function (Theodoratou et al., 2005) and do not support the conclusion that it acts as a recognition motif for either the HybG or HybD hydrogenase maturation proteins. The two variable amino acids between Cys-4 and His-552 in HybC and HyaB of *E. coli*, and which are part of the conserved D-P-C-X-A-C-X-X-H motif that forms the C-terminus of most nickel hydrogenase large subunits, are interchangeable and not essential for either HybG or endoprotease specificity; however, the exchange from AV to ST in pro-HybC did impair the efficiency of

maturation. It is likely that this effect is due to the proximity of these residues to the crucial fourth cofactor-coordinating cysteinyl residue (Cys-4), which ultimately bridges the two metals of the NiFe-cofactor in the active site, thus conferring activity upon the cofactor (Magalon and Böck, 2000; Beaton et al., 2018). The importance of the fourth cysteinyl residue in maturation was emphasized recently when the crystal structure of the immature precursor HyhL from *T. kodakarensis* revealed that a β-strand formed within the C-terminal extension and interacted with two β-strands in the N-terminus of the polypeptide to form a β-sheet structure. This conformational change displaced the Cys-4 residue away from the other three coordinating Cys residues (Kwon et al., 2018), consequently opening the active site to allow the Hyp maturation proteins to interact with and deliver the $Fe(CN)_2CO$ and nickel moieties to the precursor.

After endoproteolytic cleavage, the C-terminus is suggested to "flip"back forming a short α-helix closing the active site, thus allowing Cys-4 to bridge the two metals. This hypothesis is supported by the recently resolved structure of the mature HybC protein (Beaton et al., 2018; see also **Figure 1C**). Our limited proteolysis studies demonstrated that a major conformational change in the protein indeed occurs because HybC$_{proc}$ became significantly more resistant to trypsin treatment when compared with pro-HybC. Moreover, interaction with HybG also protected the "open" conformation of the protein against trypsin, which corroborates our proposal that HybG possibly interacts with the N-terminal region of the protein, as has been shown for the nickel delivery protein HypA during its interaction with HyhL (Kwon et al., 2018). Moreover, these findings are in accord with HybG being unable to interact with HybC$_{proc}$ (Thomas et al., 2015). Contrary to the proposed interaction of the HybD maturation endoprotease with the C-terminal extension (discussed in Kwon et al., 2018), the results presented in this communication indicate that the C-terminus is not a recognition motif for the hydrogenase-specific endoprotease, hence locating the recognition site(s) at a different place from the processing site. The two proteases

HyaD and HybD do not recognize substrates other than their own large subunit precursors HyaB and HybC, respectively, and despite substitution of the complete C-terminal oligopeptide and the P2 and P3 sites from HyaB, pro-HybC[§ST] retained its specificity for HybD.

DATA AVAILABILITY STATEMENT

The datasets generated for this study are available on request to the corresponding author.

AUTHOR CONTRIBUTIONS

CP, CT, and KN designed and performed the experiments and analyzed the data. CP and RS conceived the study, interpreted the data, and drafted the manuscript. All authors read and approved the manuscript.

REFERENCES

Albareda, M., Buchanan, G., and Sargent, F. (2017). Identification of a stable complex between a [NiFe]-hydrogenase catalytic subunit and its maturation protease. *FEBS Lett.* 591, 338–347. doi: 10.1002/1873-3468.12540

Baba, T., Ara, T., Hasegawa, M., Takai, Y., Okumura, Y., Baba, M., et al. (2006). Construction of *Escherichia coli* K-12 in-frame, single-gene knockout mutants: the Keio collection. *Mol. Syst. Biol.* 2:2006.0008. doi: 10.1038/msb4100050

Ballantine, S. P., and Boxer, D. H. (1985). Nickel-containing hydrogenase isoenzymes from anaerobically grown *Escherichia coli* K-12. *J. Bacteriol.* 163, 454–459.

Beaton, S. E., Evans, R. M., Finney, A. J., Lamont, C. M., Armstrong, F. A., Sargent, F., et al. (2018). The structure of hydrogenase-2 from *Escherichia coli*: implications for H_2-driven proton pumping. *Biochem. J.* 475, 1353–1370. doi: 10.1042/BCJ20180053

Begg, Y., Whyte, J., and Haddock, B. (1977). The identification of mutants of *Escherichia coli* deficient in formate dehydrogenase and nitrate reductase activities using dye indicator plates. *FEMS Microbiol. Lett.* 2, 47–50. doi: 10.1111/j.1574-6968.1977.tb00905.x

Blokesch, M., Magalon, A., and Böck, A. (2001). Interplay between the specific chaperone-like proteins HybG and HypC in maturation of hydrogenases 1, 2, and 3 from *Escherichia coli*. *J. Bacteriol.* 183, 2817–2822. doi: 10.1128/JB.183.9.2817-2822.2001

Böck, A., King, P., Blokesch, M., and Posewitz, M. (2006). Maturation of hydrogenases. *Adv. Microb. Physiol.* 51, 1–71. doi: 10.1016/S0065-2911(06)51001-X

Casadaban, M. J. (1976). Transposition and fusion of the *lac* genes to selected promoters in *Escherichia coli* using bacteriophage lambda and mu. *J. Mol. Biol.* 104, 541–555. doi: 10.1016/0022-2836(76)90119-4

Drapal, N., and Böck, A. (1998). Interaction of the hydrogenase accessory protein HypC with HycE, the large subunit of *Escherichia coli* hydrogenase 3 during enzyme maturation. *Biochemistry* 37, 2941–2948. doi: 10.1021/bi9720078

Fritsche, E., Paschos, A., Beisel, H. G., Böck, A., and Huber, R. (1999). Crystal structure of the hydrogenase maturating endopeptidase HybD from *Escherichia coli*. *J. Mol. Biol.* 288, 989–998. doi: 10.1006/jmbi.1999.2719

Gollin, D. J., Mortenson, L. E., and Robson, R. L. (1992). Carboxyl-terminal processing may be essential for production of active NiFe hydrogenase in *Azotobacter vinelandii*. *FEBS Lett.* 309, 371–375. doi: 10.1016/0014-5793(92)80809-U

Hedstrom, L. (2002). Serine protease mechanism and specificity. *Chem. Rev.* 102, 4501–4524. doi: 10.1021/cr000033x

Hormann, K., and Andreesen, J. R. (1989). Reductive cleavage of sarcosine and betaine by *Eubaterium acidaminophilum via* enzyme systems different from glycine reductase. *Arch. Microbiol.* 153, 50–59. doi: 10.1007/BF00277541

Karimova, G., Pidoux, J., Ullmann, A., and Ladant, D. (1998). A bacterial two-hybrid system based on a reconstituted signal transduction pathway. *Proc. Natl. Acad. Sci. USA* 95, 5752–5756.

Kitagawa, M., Ara, T., Arifuzzaman, M., Ioka-Nakamichi, T., Inamoto, E., Toyonaga, H., et al. (2005). Complete set of ORF clones of *Escherichia coli* ASKA library (a complete set of *E. coli* K-12 ORF archive): unique resources for biological research. *DNA Res.* 12, 291–299. doi: 10.1093/dnares/dsi012

Kwon, S., Watanabe, S., Nishitani, Y., Kawashima, T., Kanai, T., Atomi, H., et al. (2018). Crystal structures of a [NiFe] hydrogenase large subunit HyhL in an immature state in complex with a Ni chaperone HypA. *Proc. Natl. Acad. Sci. USA* 115, 7045–7050. doi: 10.1073/pnas.1801955115

Lacasse, M. J., and Zamble, D. B. (2016). [NiFe]-hydrogenase maturation. *Biochemistry* 55, 1689–1701. doi: 10.1021/acs.biochem.5b01328

Laemmli, U. (1970). Cleavage of structural proteins during the assembly of the head of bacteriophage T4. *Nature* 227, 680–685. doi: 10.1038/227680a0

Lowry, O., Rosebrough, N., Farr, A., and Randall, R. (1951). Protein measurement with the Folin phenol reagent. *J. Biol. Chem.* 193, 265–275.

Magalon, A., and Böck, A. (2000). Analysis of the HypC-HycE complex, a key intermediate in the assembly of the metal center of the *Escherichia coli* hydrogenase 3. *J. Biol. Chem.* 275, 21114–21120. doi: 10.1074/jbc.M000987200

Menon, N. K., Robbins, J., Vartanian, M., Patil, D., Peck, H. D. Jr., Menon, A. L., et al. (1993). Carboxy-terminal processing of the large subunit of [NiFe] hydrogenases. *FEBS Lett.* 331, 91–95. doi: 10.1016/0014-5793(93)80303-C

Miller, J. H. (1972). *Experiments in molecular genetics*. Cold Spring Harbor, NY: Cold Spring Harbor Laboratory.

Pinske, C. (2018). The ferredoxin-like proteins HydN and YsaA enhance redox dye-linked activity of the formate dehydrogenase H component of the formate hydrogenlyase complex. *Front. Microbiol.* 9:1238. doi: 10.3389/fmicb.2018.01238

Pinske, C., Jaroschinsky, M., Linek, S., Kelly, C. L., Sargent, F., and Sawers, R. G. (2015). Physiology and bioenergetics of [NiFe]-hydrogenase 2-catalyzed H_2-consuming and H_2-producing reactions in *Escherichia coli*. *J. Bacteriol.* 197, 296–306. doi: 10.1128/JB.02335-14

Pinske, C., Jaroschinsky, M., Sargent, F., and Sawers, G. (2012). Zymographic differentiation of [NiFe]-hydrogenases 1, 2 and 3 of *Escherichia coli* K-12. *BMC Microbiol.* 12:134. doi: 10.1186/1471-2180-12-134

Pinske, C., Krüger, S., Soboh, B., Ihling, C., Kuhns, M., Braussemann, M., et al. (2011). Efficient electron transfer from hydrogen to benzyl viologen by the [NiFe]-hydrogenases of *Escherichia coli* is dependent on the coexpression of the iron-sulfur cluster-containing small subunit. *Arch. Microbiol.* 193, 893–903. doi: 10.1007/s00203-011-0726-5

Redwood, M. D., Mikheenko, I., Sargent, F., and Macaskie, L. (2008). Dissecting the roles of *Escherichia coli* hydrogenases in biohydrogen production. *FEMS Microbiol. Lett.* 278, 48–55. doi: 10.1111/j.1574-6968.2007.00966.x

Rossmann, R., Maier, T., Lottspeich, F., and Böck, A. (1995). Characterisation of a protease from *Escherichia coli* involved in hydrogenase maturation. *Eur. J. Biochem.* 227, 545–550. doi: 10.1111/j.1432-1033.1995.tb20422.x

- 76 -

Rossmann, R., Sauter, M., Lottspeich, F., and Böck, A. (1994). Maturation of the large subunit (HYCE) of *Escherichia coli* hydrogenase 3 requires nickel incorporation followed by *C*-terminal processing at Arg537. *Eur. J. Biochem.* 220, 377–384. doi: 10.1111/j.1432-1033.1994.tb18634.x

Sambrook, J., Fritsch, E. F., and Maniatis, T. (1989). *Molecular cloning: A laboratory manual.* Cold Spring Harbor, New York: Cold Spring Harbor Laboratory Press.

Sawers, R. G. (2012). "Hydrogenase maturation endopeptidase" in *Handbook of proteolytic enzymes.* 3rd Edn. *Chapter 70.* eds. N. Rawlings, and G. Salvesen (Cambridge, Massachusetts, USA: Academic Press), 294–296.

Sawers, R. G., and Pinske, C. (2017). "Insights into [NiFe]-hydrogenase active site metallocluster assembly" in *Encyclopedia of inorganic and bioinorganic chemistry – Metalloprotein site assembly, Chapter eibc2484.* eds. M. K. Johnson, and R. A. Scott (Hoboken, New Jersey, USA: J. Wiley and Sons).

Schechter, I., and Berger, A. (1967). On the size of the active site in proteases. I. Papain. *Biochem. Biophys. Res. Commun.* 27, 157–162. doi: 10.1016/S0006-291X(67)80055-X

Senger, M., Stripp, S. T., and Soboh, B. (2017). Proteolytic cleavage orchestrates cofactor insertion and protein assembly in [NiFe]-hydrogenase biosynthesis. *J. Biol. Chem.* 292, 11670–11681. doi: 10.1074/jbc.M117.788125

Soboh, B., Pinske, C., Kuhns, M., Waclawek, M., Ihling, C., Trchounian, K., et al. (2011). The respiratory molybdo-selenoprotein formate dehydrogenases of *Escherichia coli* have hydrogen: benzyl viologen oxidoreductase activity. *BMC Microbiol.* 11:173. doi: 10.1186/1471-2180-11-173

Soboh, B., Stripp, S. T., Bielak, C., Lindenstrauß, U., Braussemann, M., Javaid, M., et al. (2013). The [NiFe]-hydrogenase accessory chaperones HypC and HybG of *Escherichia coli* are iron- and carbon dioxide-binding proteins. *FEBS Lett.* 587, 2512–2516. doi: 10.1016/j.febslet.2013.06.055

Theodoratou, E., Huber, R., and Böck, A. (2005). [NiFe]-hydrogenase maturation endopeptidase: structure and function. *Biochem. Soc. Trans.* 33, 108–111. doi: 10.1042/BST0330108

Theodoratou, E., Paschos, A., Magalon, A., Fritsche, E., Huber, R., and Böck, A. (2000a). Nickel serves as a substrate recognition motif for the endopeptidase involves in hydrogenase maturation. *Eur. J. Biochem.* 267, 1995–1999. doi: 10.1046/j.1432-1327.2000.01202.x

Theodoratou, E., Paschos, A., Mintz-Weber, S., and Böck, A. (2000b). Analysis of the cleavage site specificity of the endopeptidase involved in the maturation of the large subunit of hydrogenase 3 from *Escherichia coli. Arch. Microbiol.* 173, 110–116. doi: 10.1007/s002039900116

Thomas, C., Muhr, E., and Sawers, R. G. (2015). Coordination of synthesis and assembly of a modular membrane-associated [NiFe]-hydrogenase is determined by cleavage of the *C*-terminal peptide. *J. Bacteriol.* 197, 2989–2998. doi: 10.1128/JB.00437-15

- 77 -

Kapitel V – Funktion der *N*-terminalen HycE Domäne

Die *N*-terminalen Domänen der paralogen HycE und NuoCD steuern den Aufbau der jeweiligen Formiat Hydrogenlyase- und NADH-Dehydrogenase-Komplexe.

Philipp Skorupa[a], Ute Lindenstrauß[a], Sabrina Burschel[b], Christian Blumenscheit[a], Thorsten Friedrich[b] und Constanze Pinske[a,*],
Philipp Skorupa und Ute Lindenstrauß trugen gleich viel zu dieser Arbeit bei.

[a] Institut für Biologie/Mikrobiologie, Martin-Luther-Universität Halle-Wittenberg, 06108 Halle, Deutschland, Kurt-Mothes-Str. 3, 06120 Halle/Saale, Deutschland
[b] Albert-Ludwigs-University Freiburg; Institute für Biochemie/Molecular Bioenergetik; Albertstr. 21; 79104 Freiburg, Deutschland

* Korrespondierende Autorin: Constanze Pinske
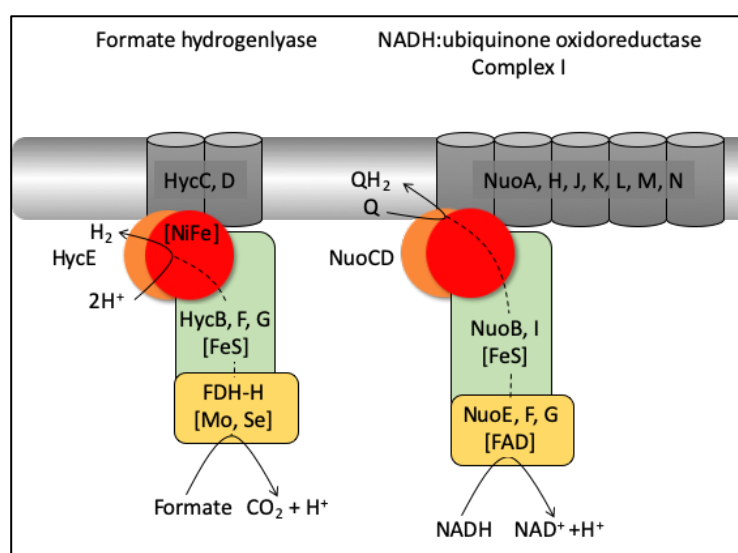
Abbildung 18: Vergleich des schematischen Aufbaus des FHL-Komplexes mit Komplex I.

Zusammenfassung:

Komplex I und der Formiat-Hydrogenlyase (FHL)-Komplex aus *Escherichia coli* enthalten jeweils das Fusionsprotein NuoCD bzw. HycE. Es wurden die *N*-terminalen, kofaktorfreien Domänen beider Proteine deletiert oder das Protein genetisch in zwei einzelne Proteine getrennt und die Enzymaktivität bestimmt. Die Deletionsvarianten verursachten die Instabilität beider Komplexe. Eine Trennung führte im Fall von FHL zum Aktivitätserhalt während Komplex I inaktiv wurde.

Der Formiat Hydrogenlyase (FHL) Komplex ist der wichtigste wasserstoffproduzierende Enzymkomplex in Enterobakterien. Er wandelt Formiat durch die Formiat-Dehydrogenase und die [NiFe]-Hydrogenase (HycE Protein) in CO_2 und H_2 um. FHL und Komplex I sind evolutionär eng verwandt und teilen eine gemeinsame Kernarchitektur. Komplex I katalysiert jedoch den grundlegend verschiedenen Elektronentransfer von NADH zu Chinon und pumpt dabei Protonen. Die katalytische FHL-Untereinheit HycE ähnelt NuoCD des *Escherichia coli-*

Komplexes I; eine Fusion von NuoC und NuoD, die in anderen Organismen separat vorhanden sind. Die *C*-terminale Domäne von HycE beherbergt den [NiFe]-Kofaktor und ähnelt anderen Hydrogenasen, während diese Domäne in NuoCD an der Chinonbindung beteiligt ist. Die *N*-terminalen Domänen dieser Proteine binden keine Kofaktoren und sind nicht am Elektronentransfer beteiligt. Da diese *N*-terminalen Domänen in einigen Organismen separate Proteine sind, wurden sie in *E. coli* deletiert, so dass sowohl FHL- als auch Komplex I-Aktivitäten im Wesentlichen nicht detektierbar waren. Dies war entweder auf eine gestörte Assemblierung oder auf Instabilität der Komplexe zurückzuführen. Das Ersetzen der *N*-terminalen Domäne von HycE durch eine *E. coli* NuoC-Proteinfusion von 180 Aminosäuren stellte die Aktivität nicht wieder her, was darauf hindeutet, dass die Domänen komplex-spezifische Funktionen haben. Ein FHL-Komplex, in dem die *N*- und *C*-terminalen Domänen von HycE genetisch getrennt wurden, behielt den größten Teil seiner Aktivität bei, während die Trennung von NuoCD den Komplex-I vollständig inaktivierte. Nur der FHL-Komplex toleriert somit die physikalische Trennung der HycE-Domänen. Zusammengenommen legen die Ergebnisse den Schluss nahe, dass die *N*-terminalen Domänen dieser Proteine Schlüsselfaktoren für die Assemblierung der Komplexe sind.

The N-terminal domains of the paralogous HycE and NuoCD govern assembly of the respective formate hydrogenlyase and NADH dehydrogenase complexes

Philipp Skorupa[1], Ute Lindenstrauß[1], Sabrina Burschel[2], Christian Blumenscheit[1] (iD), Thorsten Friedrich[2] (iD) and Constanze Pinske[1] (iD)

1 Institute of Biology/Microbiology, Martin-Luther University Halle-Wittenberg, Germany
2 Institute of Biochemistry/Molecular Bioenergetics, Albert-Ludwigs-University Freiburg, Germany

Formate hydrogenlyase (FHL) is the main hydrogen-producing enzyme complex in enterobacteria. It converts formate to CO_2 and H_2 via a formate dehydrogenase and a [NiFe]-hydrogenase. FHL and complex I are evolutionarily related and share a common core architecture. However, complex I catalyses the fundamentally different electron transfer from NADH to quinone and pumps protons. The catalytic FHL subunit, HycE, resembles NuoCD of *Escherichia coli* complex I; a fusion of NuoC and NuoD present in other organisms. The C-terminal domain of HycE harbours the [NiFe]-active site and is similar to other hydrogenases, while this domain in NuoCD is involved in quinone binding. The N-terminal domains of these proteins do not bind cofactors and are not involved in electron transfer. As these N-terminal domains are separate proteins in some organisms, we removed them in *E. coli* and observed that both FHL and complex I activities were essentially absent. This was due to either a disturbed assembly or to complex instability. Replacing the N-terminal domain of HycE with a 180 amino acid *E. coli* NuoC protein fusion did not restore activity, indicating that the domains have complex-specific functions. A FHL complex in which the N- and C-terminal domains of HycE were physically separated still retained most of its FHL activity, while the separation of NuoCD abolished complex I activity completely. Only the FHL complex tolerates physical separation of the HycE domains. Together, the findings strongly suggest that the N-terminal domains of these proteins are key determinants in complex assembly.

Protein tertiary structure describes the autonomously folding regions of a protein as a domain. Domains can serve different functions, for example binding of cofactors, recognition of a motif or catalytic activity. Evolution has shuffled domains to create the huge diversity of proteins that occur today [1]. Taken on their own, a domain sometimes behaves completely different compared to the holo-protein, as observed for fibril formation by the isolated N-terminal acylphosphatase domain of the HypF hydrogenase maturation factor [2,3]. Artificial fusion proteins have been used for many years as biochemical tools, and in many cases, these fusions have no or little impact on the function of the original protein.

It has been observed that proteins possessing coordinate functions sometimes become fused during evolution, allowing greater efficiency, based on colocation. One prominent example is the alcohol dehydrogenase

Abbreviations
BV, benzyl viologen; FdhH, formate dehydrogenase; FHL, formate hydrogenlyase; Nuo, NADH:ubiquinone oxidoreductase.

1

fusion with acetaldehyde dehydrogenase, which couples two sequential reactions without releasing the toxic intermediate acetaldehyde [4,5]. The most straightforward way for these fusion events to occur is when neighbouring genes of a polycistronic operon are joined through frameshift mutations. Clearly, evolutionary selective pressure is required for the proteins to remain fused, for example when the activity is enhanced or assembly is augmented. Protein complexes with several subunits are likely to assemble via ordered pathways, and natural selection tends to favour gene fusions to optimize assembly [6]. Gene fusion seems also to have happened to the *hycE* gene of the *Escherichia coli* hydrogenase three large subunit, HycE. Together with a formate dehydrogenase (FdhH), the HycE hydrogenase forms the catalytic components of the formate hydrogenlyase (FHL) complex in *E. coli* and other Enterobacteriacea. FHL catalyses the oxidation of formate with the concomitant reduction of protons to produce hydrogen to detoxify formate during mixed-acid fermentation [7]. Along with the FdhH and HycE, three iron-sulfur proteins, including the small subunit HycG, HycF and HycB, form the soluble part of the FHL complex. This large soluble domain is anchored to the membrane by two membrane subunits [8]. The complex is phylogenetically and structurally related to the respiratory complex I, with the NuoCD protein being the homologue of HycE [9–12]. Although the relationship is less obvious on the primary structural level, where HycE and NuoCD share only 26% (145/563) identical and 43% (244/563) similar residues, it is clearly apparent when the secondary structural elements are compared between the two proteins (Fig. 1). Complex I, or NADH:ubiquinone oxidoreductase (Nuo), is the primary energy-conserving complex of many respiratory chains and couples NADH oxidation to the translocation of four protons across the membrane [13]. NuoC varies significantly in length in different organisms [14]. Unlike most organisms, which have separate NuoC and NuoD proteins, both are fused in complex I of *E. coli* and *Bacteroides fragilis*. Moreover, the NuoC subunit is homologous to the N-terminal domain of HycE and its paralogue in *E. coli*, HyfG [14]. The crystal structures of both the soluble portion and the entire complex from *Thermus thermophilus* have been determined [15,16]. NuoC is an orthologue of Nqo5 in *T. thermophilus* and of the 30-kDa protein in *Bos taurus* [13]. Unlike its counterpart in HycE, which contains the [NiFe]-active site, NuoD is not known to harbour any cofactors, but it does have a quinone-binding site [17].

The C-terminal domain of HycE extends from amino acids 175–537 and harbours the four conserved cysteinyl residues that coordinate the bimetallic [NiFe]-cofactor required for catalysis (scheme in Fig. 1 and alignment in Fig. 2). These cysteinyl residues are not present in NuoD (Figs 1 and 2). Six pleiotropic Hyp proteins are required for synthesis of the [NiFe]-cofactor including its diatomic ligands attached to the Fe atom [18,19]. Of these proteins, the HypC and HypA proteins interact directly with HycE for Fe $(CN)_2CO$ and Ni^{2+} insertion, respectively [20,21]. In addition, HycE has a 32-amino acid C-terminal extension from amino acids 538–569 that is endoproteolytically processed after cofactor insertion and is assumed to facilitate this step by keeping the empty, cofactor-free apo-protein in an open conformation [22]. In this context, the N terminus of the unprocessed hydrogenase large subunit from *Thermococcus kodakarensis* was found to extend into the nickel-delivery protein HypA, while the C-terminal extension replaces the position of the N terminus prior to proteolytic processing [23]. A recent DFT calculation on HycE identified conserved glutamate residues in both the N- and C-terminal domains, which are proposed to govern the insertion of the Ni^{2+} ion of the cofactor, but the function of these residues has yet to be validated experimentally for HycE [24]. This strongly suggests that both domains act in concert for cofactor insertion.

The N-terminal domain of HycE, corresponding to NuoC, extends from amino acids 9–194 and thus is predicted to have a short overlap with the C-terminal domain [25]. This domain/protein bears a cofactor neither in the FHL complex nor in complex I, and its role remains enigmatic.

The N- and C-terminal domains of HycE and NuoCD are predicted to be fused via a long unstructured loop region that contacts the formate dehydrogenase or diaphorase subunits in FHL and complex I, respectively (Fig. 1). Previous work has shown that conserved residues (Glu-138, Glu-140, Asp-143) in the N-terminal domain NuoC are required for the stability of not only the NuoCD protein, but also all other subunits [26]. These residues are also conserved in the HycE protein (Figs 1 and 2). Amino acid exchanges within the N-terminal domain of HycE were better tolerated than exchanges in these conserved residues; for example, the addition of a 10-His residue stretch after Gly-83 was shown to have no effect on the stability and activity of the FHL complex because they are exposed to the surface [27]. Moreover, engineering of the HycE protein revealed that truncation of the C terminus increased H_2 production from the FHL
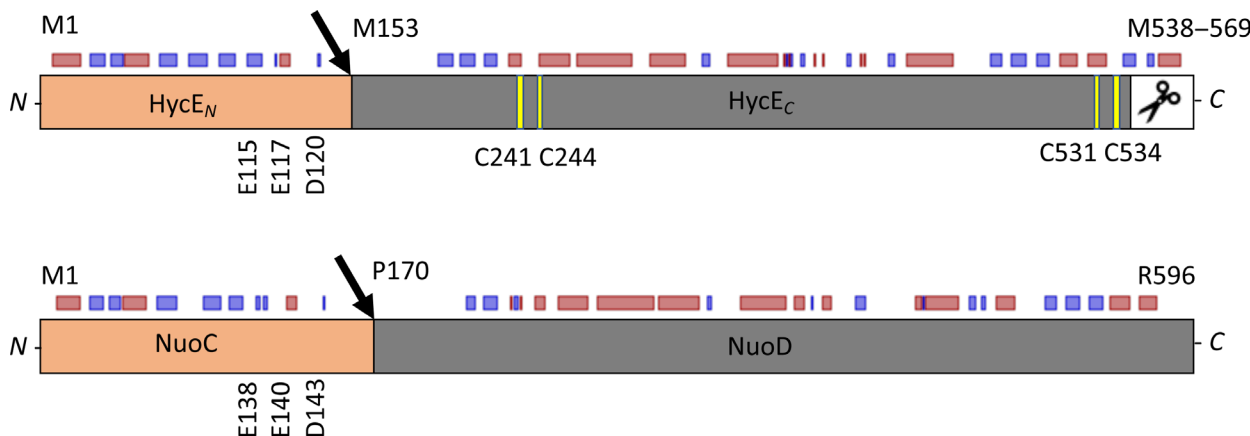
Fig. 1. Schematic representation of the HycE (top) and NuoCD (bottom) fusion proteins. The N-terminal domain of each protein is coloured in orange and the C-terminal domain in grey, and the black arrows indicate the sites where the proteins were genetically separated. The cysteinyl residues that coordinate the [NiFe]-cofactor in HycE are coloured in yellow, and the C-terminal extension that is proteolytically processed is shown in white with the scissors symbol. The locations of further relevant residues, which are mentioned in the text, are shown. The small rectangles above the respective proteins represent the secondary structure prediction (red – helix; blue – sheet) based on the Open PredictProtein server [51].

complex, despite the fact that these deletions remove the [NiFe]-binding site [28].

Therefore, in this study, we investigated the possibility of splitting the HycE and NuoCD domains into separate proteins in order to address the role of the N-terminal domain and the potential evolutionary significance of the fusion.

Methods

Growth conditions
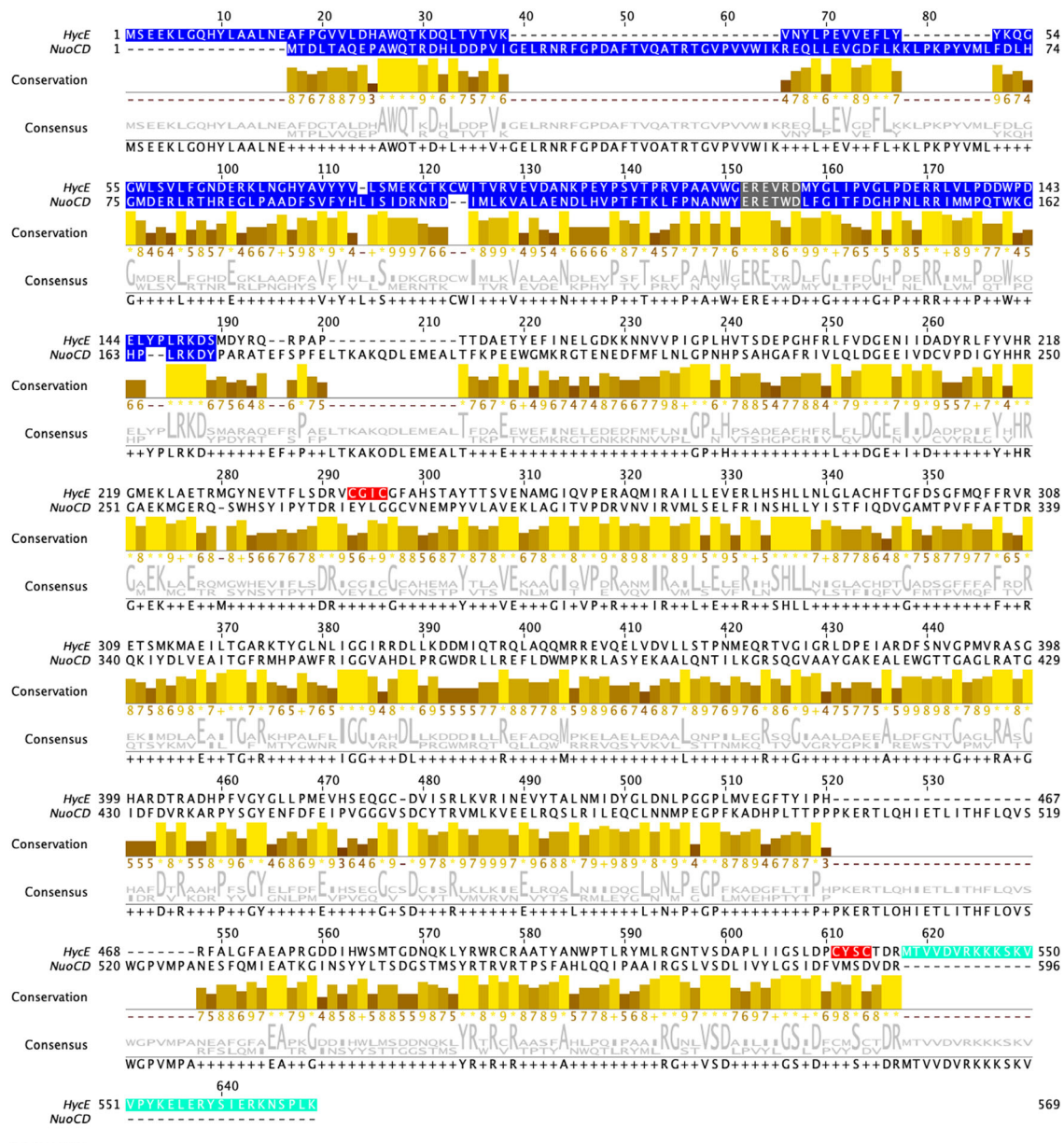
Bacterial growth was generally carried out either aerobically on LB agar plates and in shaking liquid LB cultures or anaerobically as standing liquid cultures in TGYEP medium, pH 6.5, with 0.8% (w/v) glucose included [29] at 37 °C. Alternatively, for complex I activity, aerobic cultures were grown in glycerol medium [1% (w/v) peptone, 0.5% (w/v) yeast extract, 0.8% (w/v) NaCl, 0.4% (w/v) glycerol and separately prepared 15 mM Na_3PO_4, 10 mM Na_2HPO_4 and 10 mM KH_2PO_4, pH 8.5]. Cultures were vigorously shaken at 180 r.p.m. and 37 °C. Growth experiments were performed as biological triplicates in a 96-well microtiter plate, filled with 150 μL M9 minimal medium with 25 mM acetate as sole carbon source (47.6 mM Na_2HPO_4, 22 mM KH_2PO_4, 8.4 mM NaCl, 19 mM NH_4Cl, 2 mM $MgSO_4$, 0.1 mM $CaCl_2$, 0.3 μM thiamine dichloride, 0.1% w/v trace element solution) and agitation of 150 r.p.m. in a Tecan Infinite 200 plate reader (TECAN, Männedorf, Switzerland). Strains for maintaining the pMAK705 plasmids were grown aerobically at 30 °C. When appropriate, the antibiotics ampicillin and chloramphenicol were included at 100 and 34 μg·mL^{-1}, respectively.

DNA modifications and strain construction

All strains and plasmids are listed in Table 1 and oligonucleotides in Table 2. For constructing the N-terminal truncation of HycE in strain Δ*hycE*N, the 514-bp DNA upstream region up to the encoded methionine start codon was amplified using the oligonucleotides HycEup_XbaI and HycEup_BamHI leaving the ribosome binding site intact, while the downstream 1254 bp was amplified from methionine codon 153 to the stop codon using the oligonucleotides HycEdown_BamHI and HycEdown_EcoRI. The two fragments were digested with XbaI/BamHI and BamHI/EcoRI, respectively, and ligated into pBSK(+) before being moved by XbaI/EcoRI restriction digestion to pMAK705 for chromosomal integration. The chromosomal integration into strain MG1655 was performed according to Ref. [30] and yielded the strain Δ*hycE*N. Similarly, the above pMAK705 construct was modified by introducing the *nuoC* DNA sequence into the BamHI site after amplification with the oligonucleotides nuoC_HA_FW_BamHI and nuoC_RW_BamHI. The directionality of the insert was verified by DNA sequencing, and the integration onto the chromosome of MG1655 was done independently and resulted in strain *nuoC-hycE*.

Separation of the *hycE* gene into two distinct genes on plasmid pHycE was done by the NEBaseChanger method (NEB, Ipswich, MA, USA) using the oligonucleotides HycEN+C_FW and HycEN+C_RW and resulted in plasmid pHycEN+C. This construct was subcloned onto pMAK705 and moved to the chromosome as described [30].

In trans complementation was done by cloning the DNA fragment encoding the N-terminal domain including the connecting alpha helix with AA1-168 in pJET1.2 (Thermo

Fig. 2. Alignment of HycE and NuoCD protein sequences. The alignment was performed with CLUSTAL O (1.2.4) [55] within the UniProt database and the visualization done by JALVIEW [52]; in the conservation panel, the height of the bar represents the conservation as well as the consensus logo provided according to the size of the letter. Highlighted within the sequences are the N-terminal domains (blue highlight), conserved residues within the N-terminal domain (grey highlight), hydrogenase specific C-terminal extension (cyan highlight) and [NiFe]-cofactor binding motif (red highlight).

Table 1. Strains and plasmids used in this study.

	Genotype	Reference
Strain		
MG1655	F⁻ λ⁻ *ilvG⁻ rfb-50 rph-1*	[53]
BW25113	*lacI⁺rrnB*$_{T14}$ Δ*lacZ*$_{WJ16}$ *hsdR*514 Δ*araBAD*$_{AH33}$ Δ*rhaBAD*$_{LD78}$ *rph-1* Δ*(araB–D)567* Δ*(rhaD–B)568* Δ*lacZ4787*(::*rrnB-3*) *hsdR514 rph-1*	[33,54]
JW2691	Like BW25113, but Δ*hycE*	[54]
*hycE*N+C	Like MG1655, but *hycE* separated as AA1-152 and AA153-569	This study
Δ*hycE*N	Like MG1655, but Δ*hycE* N-terminal domain corresponding to AA1-152	This study
nuoC-hycE	Like MG1655, but *hycE* N-terminal domain AA1-152 replaced with *nuoC* coding for AA1-169	This study
JW4040	Like BW25113, but Δ*fdhF*	[54]
Δ*ndh*	JW1095: like BW25113, but Δ*ndh*	[31,54]
Δ*nuoC*	BW25113 Δ*ndh*, Δ*nuoC* AA1-169	This study
nuoC+D	BW25113 Δ*ndh*, *nuoC* separated as AA1-169 and *nuoD* as AA170-596	This study
Δ*nuoC-L*	BW25113 Δ*ndh*, Δ*nuoC-L*	This study
Plasmids		
pMAK705	Temperature-sensitive replicon, Cm^R	[30]
pHycE	pACYCDuet-1, *hycE*⁺, internal His-tag, Cm^R	[34]
pHycEN+C	pACYCDuet-1, *hycE* N-terminal domain AA1-152, *hycE* C-terminal domain AA153-569 Cm^R	This study
pHycEN	pJET1.2, *hycE* N-terminal domain AA1-168, Amp^R	This study
pJET-nuoCD	pJET1.2, *nuoCD* including RBS, Amp^R	This study
pKD3	Cm^R	[33]
pCP20	Contains flippase gene for λ Red mutagenesis; Cm^R, Amp^R	[32]

Table 2. Oligonucleotides used in this study.

Oligonucleotide	Sequence 5′ → 3′
HycEup_XbaI	GCGTCTAGATGCTGCTTGGTCTGTGGGTT
HycEup_BamHI	GCGGGATCCACTCTCTTTAATCACGCCGC
HycEdown_BamHI	GCGGGATCCATGGATTATCGTCAGCGTCC
HycEdown_EcoRI	GCGGAATTCTTATTTCAGCGGCGAGTTTTTAC
nuoC_HA_FW_BamHI	GCGGGATCCATGTATCCGTATGATGTGCCGGATTATGCGACCGACTTAACCGCGCAAG
nuoC_RW_BamHI	GCGGGATCCATAATCTTTACGCAGCGGGTG
HycEN+C_FW	ATATACCATGGATTATCGTCAGCGTCC
HycEN+C_RW	CTCCTTAGCTGTCTTTACGCAGCGG
HycEN_RW_EcoRI	GCGGAATTCTTAGTAGGTTTCAGCATCGGTGG
DnuoC_5′_FW	CGCCGACAGTCACCACGGACCATTTGCAATGGTGAACAAT ccatggtccatatgaatatc
DnuoC_3′_RW_KpnI	TGGTCAGCTCAAACGGCGAGAATTCGGTAGCGCGCGCCGGCATggtaccctcct gcgattgtgtaggctggagc
DnuoLM_3′_RW	ACATGTCGATGGCAAGGAACACGCCGATAACGCCGCCCAG gcgattgtgtaggctggagc
nuoC_up_control	CGCATTGCCGTAACTAACC
nuoCD_FW_BamHI	ggatccCACGGACCATTTGCAATGGTG
nuoCD_RW_HindIII	aagcttTTAGCGGTCCACATCTGACATAAC
hycB_FW	GCGAAGCTTGATGAATCGTTTTGTAATTGCTG
hycB_RW	GCGGGATCCTCATTTAGCCTCTCCACTTT
hycF_FW	GCGCTGCAGGATGTTTACCTTTATCAAAAAAG
hycF_RW	GCGGGATCCTCAGATGGCCTCTTTCATATG
tatB_FW	GTGTTTGATATCGGTTTTTAG
tatB_RW	TTACGGTTTATCACTCGACG

Scientific, Waltham, MA, USA) using the primers HycEup_XbaI and HycEN_RW_EcoRI.

Strain BW25113 Δ*ndh* has been described before [31]. This strain was used for further modification of complex I. Deletion of the DNA sequence encoding the NuoC domain was performed by initially replacing the sequence encoding the domain with the *cat* gene from vector pKD3 (oligonucleotides DnuoC_5′_FW and DnuoC_3′_RW_KpnI) and subsequently removing the resistance cassette using vector pCP20 as described [32,33]. The DNA sequence encoding

the downstream NuoD domain received a novel ribosome binding site and start codon. The deletion of the entire region from *nuoC-L* was performed similarly, but using the oligonucleotides DnuoC_5′_FW and DnuoLM_3′_RW [33]. The *nuoC + D* strain was constructed by ordering the corresponding region as gBlocks fragment (DNA sequence in Fig. 3), which contained a stop codon after the codon encoding Y169 in *nuoC*, a ribosome binding site and a start codon for *nuoD* (IDT DNA, Coralville, IA, USA), cloning it as BamHI/BamHI fragment into pMAK705 and introducing it into BW25113 Δ*ndh*.

The pJET-nuoCD plasmid was constructed by amplification of the chromosomal *nuoCD* gene, including its own ribosome binding site, using the oligonucleotides nuoCD_FW_BamHI and nuoCD_RW_HindIII and Q5 DNA polymerase (NEB) and cloning it blunt-end into pJET1.2 vector according to the manufacturer's instructions (Thermo Scientific). Expression of the gene is under the control of the *lacUV5* promoter of the vector.

All authenticity of all DNA sequences in the plasmid inserts and strains was verified by sequencing.

RT-PCR

The RT-PCR was performed according to previously published methods [34]. RNA was isolated from strains in the

AGGAACCTGCTTTACCAAAATGGCACCGGTTATTCAGCGTCTGTATGACCAGATGCTGGAACCAAAATGGGTTATCTCAA

TGGGTGCCTGTGCCAACTCTGGTGGTATGTACGATATTTATTCCGTTGTGCAGGGCGTCGATAAATTCATCCCGGTTGAT

GTGTATATCCCGGGCTGCCCGCCGCGTCCTGAAGCGTACATGCAGGCACTGATGCTGTTGCAGGAATCTATCGGCAAAGA

ACGTCGTCCGCTCTCCTGGGTGGTTGGCGATCAGGGCGTTTATCGCGCCAATATGCAATCAGAGCGCGAACGCAAGCGCG

GTGAACGCATTGCCGTAACTAACCTGCGTACACCTGACGAGATTTAATTTGCGCCTGTCGGCAAAGGGATTTTTCTTCGC

TTATTCCTAAATCTATTTCGCGAAGCTTACTGCGCCGACAGTCACCACGGACCATTTGCAATGGTGAACAATATG<mark>TATCC</mark>

<mark>GTATGATGTGCCGGATTATGCG</mark>*ggtacc*ACCGACTTAACCGCGCAAGAACCCGCCTGGCAGACCCGCGATCATCTTGATG

ATCCGGTGATTGGCGAACTGCGCAACCGTTTTGGGCCGGATGCCTTTACTGTTCAGGCGACTCGCACCGGGGTTCCCGTT

GTGTGGATCAAGCGTGAACAATTACTGGAAGTTGGCGATTTCTTAAAGAAACTGCCGAAACCTTACGTCATGCTGTTTGA

CTTACACGGCATGGACGAACGTCTGCGCACACACCGCGAAGGGTTACCTGCCGCGGATTTTTCCGTTTTCTACCATCTGA

TTTCTATCGATCGTAACCGCGACATCATGCTGAAGGTGGCGCTGGCAGAAAACGACCTGCACGTACCGACCTTCACCAAA

CTGTTCCCGAACGCTAACTGGTATGAGCGTGAAACCTGGGATCTGTTTGGCATTACTTTCGACGGTCACCCGAACCTGCG

ACGCATCATGATGCCGCAAACCTGGAAAGGTCACCCGCTGCGTAAAGATTATtaaggag*ggtacc*ATGCCGGCGCGCGCT

ACCGAATTCTCGCCGTTTGAGCTGACCAAAGCCAAACAGGATCTGGAGATGGAAGCCCTGACCTTCAAACCGGAAGAGTG

GGGGATGAAGCGCGGCACCGAAAACGAGGACTTCATGTTCCTCAACCTCGGTCCGAACCACCCGTCGGCGCACGGGGCTT

TCCGTATCGTTTTGCAACTCGATGGCGAAGAGATTGTCGACTGCGTACCAGACATCGGTTACCACCACCGTGGTGCGGAG

AAAATGGGCGAACGCCAGTCCTGGCACAGCTACATTCCGTATACTGACCGTATCGAATACCTCGGCGGCTGCGTTAACGA

AATGCCTTACGTGCTGGCGGTAGAGAAACTGGCCGGGATCACCGTGCCGGATCGCGTTAACGTCATTCGCGTTATGCTCT

CCGAACTGTTCCGCATCAACAGTCACCTGCTGTATATCTCGACCTTTATTCAGGACGTCG

Legend:

XX	KpnI site
<mark>XX</mark>	HA-epitope tag
ATG	start/stop codons
<u>XX</u>	*nuoC*

Fig. 3. DNA sequence of *nuoC+D* ordered as gBlocks fragment. The 1500-bp fragment above was obtained from IDT DNA and designed to contain the *nuoC* upstream region, *nuoC* as independent gene (start and stop codons are shown in red; gene is underlined), DNA sequence coding for an included HA-epitope tag (yellow highlight) and a ribosome binding site for the downstream *nuoD* gene linked to the start codon by a KpnI restriction site (italics).

exponential growth phase using the SV Total RNA Isolation System according to the manufacturer's instructions (Promega, Fitchburg, WI, USA). An extra DNase I digestion step was performed using RQ1 RNase-Free DNase (Promega). The RT-PCR to generate cDNA was performed using M-MLV Reverse Transcriptase, RNase H Minus and random hexamer primers according to the manufacturer's instructions (Promega). The presence of transcripts was tested with gene-specific oligonucleotides, which are listed in Table 2, by using 17 PCR cycles to remain within the semi-quantitative part of the amplification reaction.

Western blotting and signal quantification

Aliquots of 50 µg total proteins of anaerobically grown cells were separated on a 10% (w/v acrylamide) SDS/PAGE, transferred to a nitrocellulose membrane and challenged with antibodies raised against HycG (1 : 3000, a kind gift from A. Böck/R. G. Sawers) [35,36]. The secondary antibody used was conjugated to HRP enzyme (Bio-Rad, Hercules, CA, USA), and the light signal generated by the ECL reaction (Thermo Scientific) was recorded with a film. The signal intensities were analysed using IMAGEJ software [37].

Enzymatic assays

Hydrogenase activity was determined as H_2-dependent benzyl viologen (BV) reduction using 50 mM MOPS buffer, pH 7.0, with 4 mM BV in a stoppered 1.6-mL cuvette with 0.8 mL H_2 gas headspace as described [38]. For kinetic determination of FHL activity, cell suspensions were applied to a modified Clark-type electrode (Oxytherm, Hansatech Instruments, Norfolk, UK), which was equipped with an OXY/ECU module to reverse the polarizing voltage to −0.7 V, where the electrode disc is only sensitive to H_2 (Hansatech Instruments). A volume of 2 mL degassed MOPS buffer, pH 7.0, was used, and the reaction was started with 15 mM formate. The H_2 content of the gas headspace of a 15-mL Hungate tube filled with 7 mL culture was determined by gas chromatography using a GC2010 Plus Gas Chromatograph (Shimadzu, Kyōto, Japan) as described [39].

To measure complex I activity, the NADH-dependent oxidase activity was determined on a Clark-type electrode sensitive to O_2 (Hansatech Instruments) and was performed essentially identical to the H_2 measurements, with the exception that 1.25 mM NADH was used as substrate [31]. Similarly, the succinate oxidase activity was monitored in the presence of 10 mM succinate. Protein concentrations were determined by the method of Ref. [40].

Sucrose gradient centrifugation

The sucrose gradients were prepared and NADH/ferricyanide oxidoreductase activity was determined basically as described

[31]. Briefly, membrane extracts from cells grown under the appropriate growth conditions were prepared after cell rupture with an Emulsiflex (EF-C5; Avestin Europe, Mannheim, Germany) in the presence of PMSF (0.1 mM) and DNase at 160 000 *g*. The sediment was resuspended in buffer A (50 mM MES/NaOH, 50 mM NaCl) with 1% (w/v) DDM and 5 mM $MgCl_2$. After solubilization, the membrane fraction was briefly centrifuged and subsequently applied to a freshly poured 24 mL linear sucrose gradient ranging from 5% to 30% (w/v) sucrose in buffer A supplemented with 5 mM $MgCl_2$. After centrifugation for 16 h at 140 000 *g*, the gradient was fractionated into 24 × 1 mL fractions. The NADH/ferricyanide oxidoreductase activity of 50 µL from each fraction was assayed in 1 mL buffer A containing 1 mM ferricyanide (AppliChem, Darmstadt, Germany). The reaction was started by an addition of 0.2 mM NADH, and the reaction was followed by monitoring the slope at 410 nm in an Ultrospec photometer (Amersham Pharmacia Biotech, Amersham, UK). The rate was calculated using an ε_{410} of $1 \text{ mM}^{-1} \cdot \text{cm}^{-1}$. Protein concentration was determined by biuret assay [41].

Results and Discussion

Formate hydrogenlyase complex retains activity after separation of the N- and C-terminal domains of HycE

In order to investigate the effect of dividing the HycE protein into two separate domains on the activity and stability of the FHL complex, the efficiency of conversion of formate to H_2 and CO_2 was quantified by measuring the headspace H_2 content of the culture after fermentative growth. This activity represents the total yield of H_2 after growth on glucose medium, but also provides an accurate indication of the activity of the FHL complex, and is particularly useful for assessing low FHL activities. The parental strain produced 7.03 µmol H_2·mL culture^{-1}·$OD_{600 \text{ nm}}$$^{-1}$, while H_2 production was basically absent in the negative control strain JW2691, which lacks the *hycE* gene encoding the catalytic subunit HycE. This strain can be partially (71%) complemented for H_2 production by introducing plasmid pHycE carrying the *hycE* gene. We have previously observed that *hycE* cannot fully complement a Δ*hycE* strain when provided *in trans*, and we assume this to be due to the altered chromosomal context [42]. Surprisingly, the Δ*hycE* strain can also be complemented by the plasmid pHycEN+C, which consists of the same insert sequence as on pHycE with the exception that it includes a stop codon within *hycE* (Table 3). This 'split', or separated, *hycE* gene in the chromosomal context in strain *hycE*N+C also resulted

Table 3. Hydrogenase activities and their percentage of the parental activities. The activities were determined from three biological replicates.

Strain (+Plasmid)	H_2-headspace quantification ($\mu mol \cdot OD_{600 \, nm}^{-1} \cdot mL^{-1}$)		Formate-dependent H_2 evolution (nmol $H_2 \cdot mg^{-1} \cdot min^{-1}$)		Total hydrogenase activity H_2:BV (U·mg^{-1})	
MG1655 (parental)	7.03 ± 0.28	100%	636 ± 28	100%	1.12 ± 0.37	100%
JW2691 (Δ*hycE*)	0.04 ± 0.07	< 1%	1 ± 2	< 1%	0.32 ± 0.10	29%
JW2691 + pHycE	4.99 ± 0.71	71%	190 ± 62	30%	0.56 ± 0.32	50%
JW2691 + pHycEN+C	7.46 ± 1.94	106%	337 ± 173	53%	0.64 ± 0.53	57%
*hycE*N+C	7.23 ± 0.39	103%	350 ± 19	55%	0.67 ± 0.34	60%
Δ*hycE*N	< 0.01	< 1%	1 ± 2	< 1%	0.19 ± 0.05	17%
Δ*hycE*N + pHycEN	3.23 ± 0.19	46%	73 ± 15	11%	0.39 ± 0.18	35%
nuoC-hycE	< 0.01	< 1%	1 ± 2	< 1%	0.19 ± 0.01	17%

in H_2 accumulation to a level similar to that of the parental strain. Strain Δ*hycE*N, which carried a truncation of the N-terminal domain of HycE, but retained a protein fragment of the C-terminal domain, was unable to evolve H_2, a phenotype like that of the *hycE* deletion strain. The Δ*hycE*N strain could be complemented *in trans*, however, by introducing a plasmid encoding the missing N-terminal portion of HycE, which restored almost 50% of the H_2 production (Table 3). Complementation could not be achieved by using a fusion of the related NuoC to the C-terminal domain of HycE. Hence, despite sharing structural similarity, they fulfil distinct roles in both complexes. These assays also showed that the HycE protein, when physically separated into N- and C-terminal domains, was as efficient as the native HycE protein in converting formate to H_2 and CO_2 during mixed-acid fermentation.

In addition to the headspace analysis, which measures accumulation of H_2 over 16 h, cell suspensions were assayed on a modified Clark-type electrode with formate as substrate allowing quantitative measurement of the specific activity of the FHL complex. These measurements verified the absence of activity in strains JW2691 (Δ*hycE*), Δ*hycE*N and *nuoC-hycE*. As could be shown for the H_2-headspace measurement, the pHycE and pHycEN plasmids were functional, but were only able to complement the corresponding deletion strains JW2691 (Δ*hycE*) and Δ*hycE*N, to 30% and 11% of the level of the wild-type strain, respectively (Table 3). While determination of the accumulated H_2 revealed 100% complementation of H_2 production, the direct FHL assay led to approximately 50% of the FHL activity rate of the parental strain when the domain-split HycE protein was introduced either *in trans* on plasmid pHycEN+C in strain JW2691 (Δ*hycE*) or after chromosomal integration in strain *hycE*N+C (Table 2). This result revealed that the two physically separated domains of HycE retain

half of the activity of the fused, native protein, despite being fully functional in conversion of glucose during growth. Moreover, the findings demonstrate that providing each component in multiple copies did not result in higher activity, indicating that the amount of the two domains in the complex did not limit the reaction rate.

The samples used in the electrode experiments were subsequently used to generate crude extracts, allowing spectrophotometric quantification of total hydrogenase activity, which is a composite of Hyd-1, Hyd-2 and the Hyd-3 component of the FHL complex. Hyd-1 and Hyd-2 are both H_2-oxidizing hydrogenases, which allow the cell to scavenge some of the FHL-produced H_2. Under these conditions, Hyd-3 is generally the major contributor to the total hydrogenase activity [42]. A fourth hydrogenase, predicted to form a second FHL complex, is usually not expressed under the conditions used in this study and does not contribute to the activity [43,44]. Here, the residual total hydrogenase activity in the Δ*hycE* strain JW2691, representing the combined activities of Hyd-1 and Hyd-2, was approximately 30% of that of the wild-type strain MG1655 (Table 3). Strains Δ*hycE*N and *nuoC-hycE* showed levels of total hydrogenase activity of 17% of the parental, which, surprisingly, is lower than when only Hyd-1 and Hyd-2 are present. Using this assay, the HycE protein separated into two domains complemented to a level of 60% of the wild-type activity, which was slightly higher than the activity recovered by complementation with a plasmid, pHycE13, encoding the native HycE polypeptide. The formate dehydrogenase H activity, which is the other catalytic component of the FHL complex, followed these trends, but with slightly greater variation (Table 4). This indicates that the formate dehydrogenase polypeptide was able to stably interact with the complex carrying the separated domains of HycE.

Table 4. Formate dehydrogenase H activity measured in crude extracts and the percentage of the parental activity. The activities were determined from three biological replicates.

Strain/plasmid	FDH-H formate: BV (U mg^{-1})	% of parental activity
MG1655	2.61 ± 2.71	100
JW2691 ($\Delta hycE$)	0.15 ± 0.24	6
JW2691 + pHycE13	0.03 ± 0.03	1
JW2691 + pHycEN+C	0.43 ± 0.73	16
*hycE*N+C	0.46 ± 0.51	18
Δ*hycE*N	0.14 ± 0.72	5
Δ*hycE*N + pHycEN	0.34 ± 0.54	13
nuoC-hycE	0.14 ± 0.24	5

Modifications of the HycE N-terminal domain do not influence transcription of the *hyc* operon

Bacterial operons often contain internal promoters and regulatory elements [45]. In the case of the *hyc* operon, computational evidence predicts a further sigma 70-dependent promoter in front of *hycI*, the last gene of the operon [46]. Therefore, it was investigated whether the genomic modifications in strains $\Delta hycE$N and *nuoC-hycE*, which completely lacked FHL activity, influenced the transcription of the downstream genes. Reverse transcriptase PCR on RNA isolated from those strains in comparison with cDNA obtained from the parental strain MG1655 showed similarly intensive bands for the upstream *hycB* gene, as well as for the downstream *hycF* gene (Fig. 4). Despite this analysis not being quantitative, the overall levels of transcripts
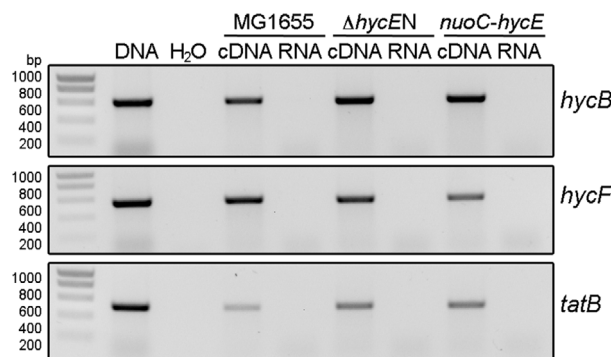
Fig. 4. Transcriptional analysis of the *hyc* operon after genomic modifications. RNA was isolated from strains MG1655, $\Delta hycE$N and *nuoC-hycE*, and reverse transcription was performed and subsequently PCR on the cDNA and, for control of DNA contamination, also from the RNA and water. The transcripts that were analysed are *hycB*, *hycF* and *tatB* as labelled on the right side. The first lane shows the size of the correct PCR fragment when obtained from genomic DNA, and the size of the ladder (SmartLadder; Eurogentec, Seraing, Belgium) is shown on the very left.

were similar, as shown for the transcripts of the constitutive mRNA of the *tatB* gene (Fig. 4). It is concluded, therefore, that the introduced genetic modifications do not alter the transcription of up- and downstream genes within the operon.

Presence of the small subunit protein HycG correlates with the FHL activities

Analysis of the hydrogenase small subunit HycG of the FHL complex by quantitative western blotting showed that the protein amount is subject to change [8]. The absence of HycE in the $\Delta hycE$ strain JW2691 caused an approximate 70% reduction in HycG levels compared to the wild-type (Fig. 5). A similar observation for a $\Delta hycE$ strains was made previously [8]. Generally, for hydrogenase assembly to occur, the large subunit must receive its [NiFe]-cofactor and therefore interact with various delivery proteins and undergo endoproteolytic processing [19,47]. Only then is the protein primed for interaction with its small subunit, and this allows the subsequent initiation of the assembly of the entire FHL complex. However, if processing of the large subunit is delayed or prevented, the small subunit is rapidly degraded [47]. This reduced amount of HycG was also observed in the $\Delta hycE$N strain, both with and without *in trans* complementation, and the *nuoC-hycE* fusion strain (Fig. 5). The strains *hycE*N+C and, to a lesser extent, the complementation of $\Delta hycE$ with pHycE and pHycEN+C show high amounts of HycG, which correlates with their FHL activities. This indicates that the absence of hydrogenase activity, which was observed for some of the HycE variants, correlates with loss of complex integrity and suggests that the N-terminal domain could be the driving force for assembly of the core FeS-carrying proteins.

It is notable in this context that the $\Delta fdhF$ strain JW4040, despite lacking FHL activity due to the absence of the electron-input subunit FdhH, showed high amounts of HycG (Fig. 5). As FdhH is only loosely associated with the FHL complex, this result indicates that this subunit is not required for the stable assembly of the core FHL complex [27] and that the core FHL complex remains stable even without electron flow through the complex.

Removal or separation of NuoC causes complete loss of complex I activity

Based on the findings made with HycE, it was decided to test whether the homologous protein of complex I, NuoCD, also revealed similar properties when the two-domain fusion protein was separated into two
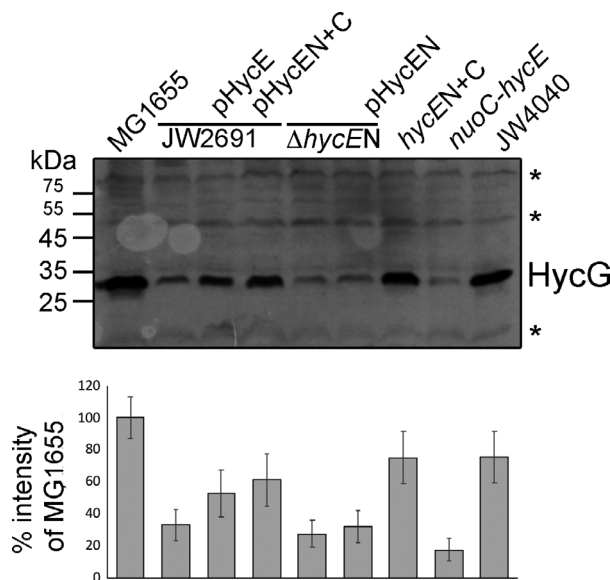
Fig. 5. Analysis of HycG levels in HycE variant strains. The amount of HycG protein from anaerobically grown samples was analysed by western blotting using antibodies raised against HycG. A protein amount of 50 µg of strains MG1655, JW2691 (ΔhycE), ΔhycEN, hycEN+C, nuoC-hycE and JW4040 (ΔfdhF) was separated by SDS/PAGE either directly or after complementation with the plasmids as indicated. Unspecific and nonhydrogenase related cross-reactions of the antibody served as an internal loading control and are indicated by an asterisk on the right side of the panel. The histograms in the lower panel show the quantification of the HycG band intensity (±SD) in comparison with the HycG protein amount in MG1655 using IMAGEJ.

Table 5. NADH and succinate oxidase activity of various *Escherichia coli* complex I deletion strains. The activities were determined from at least two biological replicates.

Strain	NADH oxidase activity (mU· mg protein^{-1})	% Activity of parental	Succinate oxidase activity (mU·mg protein^{-1})
Δ*ndh*	213 ± 12	100	63 ± 14
Δ*ndh*, Δ*nuoC*	3 ± 1	1	50 ± 7
Δ*ndh*, *nuoC+D*	8 ± 2	4	40 ± 15
Δ*ndh*, Δ*nuoC-L*	9 ± 8	4	48 ± 7

oxidase activity of 4%. The two mutant strains Δ*nuoC* and *nuoC + D* had almost no NADH oxidase activity, which indicated a loss of complex I activity (Table 5). A previous study established that deletion of any of the *nuo*-genes encoding complex I abolished its ability to transfer electrons into the respiratory chain [48]. In order to rule out a general effect of the mutations on the respiratory chain, succinate oxidase activity was assessed, which uses succinate dehydrogenase, complex II, instead of complex I to channel electrons into the quinone pool. Succinate oxidase activity was very similar in these strains, ranging from 40 to around 60 mU per mg protein (Table 5), demonstrating that the lack of NADH oxidase activity is specifically due to the absence of complex I.

The detergent-solubilized membrane fractions were subjected to a sucrose gradient centrifugation in order to determine the stability and the assembly of the complex in the mutant strains. The fractions were separately assayed for NADH/ferricyanide oxidoreductase activity, which indicates the presence of the FMN-containing subunit NuoF, which is part of the diaphorase domain of complex I. The activity peaks in fraction 14, corresponding to intact complex I as observed in the Δ*ndh* strain (shaded area in Fig. 6). Complex I mutant strain Δ*nuoC-L*, which lacks the diaphorase proteins NuoEFG, did not show activity in these fractions. Fractions 5–9 contained a broader, more disperse activity peak, which was originally thought to include the diaphorase activity that had dissociated from the complex. However, because it is also present in the membrane preparations of the Δ*nuoC-L* strain, this seems unlikely and rather represents an unspecific reaction of the ferricyanide. Furthermore, the activity profile of the extract from strains Δ*nuoC* and *nuoC + D* resembles the negative control, indicating that NuoF is absent.

Assuming that the mutations could destabilize complex I after extraction from the membrane, but nevertheless allowed retention of a residual activity in whole cells, the strains were subjected to growth experiments

distinct proteins. Strain *nuoC + D,* in which the gene encoding NuoCD was physically separated into two genes, was generated. Additionally, the DNA encoding the NuoC domain was deleted in strain Δ*nuoC* to examine the consequences on complex I assembly and activity. All changes were introduced into a strain lacking the *ndh* gene, which codes for the alternative NADH dehydrogenase, and whose presence would interfere with the NADH oxidase activity assay. As a control, a double-deletion strain Δ*nuoC-L* was constructed, which, in addition to the Δ*ndh* deletion, was also devoid of most of the genes of the *nuo* operon, including *nuoEFG* encoding the diaphorase domain and part of the membrane domain (*nuoHIJKL*).

The functionality of complex I was initially tested by monitoring the NADH oxidase activity, which is catalysed by complex I and the cytochrome *bo₃* and cytochrome *bd* oxidases. The strain Δ*ndh,* lacking the alternative NADH dehydrogenase, showed an activity of 0.2 U·mg^{-1} (Table 5), which also has been observed in a previous study [31]. The negative control strain lacking complex I (strain Δ*nuoC-L*) had only a residual

Fig. 6. Stability of complex I in various *Escherichia coli* deletion mutants. NADH/ferricyanide oxidoreductase activity of sucrose gradient fractions loaded with detergent extracts. The gradients were normalized to a total load of 20 mg protein. The shaded area represents the distribution of holo-complex I (scale right). Strains are Δ*ndh* – grey circles with grey connecting line; Δ*nuoC* – red triangles with black border; *nuoC+D* – black triangles; and Δ*nuoC-L* – grey squares.
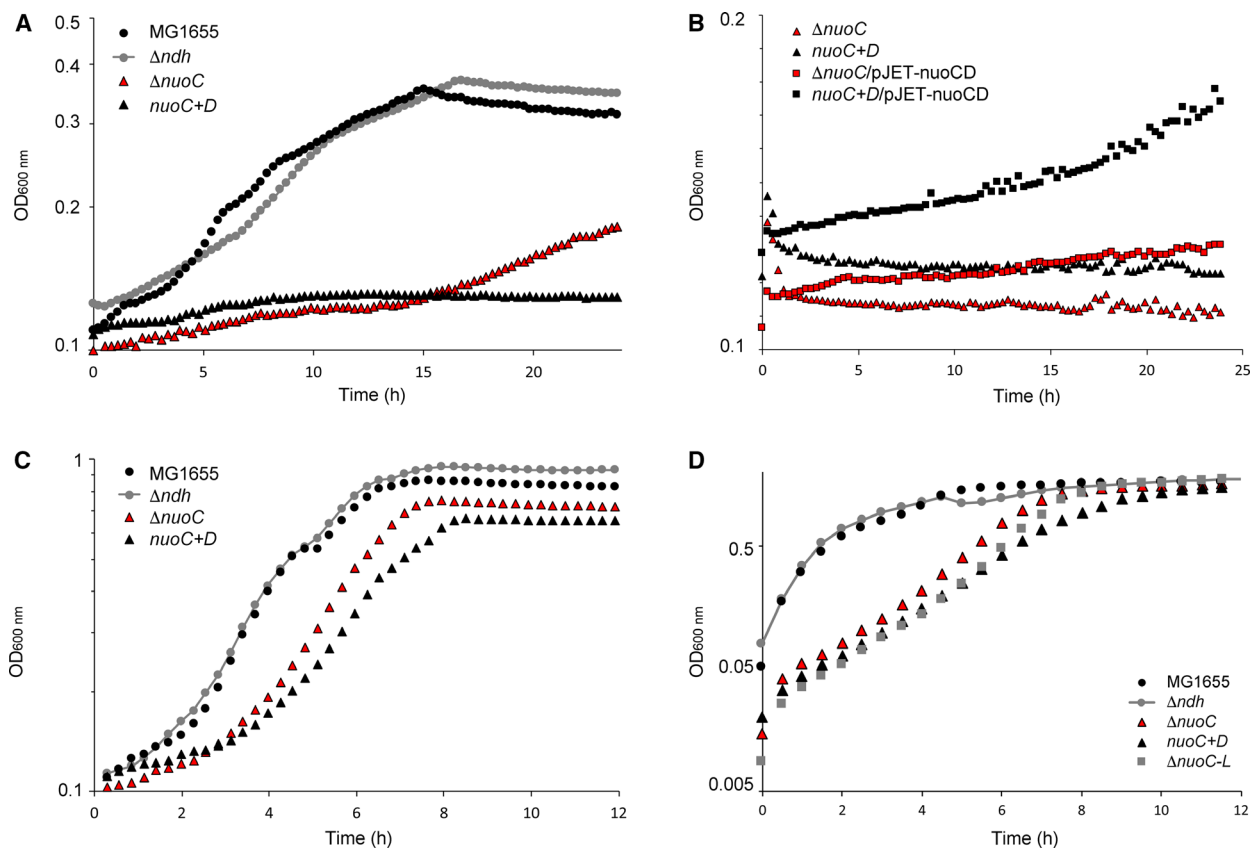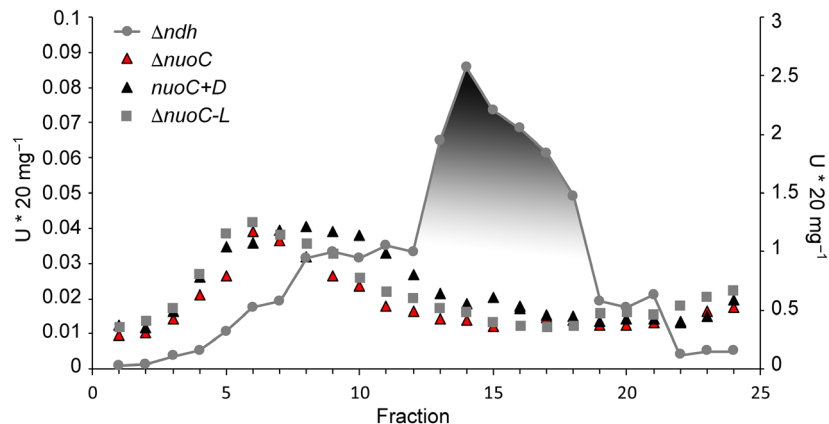
Fig. 7. Aerobic growth phenotype of complex I mutants in (A) in acetate minimal medium (B) after complementation (C) glucose minimal medium and (D) glycerol/LB medium. All growth curves were recorded in a plate reader with 150 r.p.m. shaking in 150 µL volume. The graphs represent the average of three biological triplicates. For all graphs: BW25113 – black circles; Δ*ndh* – grey circles with grey connecting line; Δ*nuoC* – red triangles with black border; *nuoC+D* – black triangles; and Δ*nuoC-L* – grey squares. For panel 7B only: Δ*nuoC*/pJET-nuoCD – red squares with black border; and *nuoC+D*/pJET-nuoCD – black squares.

in an *in vivo* assay (Fig. 7A). The cells were grown aerobically with acetate as sole nonfermentable carbon source, which requires activity of complex I in order to maintain the NADH/NAD$^+$ ratio within the cells. This in turn is necessary for the function of the TCA

cycle and the glyoxylate shunt to produce amino acids [49]. The growth monitoring during 24 h showed that the Δ*ndh* strain had no growth defect compared to the parental strain, as observed before [31]. In contrast, both the Δ*nuoC* strain and the *nuoC + D* strain did not

grow within the first 16 h of the experiment, while eventually the Δ*nuoC* strain showed a slight increase in cell density (Fig. 7A). The absence of growth with acetate, as in the Δ*nuoC* and *nuoC + D* strains, typically indicates lack of complex I activity. A complementation of the strains Δ*nuoC* and *nuoC + D* with a plasmid encoding the *nuoCD* gene, including its ribosome binding site, was attempted (Fig. 7B). However, the growth of the Δ*nuoC* or *nuoC + D* strain on acetate-containing minimal medium could only be restored to a small degree with the *nuoCD* plasmid, attaining optical densities of 0.18 (*nuoC + D*), while the parental strain grew to an OD of 0.33. This could indicate a dominant phenotype of the chromosomal *nuoCD* modification; however, it also does not entirely exclude effects caused by disruption of the *nuo* operon. All strains were in parallel subjected to growth in glucose medium, where they exhibited no difference in growth behaviour (Fig. 7C). Furthermore, glycerol medium was also tested, where the strains still attained the same final optical density in the stationary phase (Fig. 7D). The Δ*ndh* strain and its BW25113 parental derivative grew very similarly, with a growth rate μ of 1.45 and 1.74 h^{-1}, respectively. In contrast, the strains Δ*nuoC*, *nuoC + D* and Δ*nuoC-L* had significantly, but similarly, diminished growth rates of 0.54, 0.46 and 0.52 h^{-1}, respectively.

Therefore, all of the growth experiments indicate that the *nuoC* deletion and separation of *nuoCD* into two genes abolish complex I activity in whole cells in *in vivo* experiments. The absence of activity in the Δ*nuoC* strain was not surprising, because even single amino acid exchanges in NuoC had a similar effect [26]. What was surprising, however, was the different effects of separating the paralogous genes into two parts in the case of FHL and complex I. The FHL complex tolerated the introduced changes, while complex I presumably did not assemble anymore. The region within the proteins where separation of the domains occurred was based on protein alignments and the presence of the Met153 residue in HycE, which was directly hijacked as initiation codon (see alignment in Fig. 2). However, the amino acid sequence in this region is not as conserved as other regions of the protein, and without further structural information of HycE and NuoCD, it is very difficult to predict the location of the loop region and its function in connecting the modules of the complexes.

Conclusions

The research conducted here on the function of the N-terminal domains of the HycE and NuoCD subunits

of the *E. coli* FHL complex and complex I, respectively, reveals that these domains have been evolutionarily conserved and appear to have an important role in complex assembly. It is still not understood what the regulatory steps in the assembly of these large complexes are, but it is reasonable to assume that assembly must involve a highly ordered sequence of events, where accumulated subcomplexes represent intermediate steps [12,50]. The FeS proteins tend to be unstable in the absence of other components, and thus, the nucleation of the core complex (HycB, E, F, G or NuoB, CD, H, I, L) probably starts with the catalytic subunit HycE and its paralogue NuoCD, respectively. These subunits reside next to the membrane interface, while the formate dehydrogenase or NuoEFG proteins represent the last complex-specific steps in the separate evolution of the two complexes and are located further away from the membrane [12]. We identified the N-terminal domains of the HycE and NuoCD proteins as key determinants in initiating the assembly of this core complex. The different effects of splitting the proteins in two parts show that despite the existing phylogenetic relationship between the FHL and complex I, the latter tolerates splitting of the *nuoCD* gene less well.

Acknowledgements

Conflict of interest

The authors declare no conflict of interest.

Author contributions

PS and SB investigated complex I activity; UL, CB and CP investigated FHL activity; TF and CP supervised the study, provided resources and validated the results; and CP wrote the original draft.

References

1 Heringa J and Taylor WR (1997) Three-dimensional domain duplication, swapping and stealing. *Curr Opin Struct Biol* **7**, 416–421.

2 Rosano C, Zuccotti S, Stefani M, Bucciantini M, Ramponi G and Bolognesi M (2002) Crystallization and preliminary X-ray characterization of the acylphosphatase-like domain from the *Escherichia coli* hydrogenase maturation factor HypF. *Acta Crystallogr D Biol Crystallogr* **58**, 524–525.

3 Chiti F, Bucciantini M, Capanni C, Taddei N, Dobson CM and Stefani M (2001) Solution conditions can promote formation of either amyloid protofilaments or mature fibrils from the HypF *N*-terminal domain. *Protein Sci* **10**, 2541–2547.

4 Koo OK, Jeong D-W, Lee JM, Kim MJ, Lee J-H, Chang HC, Kim JH and Lee HJ (2005) Cloning and characterization of the bifunctional alcohol/acetaldehyde dehydrogenase gene (*adhE*) in *Leuconostoc mesenteroides* isolated from kimchi. *Biotechnol Lett* **27**, 505–510.

5 Sawers RG and Clark D (2004) Fermentative pyruvate and acetyl-coenzyme A metabolism. In *EcoSal – Escherichia coli and Salmonella: Cellular and Molecular Biology* (Stewart V ed). Chapter 3.5.4. American Society for Microbiology, Washington, DC. https://doi.org/10.1128/ecosalplus.3.5.

6 Marsh JA, Hernández H, Hall Z, Ahnert SE, Perica T, Robinson CV and Teichmann SA (2013) Protein complexes are under evolutionary selection to assemble via ordered pathways. *Cell* **153**, 461–470.

7 Pinske C and Sawers RG (2016) Anaerobic formate and hydrogen metabolism. In *EcoSal Plus2016* (Stewart V ed). American Society for Micrbiology, Washington, DC, ESP–0011–2016.

8 Sauter M, Böhm R and Böck A (1992) Mutational analysis of the operon (*hyc*) determining hydrogenase 3 formation in *Escherichia coli*. *Mol Microbiol* **6**, 1523–1532.

9 Marreiros BC, Batista AP, Duarte AMS and Pereira MM (2012) A missing link between complex I and group 4 membrane-bound [NiFe] hydrogenases. *Biochim Biophys Acta* **1827**, 198–209.

10 Böhm R, Sauter M and Böck A (1990) Nucleotide sequence and expression of an operon in *Escherichia coli* coding for formate hydrogenlyase components. *Mol Microbiol* **4**, 231–243.

11 Albracht SP (1993) Intimate relationships of the large and the small subunits of all nickel hydrogenases with two nuclear-encoded subunits of mitochondrial NADH: ubiquinone oxidoreductase. *Biochim Biophys Acta* **1144**, 221–224.

12 Friedrich T and Scheide D (2000) The respiratory complex I of bacteria, archaea and eukarya and its module common with membrane-bound multisubunit hydrogenases. *FEBS Lett* **479**, 1–5.

13 Hirst J (2013) Mitochondrial complex I. *Annu Rev Biochem* **82**, 551–575.

14 Moparthi V and Hägerhäll C (2011) The evolution of respiratory chain complex I from a smaller last

common ancestor consisting of 11 protein subunits. *J Mol Evol* **72**, 484–497.

15 Baradaran R, Berrisford JM, Minhas GS and Sazanov LA (2013) Crystal structure of the entire respiratory complex I. *Nature* **494**, 443–448.

16 Sazanov LA and Hinchliffe P (2006) Structure of the hydrophilic domain of respiratory complex I from *Thermus thermophilus*. *Science* **311**, 1430–1436.

17 Yu H, Wu C-H, Schut GJ, Haja DK, Zhao G, Peters JW, Adams MWW and Li H (2018) Structure of an ancient respiratory system. *Cell* **173**, 1636–1649.e16.

18 Forzi L and Sawers RG (2007) Maturation of [NiFe]-hydrogenases in *Escherichia coli*. *Biometals* **20**, 565–578.

19 Sawers RG and Pinske C (2017) NiFe-hydrogenase assembly. In *Encyclopedia of Inorganic and Bioinorganic Chemistry*. John Wiley & Sons, Ltd, Hoboken, NJ. https://doi.org/10.1002/9781119951438.eibc2484.

20 Drapal N and Böck A (1998) Interaction of the hydrogenase accessory protein HypC with HycE, the large subunit of *Escherichia coli* hydrogenase 3 during enzyme maturation. *Biochemistry* **37**, 2941–2948.

21 Chan Chung KC and Zamble DB (2011) Protein interactions and localization of the *Escherichia coli* accessory protein HypA during nickel insertion to [NiFe] hydrogenase. *J Biol Chem* **286**, 43081–43090.

22 Rossmann R, Sauter M, Lottspeich F and Böck A (1994) Maturation of the large subunit (HYCE) of *Escherichia coli* hydrogenase 3 requires nickel incorporation followed by C-terminal processing at Arg537. *Eur J Biochem* **220**, 377–384.

23 Kwon S, Watanabe S, Nishitani Y, Kawashima T, Kanai T, Atomi H and Miki K (2018) Crystal structures of a [NiFe] hydrogenase large subunit HyhL in an immature state in complex with a Ni chaperone HypA. *Proc Natl Acad Sci USA* **115**, 7045–7050.

24 Albareda M, Pacios LF and Palacios JM (2019) Computational analyses, molecular dynamics, and mutagenesis studies of unprocessed form of [NiFe] hydrogenase reveal the role of disorder for efficient enzyme maturation. *Biochim Biophys Acta Bioenerg* **1860**, 325–340.

25 Finn RD, Attwood TK, Babbitt PC, Bateman A, Bork P, Bridge AJ, Chang HY, Dosztányi Z, El-Gebali S, Fraser M *et al.* (2017) InterPro in 2017—beyond protein family and domain annotations. *Nucleic Acids Res* **45**, D190–D199.

26 Castro-Guerrero N, Sinha PK, Torres-Bacete J, Matsuno-Yagi A and Yagi T (2010) Pivotal roles of three conserved carboxyl residues of the NuoC (30k) segment in the structural integrity of proton-translocating NADH-quinone oxidoreductase from *Escherichia coli*. *Biochemistry* **49**, 10072–10080.

27 McDowall JS, Murphy BJ, Haumann M, Palmer T, Armstrong FA and Sargent F (2014) Bacterial formate

hydrogenlyase complex. *Proc Natl Acad Sci USA* **111**, E3948–E3956.

28 Maeda T, Sanchez-Torres V and Wood TK (2008) Protein engineering of hydrogenase 3 to enhance hydrogen production. *Appl Microbiol Biotechnol* **79**, 77–86.

29 Begg YA, Whyte JN and Haddock BA (1977) The identification of mutants of *Escherichia coli* deficient in formate dehydrogenase and nitrate reductase activities using dye indicator plates. *FEMS Microbiol Lett* **2**, 47–50.

30 Hamilton CM, Aldea M, Washburn BK, Babitzke P and Kushner SR (1989) New method for generating deletions and gene replacements in *Escherichia coli*. *J Bacteriol* **171**, 4617–4622.

31 Burschel S, Kreuzer Decovic D, Nuber F, Stiller M, Hofmann M, Zupok A, Siemiatkowska B, Gorka M, Leimkühler S and Friedrich T (2019) Iron-sulfur cluster carrier proteins involved in the assembly of *Escherichia coli* NADH:ubiquinone oxidoreductase (complex I). *Mol Microbiol* **111**, 31–45.

32 Cherepanov P and Wackernagel W (1995) Gene disruption in *Escherichia coli*: Tc^R and Km^R cassettes with the option of Flp-catalyzed excision of the antibiotic-resistance determinant. *Gene* **158**, 9–14.

33 Datsenko K and Wanner B (2000) One-step inactivation of chromosomal genes in *Escherichia coli* K-12 using PCR products. *Proc Natl Acad Sci USA* **97**, 6640–6645.

34 Lindenstrauß U, Skorupa P, McDowall JS, Sargent F and Pinske C (2017) The dual-function chaperone HycH improves assembly of the formate hydrogenlyase complex. *Biochem J* **474**, 2937–2950.

35 Laemmli U (1970) Cleavage of structural proteins during the assembly of the head of bacteriophage T4. *Nature* **227**, 680–685.

36 Towbin H, Staehelin T and Gordon J (1979) Electrophoretic transfer of proteins from polyacrylamide gels to nitrocellulose sheets: procedure and some applications. *Proc Natl Acad Sci USA* **76**, 4350–4354.

37 Abràmoff M, Magalhaes P and Ram S (2004) Image processing with ImageJ. *Biophoton Int* **11**, 36–42.

38 Ballantine S and Boxer D (1985) Nickel-containing hydrogenase isoenzymes from anaerobically grown *Escherichia coli* K-12. *J Bacteriol* **163**, 454–459.

39 Pinske C (2018) The ferredoxin-like proteins HydN and YsaA enhance redox dye-linked activity of the formate dehydrogenase H component of the formate hydrogenlyase complex. *Front Microbiol* **9**, 1238.

40 Lowry O, Rosebrough N, Farr A and Randall R (1951) Protein measurement with the Folin phenol reagent. *J Biol Chem* **193**, 265–275.

41 Lubran MM (1978) The measurement of total serum proteins by the Biuret method. *Ann Clin Lab Sci* **8**, 106–110.

42 Pinske C, Krüger S, Soboh B, Ihling C, Kuhns M, Braussemann M, Jaroschinsky M, Sauer C, Sargent F, Sinz A *et al.* (2011) Efficient electron transfer from hydrogen to benzyl viologen by the [NiFe]-hydrogenases of *Escherichia coli* is dependent on the coexpression of the iron-sulfur cluster-containing small subunit. *Arch Microbiol* **193**, 893–903.

43 Andrews SC, Berks BC, McClay J, Ambler A, Quail MA, Golby P and Guest JR (1997) A 12-cistron *Escherichia coli* operon (*hyf*) encoding a putative proton-translocating formate hydrogenlyase system. *Microbiology* **143** (Pt 11), 3633–3647.

44 Redwood MD, Mikheenko IP, Sargent F and Macaskie LE (2008) Dissecting the roles of *Escherichia coli* hydrogenases in biohydrogen production. *FEMS Microbiol Lett* **278**, 48–55.

45 Sawers RG (2006) Differential turnover of the multiple processed transcripts of the *Escherichia coli* foc A-*pflB* operon. *Microbiology* **152**, 2197–2205.

46 Huerta AM and Collado-Vides J (2003) Sigma70 promoters in *Escherichia coli*: specific transcription in dense regions of overlapping promoter-like signals. *J Mol Biol* **333**, 261–278.

47 Pinske C and Sawers RG (2014) The importance of iron in the biosynthesis and assembly of [NiFe]-hydrogenases. *Biomol Concepts* **5**, 55–70.

48 Erhardt H, Steimle S, Muders V, Pohl T, Walter J and Friedrich T (2012) Disruption of individual *nuo*-genes leads to the formation of partially assembled NADH:ubiquinone oxidoreductase (complex I) in *Escherichia coli*. *Biochim Biophys Acta* **1817**, 863–871.

49 Prüß BM, Nelms JM, Park C and Wolfe AJ (1994) Mutations in NADH:ubiquinone oxidoreductase of *Escherichia coli* affect growth on mixed amino acids. *J Bacteriol* **176**, 2143–2150.

50 McDowall JS, Hjersing MC, Palmer T and Sargent F (2015) Dissection and engineering of the *Escherichia coli* formate hydrogenlyase complex. *FEBS Lett* **589**, 3141–3147.

51 Yachdav G, Kloppmann E, Kajan L, Hecht M, Goldberg T, Hamp T, Hönigschmid P, Schafferhans A, Roos M, Bernhofer M *et al.* (2014) PredictProtein – an open resource for online prediction of protein structural and functional features. *Nucleic Acids Res* **42**, W337–W343.

52 Waterhouse AM, Procter JB, Martin DMA, Clamp M and Barton GJ (2009) Jalview version 2 – a multiple sequence alignment editor and analysis workbench. *Bioinformatics* **25**, 1189–1191.

53 Blattner FR, Plunkett G, Bloch CA, Perna NT, Burland V, Riley M, Collado-Vides J, Glasner JD, Rode CK, Mayhew GF *et al.* (1997) The complete genome sequence of *Escherichia coli* K-12. *Science* **277**, 1453–1462.

54 Baba T, Ara T, Hasegawa M, Takai Y, Okumura Y, Baba M, Datsenko K, Tomita M, Wanner B and Mori H (2006) Construction of *Escherichia coli* K-12 in-frame, single-gene knockout mutants: the Keio collection. *Mol Syst Biol* **2**, 2006 0008.

55 Sievers F, Wilm A, Dineen D, Gibson TJ, Karplus K, Li W, Lopez R, McWilliam H, Remmert M and Söding J *et al.* (2011) Fast, scalable generation of high-quality protein multiple sequence alignments using Clustal Omega. *Mol Syst Biol* **7**, 539.

Kapitel VI – Phänotyp von HycH

Das Doppelfunktions-Chaperon HycH verbessert die Assemblierung des Formiat Hydrogenlyase Komplexes

Ute Lindenstrauß[a], Philipp Skorupa[a], Jennifer S. McDowall[b], Frank Sargent[b] und Constanze Pinske[a,*]

[a] Institut für Biologie/Mikrobiologie, Martin-Luther-Universität Halle-Wittenberg, 06108 Halle, Deutschland, Kurt-Mothes-Str. 3, 06120 Halle/Saale, Deutschland
[b] University of Dundee; School of Life Sciences; Division of Molecular Microbiology; Dow Street; DD1 5EH Dundee, UK

* Korrespondierende Autorin: Constanze Pinske

Zusammenfassung:

Der Aufbau von Multiproteinkomplexen erfordert die konzertierte Synthese und Reifung ihrer Komponenten sowie deren koordinierte Wechselwirkung. Der membrangebundene Formiat-Hydrogenlyase (FHL)-Komplex ist das primäre wasserstoffproduzierende Enzym in *Escherichia coli* und besteht aus sieben Untereinheiten, die hauptsächlich im *hycA-I*-Operon der [NiFe]-Hydrogenase-3 (Hyd-3) kodiert sind. Das HycH-Protein hat eine akzessorische Funktion und ist nicht Teil des finalen strukturellen FHL-Komplexes. Hier wurde ein Mutantenstamm ohne HycH charakterisiert und festgestellt, dass er aufgrund der Instabilität der Elektronentransfer-Untereinheiten eine signifikant verringerte FHL-Aktivität aufwies. Es wurde gezeigt, dass HycH in verschiedenen Stadien während der Reifung und des Zusammenbaus des Komplexes spezifisch mit dem Apo-Protein HycE, der katalytischen Hydrogenase-Untereinheit des FHL-Komplexes, interagiert. Varianten von HycH wurden mit dem Ziel erzeugt, interagierende Reste und solche, welche die Aktivität beeinflussen, zu identifizieren. Bei Austausch der Reste R70/71/K72, Y79, E81 und Y128 war die Interaktion mit HycE gestört, ohne dabei die FHL-Aktivität zu beeinflussen. Im Gegensatz dazu wurde die FHL-Aktivität, jedoch nicht die Wechselwirkung mit HycE, durch den H37-Austausch gegen polare Resten negativ beeinflusst. Schließlich wurde festgestellt, dass eine HycH Y30-Variante instabil war. Zudem konnte eine überlappende Funktion zwischen HycH und seinem homologen Gegenstück HyfJ aus dem für [NiFe]-Hydrogenase 4 (Hyd-4) kodierenden Operon identifiziert werden. Dies ist das erste Beispiel für die gemeinsame Nutzung von Reifungsmaschinerie-Komponenten zwischen Hyd-3- und Hyd-4-Komplexen. Die hier präsentierten Daten zeigen, dass HycH eine neuartige Doppelrolle als Assemblierungs-Chaperon für eine cytoplasmatische [NiFe]-Hydrogenase spielt.

Bedeutung

Die biologische Wasserstoffproduktion in Kombination mit moderner Brennstoffzellentechnologie könnte unsere Energienutzung dauerhaft verändern.

Bakteriell hergestellter Wasserstoff stammt aus der Aktivität von Hydrogenasen, bei denen es sich um metallhaltige Enzymkomplexe mit mehreren Untereinheiten handelt. Die Nutzung dieses Wasserstoffs erfordert ein detailliertes molekulares Verständnis der Kofaktor-Insertion, Kenntnis der Reihenfolge der Assemblierung und wie dies zur Optimierung der Aktivität verwendet werden kann. Hier nutzen wir den Modellorganismus *Escherichia coli*, um die Proteine zu untersuchen, die an der Assemblierung des sieben Untereinheiten enthaltenden Formiat-Hydrogenlyase-Komplexes für die H_2-Produktion beteiligt sind. Wir haben das HycH-Protein als Interaktionspartner für die katalytische Untereinheit identifiziert, bevor diese mit den Elektronentransfer-Untereinheiten interagiert. Unsere Ergebnisse liefern neue Einblicke in die Anforderungen eines Metalloenzymkomplexes mit mehreren Untereinheiten.

Research Article

The dual-function chaperone HycH improves assembly of the formate hydrogenlyase complex

Ute Lindenstrauß[1], Philipp Skorupa[1], Jennifer S. McDowall[2], Frank Sargent[2] and Constanze Pinske[1]

[1]Martin-Luther University Halle-Wittenberg, Institute of Biology/Microbiology, Kurt-Mothes-Str. 3, 06120 Halle, Germany; [2]School of Life Sciences, Division of Molecular Microbiology, University of Dundee, Dow Street, DD1 5EH Dundee, U.K.

Correspondence: Constanze Pinske (constanze.pinske@mikrobiologie.uni-halle.de)

The assembly of multi-protein complexes requires the concerted synthesis and maturation of its components and subsequently their co-ordinated interaction. The membrane-bound formate hydrogenlyase (FHL) complex is the primary hydrogen-producing enzyme in *Escherichia coli* and is composed of seven subunits mostly encoded within the *hycA-I* operon for [NiFe]-hydrogenase-3 (Hyd-3). The HycH protein is predicted to have an accessory function and is not part of the final structural FHL complex. In this work, a mutant strain devoid of HycH was characterised and found to have significantly reduced FHL activity due to the instability of the electron transfer subunits. HycH was shown to interact specifically with the unprocessed species of HycE, the catalytic hydrogenase subunit of the FHL complex, at different stages during the maturation and assembly of the complex. Variants of HycH were generated with the aim of identifying interacting residues and those that influence activity. The R70/71/K72, the Y79, the E81 and the Y128 variant exchanges interrupt the interaction with HycE without influencing the FHL activity. In contrast, FHL activity, but not the interaction with HycE, was negatively influenced by H37 exchanges with polar residues. Finally, a HycH Y30 variant was unstable. Surprisingly, an overlapping function between HycH with its homologous counterpart HyfJ from the operon encoding [NiFe]-hydrogenase-4 (Hyd-4) was identified and this is the first example of sharing maturation machinery components between Hyd-3 and Hyd-4 complexes. The data presented here show that HycH has a novel dual role as an assembly chaperone for a cytoplasmic [NiFe]-hydrogenase.

Die Publikation kann unter https://portlandpress.com/biochemj/article/474/17/2937/49490/The-dual-function-chaperone-HycH-improves-assembly aufgerufen werden. Sie nimmt die Seiten 97-110 der Druckversion der Habilitationsschrift ein.

Bibliographie

Abou Hamdan A, Dementin S, Liebgott P-P, Gutierrez-Sanz O, Richaud P, De Lacey AL, Rousset M, Bertrand P, Cournac L & Léger C (2012) Understanding and tuning the catalytic bias of hydrogenase. *J Am Chem Soc* **134:** 8368–8371

Adamson H, Robinson M, Wright JJ, Flanagan LA, Walton J, Elton D, Gavaghan DJ, Bond AM, Roessler MM & Parkin A (2017) Retuning the catalytic bias and overpotential of a [NiFe]-hydrogenase via a single amino acid exchange at the electron entry/exit site. *J Am Chem Soc* **139:** 10677–10686

Andrews SC, Berks BC, McClay J, Ambler A, Quail MA, Golby P & Guest JR (1997) A 12-cistron *Escherichia coli* operon (*hyf*) encoding a putative proton-translocating formate hydrogenlyase system. *Microbiology (Reading, Engl)* **143 (Pt 11):** 3633–3647

Bagramyan K, Mnatsakanyan N, Poladian A, Vassilian A & Trchounian A (2002) The roles of hydrogenases 3 and 4, and the F_0F_1-ATPase, in H_2 production by *Escherichia coli* at alkaline and acidic pH. *FEBS Lett* **516:** 172–178

Bagramyan K, Vassilian A, Mnatsakanyan N & Trchounian A (2001) Participation of *hyf*-encoded hydrogenase 4 in molecular hydrogen release coupled with proton-potassium exchange in *Escherichia coli*. *Membrane & cell biology* **14:** 749–763

Batista AP, Marreiros BC & Pereira MM (2013) The antiporter-like subunit constituent of the universal adaptor of complex I, group 4 membrane-bound [NiFe]-hydrogenases and related complexes. *Biol Chem* **394:** 659–666

Bay SK, Dong X, Bradley JA, Leung PM, Grinter R, Jirapanjawat T, Arndt SK, Cook PLM, LaRowe DE, Nauer PA, Chiri E & Greening C (2021) Trace gas oxidizers are widespread and active members of soil microbial communities. *Nat Microbiol* **6:** 246–256

Beaton SE, Evans RM, Finney AJ, Lamont CM, Armstrong FA, Sargent F & Carr SB (2018) The structure of hydrogenase-2 from *Escherichia coli*: implications for H_2-driven proton pumping. *Biochem J* **475:** 1353–1370

Benoit SL, Maier RJ, Sawers RG & Greening C (2020) Molecular hydrogen metabolism: a widespread trait of pathogenic bacteria and protists. *Microbiol Mol Biol Rev* **84:** 100

Beyer L, Doberenz C, Falke D, Hunger D, Suppmann B & Sawers RG (2013) Coordination of FocA and pyruvate formate-lyase synthesis in *Escherichia coli* demonstrates preferential translocation of formate over other mixed-acid fermentation products. *J Bacteriol* **195:** 1428–1435

Böck A, Forchhammer K, Heider J, Leinfelder W, Sawers RG, Veprek B & Zinoni F (1991) Selenocysteine: the 21st amino acid. *Mol Microbiol* **5:** 515–520

Böck A, King PW, Blokesch M & Posewitz MC (2006) Maturation of hydrogenases. *Adv Microb Physiol* **51:** 1–71

Böhm R, Sauter M & Böck A (1990) Nucleotide sequence and expression of an operon in *Escherichia coli* coding for formate hydrogenlyase components. *Mol Microbiol* **4:** 231–243

Brandt U & Trumpower B (1994) The protonmotive Q cycle in mitochondria and bacteria. *Crit Rev Biochem Mol Biol* **29:** 165–197

Brenner DJ & Farmer JJ III (2015). *Enterobacteriaceae* . In Bergey's Manual of Systematics of Archaea and Bacteria (eds ME Trujillo, S Dedysh, P DeVos, B Hedlund, P Kämpfer, FA Rainey & WB Whitman). https://doi.org/10.1002/9781118960608.fbm00222

Buckel W & Thauer RK (2018) Flavin-based electron bifurcation, ferredoxin, flavodoxin, and anaerobic respiration with protons (Ech) or NAD^+ (Rnf) as electron acceptors: A historical review. *Front Microbiol* **9:** 3704

Burton R, Can M, Esckilsen D, Wiley S & Ragsdale SW (2018) Production and properties of enzymes that activate and produce carbon monoxide. *Meth Enzymol* **613:** 297–324

Caserta G, Lorent C, Pelmenschikov V, Schoknecht J, Yoda Y, Hildebrandt P, Cramer SP, Zebger I & Lenz O (2020) *In vitro* assembly as a tool to investigate catalytic intermediates of [NiFe]-hydrogenase. *ACS Catal.:* 13890–13894

Dreier JP, Major S, Foreman B, Winkler MKL, Kang E-J, Milakara D, Lemale CL, DiNapoli V, Hinzman JM, Woitzik J, Andaluz N, Carlson A & Hartings JA (2018) Terminal spreading depolarization and electrical silence in death of human cerebral cortex. *Ann Neurol* **83:** 295–310

Duarte AG, Catarino T, White GF, Lousa D, Neukirchen S, Soares CM, Sousa FL, Clarke TA & Pereira IAC (2018) An electrogenic redox loop in sulfate reduction reveals a likely widespread mechanism of energy conservation. *Nature Communications* **9:** 5448

Dubini A & Sargent F (2003) Assembly of Tat-dependent [NiFe] hydrogenases: identification of precursor-binding accessory proteins. *FEBS Lett* **549:** 141–146

Dubini A, Pye R, Jack R, Palmer T & Sargent F (2002) How bacteria get energy from hydrogen: a genetic analysis of periplasmic hydrogen oxidation in *Escherichia coli*. *International Journal of Hydrogen Energy* **27:** 1413–1420

Finney AJ & Sargent F (2019) Formate hydrogenlyase: A group 4 [NiFe]-hydrogenase in tandem with a formate dehydrogenase. *Adv Microb Physiol* **74:** 465–486

Finney AJ, Buchanan G, Palmer T, Coulthurst SJ & Sargent F (2020) Activation of a [NiFe]-hydrogenase-4 isoenzyme by maturation proteases. *Microbiology (Reading, Engl)* **14:** 749

Finney AJ, Lowden R, Fleszar M, Albareda M, Coulthurst SJ & Sargent F (2019) The plant pathogen *Pectobacterium atrosepticum* contains a functional formate hydrogenlyase-2 complex. *Mol Microbiol* **112:** 1440–1452

Forzi L & Sawers RG (2007) Maturation of [NiFe]-hydrogenases in *Escherichia coli*. *Biometals* **20:** 565–578

Friedrich T & Scheide D (2000) The respiratory complex I of bacteria, archaea and eukarya and its module common with membrane-bound multisubunit hydrogenases. *FEBS Lett* **479:** 1–5

Fuchs G, Hrsg. Allgemeine Mikrobiologie. 10., unveränderte Auflage. Stuttgart: Thieme; 2017.

Fujishiro T, Bai L, Xu T, Xie X, Schick M, Kahnt J, Rother M, Hu X, Ermler U & Shima S (2016) Identification of HcgC as a SAM-dependent pyridinol methyltransferase in [Fe]-hydrogenase cofactor biosynthesis. *Angew Chem Int Ed Engl* **55:** 9648–9651

Fujishiro T, Ermler U & Shima S (2014) A possible iron delivery function of the dinuclear iron center of HcgD in [Fe]-hydrogenase cofactor biosynthesis. *FEBS Lett* **588:** 2789–2793

Fujishiro T, Tamura H, Schick M, Kahnt J, Xie X, Ermler U & Shima S (2013) Identification of the HcgB enzyme in [Fe]-hydrogenase-cofactor biosynthesis. *Angew Chem Int Ed Engl* **52:** 12555–12558

Gilbert JA & Neufeld JD (2014) Life in a World without Microbes. *PLoS Biol.* **12:** e1002020

Greening C, Biswas A, Carere CR, Jackson CJ, Taylor MC, Stott MB, Cook GM & Morales SE (2016) Genomic and metagenomic surveys of hydrogenase distribution indicate H_2 is a widely utilised energy source for microbial growth and survival. *The ISME journal* **10:** 761–777

Greening C, Villas-Bôas SG, Robson JR, Berney M & Cook GM (2014) The growth and survival of *Mycobacterium smegmatis* is enhanced by co-metabolism of atmospheric H_2. *PLoS ONE* **9:** e103034

Hedderich R & Forzi L (2005) Energy-converting [NiFe] hydrogenases: more than just H_2 activation. *J Mol Microbiol Biotechnol* **10:** 92–104

Herrmann G, Jayamani E, Mai G & Buckel W (2008) Energy conservation via electron-transferring flavoprotein in anaerobic bacteria. *J Bacteriol* **190:** 784–791

Jormakka M, Byrne B & Iwata S (2003) Protonmotive force generation by a redox loop mechanism. *FEBS Lett* **545:** 25–30

Kampjut D & Sazanov LA (2020) The coupling mechanism of mammalian respiratory complex I. *Science* **370:** eabc4209

Kim YJ, Lee HS, Kim ES, Bae SS, Lim JK, Matsumi R, Lebedinsky AV, Sokolova TG, Kozhevnikova DA, Cha S-S, Kim S-J, Kwon KK, Imanaka T, Atomi H, Bonch-Osmolovskaya EA, Lee J-H & Kang SG (2010) Formate-driven growth coupled with H_2 production. *Nature* **467:** 352–355

Kleinhaus JT, Wittkamp F, Yadav S, Siegmund D & Apfel U-P (2020) [FeFe]-Hydrogenases: maturation and reactivity of enzymatic systems and overview of biomimetic models. *Chemical Society Reviews* **114:** 4081

Konings WN (2002) The cell membrane and the struggle for life of lactic acid bacteria. In *Lactic Acid Bacteria: Genetics, Metabolism and Applications* pp 3–27. Dordrecht: Springer, Dordrecht

Kuchenreuther JM, George SJ, Grady-Smith CS, Cramer SP & Swartz JR (2011) Cell-free H-cluster synthesis and [FeFe] hydrogenase activation: all five CO and CN^- ligands derive from tyrosine. *PLoS ONE* **6:** e20346

Kwon S, Watanabe S, Nishitani Y, Kawashima T, Kanai T, Atomi H & Miki K (2018) Crystal structures of a [NiFe] hydrogenase large subunit HyhL in an immature state in complex with a Ni chaperone HypA. *Proc Natl Acad Sci USA* **115:** 7045–7050

Lacasse MJ & Zamble DB (2016) [NiFe]-hydrogenase maturation. *Biochemistry* **55:** 1689–1701

Lim JK, Mayer F, Kang SG & Müller V (2014) Energy conservation by oxidation of formate to carbon dioxide and hydrogen via a sodium ion current in a hyperthermophilic archaeon. *Proc Natl Acad Sci USA* **111:** 11497–11502

Lin W-Y & Liaw S-J (2020) Deacidification by FhlA-dependent hydrogenase is involved in urease activity and urinary stone formation in uropathogenic *Proteus mirabilis*. *Sci Rep* **10:** 1–14

Lindenstrauß U & Pinske C (2019) Dissection of the hydrogen metabolism of the enterobacterium *Trabulsiella guamensis*: Identification of a formate-dependent and essential formate hydrogenlyase complex exhibiting phylogenetic similarity to complex I. *J Bacteriol* **201:** 1480

Lindenstrauß U, Skorupa P, McDowall JS, Sargent F & Pinske C (2017) The dual-function chaperone HycH improves assembly of the formate hydrogenlyase complex. *Biochem J* **474:** 2937–2950

Lubek D, Simon AH & Pinske C (2019) Amino acid variants of the HybB membrane subunit of *Escherichia coli* [NiFe]-hydrogenase-2 support a role in proton transfer. *FEBS Lett* **156:** 2194–2203

Lubitz W, Ogata H, Rüdiger O & Reijerse E (2014) Hydrogenases. *Chem Rev* **114:** 4081–4148

Magalon A & Mendel RR. Biosynthesis and Insertion of the Molybdenum Cofactor. In *EcoSal Plus. 2015;6(2)*. V. Stewart (Ed.), doi: 10.1128/ecosalplus.ESP-0006-2013.

Maier L, Vyas R, Cordova CD, Lindsay H, Schmidt TSB, Brugiroux S, Periaswamy B, Bauer R, Sturm A, Schreiber F, Mering von C, Robinson MD, Stecher B & Hardt W-D (2013) Microbiota-derived hydrogen fuels *Salmonella* Typhimurium invasion of the gut ecosystem. *Cell Host Microbe* **14:** 641–651

Marloth JT & Pinske C (2020) Susceptibility of the formate hydrogenlyase reaction to the protonophore CCCP depends on the total hydrogenase composition. *Inorganics* **8:** 38

Marreiros BC, Batista AP, Duarte AMS & Pereira MM (2012) A missing link between complex I and group 4 membrane-bound [NiFe] hydrogenases. *Biochim Biophys Acta* **1827:** 198–209

McWhorter AC, Haddock RL, Nocon FA, Steigerwalt AG, Brenner DJ, Aleksić S, Bockemühl J & Farmer JJ (1991) *Trabulsiella guamensis*, a new genus and species of the family *Enterobacteriaceae* that resembles *Salmonella* subgroups 4 and 5. *J Clin Microbiol* **29:** 1480–1485

Menon NK, Chatelus CY, Dervartanian M, Wendt JC, Shanmugam KT, Peck HD & Przybyla AE (1994) Cloning, sequencing, and mutational analysis of the *hyb* operon encoding *Escherichia coli* hydrogenase 2. *J Bacteriol* **176:** 4416–4423

Miki K, Atomi H & Watanabe S (2020) Structural insight into [NiFe] hydrogenase maturation by transient complexes between Hyp Proteins. *Acc. Chem. Res.* **53:** 875–886

Mitchell P (1961) Coupling of phosphorylation to electron and hydrogen transfer by a chemi-osmotic type of mechanism. *Nature* **191:** 144–148

Nutschan K, Golbik RP & Sawers RG (2019) The iron-sulfur-containing HypC-HypD scaffold complex of the [NiFe]-hydrogenase maturation machinery is an ATPase. *FEBS Open Bio* **193:** 265

Padan E & Landau M (2016) Sodium-proton (Na^+/H^+) antiporters: Properties and roles in health and disease. *Met Ions Life Sci* **16:** 391–458

Peters JW, Schut GJ, Boyd ES, Mulder DW, Shepard EM, Broderick JB, King PW & Adams MWW (2015) [FeFe]- and [NiFe]-hydrogenase diversity, mechanism, and maturation. *Biochim Biophys Acta* **1853:** 1350–1369

Pinske C (2019) Bioenergetic aspects of archaeal and bacterial hydrogen metabolism. *Adv Microb Physiol* **74:** 487–514

Pinske C & Sargent F (2016) Exploring the directionality of *Escherichia coli* formate hydrogenlyase: a membrane-bound enzyme capable of fixing carbon dioxide to organic acid. *Microbiologyopen* **5:** 721–737

Pinske C & Sawers RG (2014). The importance of iron in the biosynthesis and assembly of [NiFe]-hydrogenases. *Biomolecular Concepts* 5, 1, 55-70, Available From: De Gruyter https://doi.org/10.1515/bmc-2014-0001

Pinske C & Sawers R. 2016. Anaerobic Formate and Hydrogen Metabolism, In *EcoSal Plus 2016,* V. Stewart (Ed.); doi:10.1128/ecosalplus.ESP-0011-2016

Pinske C, Jaroschinsky M, Linek S, Kelly CL, Sargent F & Sawers RG (2015a) Physiology and bioenergetics of [NiFe]-hydrogenase 2-catalyzed H_2-consuming and H_2-producing reactions in *Escherichia coli. J Bacteriol* **197:** 296–306

Pinske C, Krüger S, Soboh B, Ihling C, Kuhns M, Braussemann M, Jaroschinsky M, Sauer C, Sargent F, Sinz A & Sawers RG (2011) Efficient electron transfer from hydrogen to benzyl viologen by the [NiFe]-hydrogenases of *Escherichia coli* is dependent on the coexpression of the iron-sulfur cluster-containing small subunit. *Arch Microbiol* **193:** 893–903

Pinske C, Sargent F & Sawers RG (2015b) SlyD-dependent nickel delivery limits maturation of [NiFe]-hydrogenases in late-stationary phase *Escherichia coli* cells. *Metallomics* **7:** 683–690

Pinske C, Thomas C, Nutschan K & Sawers RG (2019) Delimiting the function of the *C*-terminal extension of the *Escherichia coli* [NiFe]-hydrogenase 2 large subunit precursor. *Front Microbiol* **10:** 2223

Py B & Barras F (2015) Genetic approaches of the Fe-S cluster biogenesis process in bacteria: Historical account, methodological aspects and future challenges. *Biochim Biophys Acta* **1853:** 1429–1435
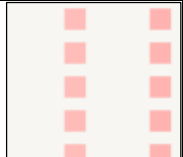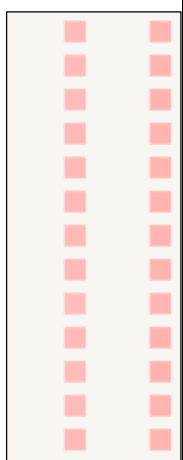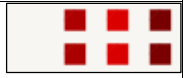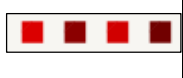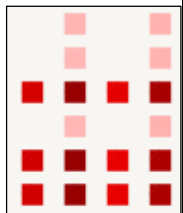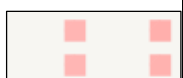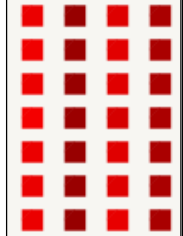
Redwood MD, Mikheenko IP, Sargent F & Macaskie LE (2008) Dissecting the roles of *Escherichia coli* hydrogenases in biohydrogen production. *FEMS Microbiol Lett* **278 :** 48–55

Rossmann R, Maier T, Lottspeich F & Böck A (1995) Characterisation of a protease from *Escherichia coli* involved in hydrogenase maturation. *Eur J Biochem* **227:** 545–550

Sargent F, Ballantine S, Rugman P, Palmer T & Boxer D (1998) Reassignment of the gene encoding the *Escherichia coli* hydrogenase 2 small subunit-identification of a soluble precursor of the small subunit in a *hypB* mutant. *Eur J Biochem* **255:** 746–754

Sauter M, Böhm R & Böck A (1992) Mutational analysis of the operon (*hyc*) determining hydrogenase 3 formation in *Escherichia coli. Mol Microbiol* **6:** 1523–1532

Sawers RG (2005) Formate and its role in hydrogen production in *Escherichia coli*. *Biochemical Society Transactions* **33:** 42–46

Sawers RG & Clark DP (2004) Kapitel: Fermentative Pyruvate and Acetyl-Coenzyme A Metabolism. In *EcoSal Plus 2004,* V. Stewart (Ed.) doi:10.1128/ecosalplus.3.5.3

Sawers RG & Pinske C (2017). NiFe-Hydrogenase Assembly. In *Encyclopedia of Inorganic and Bioinorganic Chemistry*, John Wiley & Sons, Inc., R.A. Scott (Ed.). https://doi.org/10.1002/9781119951438.eibc2484

Sawers RG, Ballantine S & Boxer D (1985) Differential expression of hydrogenase isoenzymes in *Escherichia coli* K-12: evidence for a third isoenzyme. *J Bacteriol* **164:** 1324–1331

Schäfer C, Friedrich B & Lenz O (2013) Novel, oxygen-insensitive group 5 [NiFe]-hydrogenase in *Ralstonia eutropha*. *Appl Environ Microbiol* **79:** 5137–5145

Schechter I & Berger A (1967) On the size of the active site in proteases. I. Papain. *Biochem Biophys Res Commun* **425:** 497-502.

Schut GJ & Adams MWW (2009) The iron-hydrogenase of *Thermotoga maritima* utilizes ferredoxin and NADH synergistically: a new perspective on anaerobic hydrogen production. *J Bacteriol* **191:** 4451–4457

Self W, Hasona A & Shanmugam K (2004) Expression and regulation of a silent operon, *hyf*, coding for hydrogenase 4 isoenzyme in *Escherichia coli*. *J Bacteriol* **186:** 580–587

Shepard EM, Mus F, Betz JN, Byer AS, Duffus BR, Peters JW & Broderick JB (2014) [FeFe]-hydrogenase maturation. *Biochemistry* **53:** 4090–4104

Shima S & Thauer RK (2007) A third type of hydrogenase catalyzing H_2 activation. *Chem. Record* **7:** 37–46

Skibinski DAG, Golby P, Chang Y-S, Sargent F, Hoffman R, Harper R, Guest JR, Attwood MM, Berks BC & Andrews SC (2002) Regulation of the hydrogenase-4 operon of *Escherichia coli* by the sigma(54)-dependent transcriptional activators FhlA and HyfR. *J Bacteriol* **184:** 6642–6653

Skorupa P, Lindenstrauß U, Burschel S, Blumenscheit C, Friedrich T & Pinske C (2020) The *N*-terminal domains of the paralogous HycE and NuoCD govern assembly of the respective formate hydrogenlyase and NADH dehydrogenase complexes. *FEBS Open Bio* **10:** 371–385

Soboh B, Stripp ST, Muhr E, Granich C, Braussemann M, Herzberg M, Heberle J & Gary Sawers R (2012) [NiFe]-hydrogenase maturation: isolation of a HypC-HypD complex carrying diatomic CO and CN⁻ ligands. *FEBS Lett* **586:** 3882–3887

Steiner J & Sazanov L (2020) Structure and mechanism of the Mrp complex, an ancient cation/proton antiporter. *Elife* **9:** 213

Stephenson M & Stickland LH (1932) Hydrogenlyases: Bacterial enzymes liberating molecular hydrogen. *Biochem J* **26:** 712–724

Søndergaard D, Pedersen CNS & Greening C (2016) HydDB: A web tool for hydrogenase classification and analysis. *Sci Rep* **6:** 34212

Taglicht D, Padan E & Schuldiner S (1993) Proton-sodium stoichiometry of NhaA, an electrogenic antiporter from *Escherichia coli*. *J Biol Chem* **268:** 5382–5387

Thauer RK (2011) Hydrogenases and the global H_2 cycle. *European Journal of Inorganic Chemistry* **2011:** 919–921

Thauer RK, Jungermann K & Decker K (1977) Energy conservation in chemotrophic anaerobic bacteria. *Bacteriol Rev* **41:** 100–180

Thauer RK, Kaster A-K, Goenrich M, Schick M, Hiromoto T & Shima S (2010) Hydrogenases from methanogenic archaea, nickel, a novel cofactor, and H_2 storage. *Annu Rev Biochem* **79:** 507–536

Theodoratou E, Paschos A, Mintz-Weber & Böck A (2000) Analysis of the cleavage site specificity of the endopeptidase involved in the maturation of the large subunit of hydrogenase 3 from *Escherichia coli*. *Arch Microbiol* **173:** 110–116

Unden G & Bongaerts J (1997) Alternative respiratory pathways of *Escherichia coli*: energetics and transcriptional regulation in response to electron acceptors. *Biochim Biophys Acta* **1320:** 217–234

Vignais PM, Billoud B & Meyer J (2001) Classification and phylogeny of hydrogenases. *FEMS Microbiol Rev* **25:** 455–501

Vignais PM (2008) Hydrogenases and H^+-reduction in primary energy conservation. *Results Probl Cell Differ* **45:** 223–252

Vivijs B, Haberbeck LU, Baiye Mfortaw Mbong V, Bernaerts K, Geeraerd AH, Aertsen A & Michiels CW (2015) Formate hydrogen lyase mediates stationary-phase deacidification and increases survival during sugar fermentation in acetoin-producing enterobacteria. *Front Microbiol* **6:** 150

Volbeda A & Fontecilla-Camps JC (2012) The Evolutionary Relationship Between Complex I and [NiFe]-Hydrogenase. Sazanov L. (eds) In *A Structural Perspective on Respiratory Complex I* pp 109–121. Dordrecht: Springer Netherlands

Watanabe T, Wagner T, Huang G, Kahnt J, Ataka K, Ermler U & Shima S (2019) The bacterial [Fe]-hydrogenase paralog HmdII uses tetrahydrofolate derivatives as substrates. *Angew Chem Int Ed Engl* **58:** 3506–3510

Wraight CA (2006) Chance and design--proton transfer in water, channels and bioenergetic proteins. *Biochim Biophys Acta* **1757:** 886–912

Yu H, Wu C-H, Schut GJ, Haja DK, Zhao G, Peters JW, Adams MWW & Li H (2018) Structure of an ancient respiratory system. *Cell* **173:** 1636–1649.e16

Zickermann V, Wirth C, Nasiri H, Siegmund K, Schwalbe H, Hunte C & Brandt U (2015) Structural biology. Mechanistic insight from the crystal structure of mitochondrial complex I. *Science* **347:** 44–49
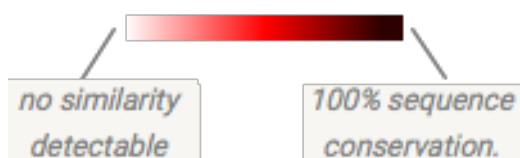
Anhang: Enterobakterielle FHL-Komplexe

Domäne: Bacteria
Phylum (Abteilung): Proteobacteria
Klasse: Gammaproteobacteria
Odnung: Enterobacterales (dt. Enterobakterien)

Familie/Gattung	Art	HyfE HyfG HycI HycE	HycJ	VP
Budviciaceae • Budvicia • Leminorella • Pragia	*Leminorella grimontii*	■ ■ ■ ■		0
Enterobacteriaceae • Biostraticola • Buttiauxella • Cedecea • Citrobacter • Cronobacter • Enterobacter • Escherichia • Gibbsiella • Klebsiella • Kluyvera • Leclercia • Mangrovibacter • Plesiomonas • Pseudescherichia • Raoultella • Saccharobacter • Salmonella • Shigella • Shimwellia • Thorsellia • Trabulsiella • Yokenella	*Buttiauxella agrestis*	■ ■ ■		0
	Cedecea neteri	■ ■ ■ ■		50
	Citrobacter amalonaticus	■ ■ ■		0
	Citrobacter farmeri	■ ■ ■		0
	Citrobacter rodentium	■ ■ ■		0
	Citrobacter sp. 302	■ ■ ■		0
	Citrobacter sp. S77	■ ■ ■		0
	Citrobacter sedlakii	■ ■ ■		0
	Citrobacter youngae	■ ■ ■		0
	Cronobacter condiment	■ ■ ■		?
	Enterobacter cloacae JD6301	■ ■ ■		100
	Enterobacter cloacae EcWSU1	■ ■ ■		100
	Enterobacter cloacae ATCC13047	■ ■ ■		100
	Enterobacter asburiae LF7a	■ ■ ■		2
	Enterobacter lignolyticus	■ ■ ■		?
	Enterobacter aerogenes	■ ■ ■		98
	Enterobacter sp. R4368	■ ■ ■ ■		?
	Enterobacter sp. 638	■ ■ ■		?
	Escherichia coli K12 W3110	■ ■ ■ ■		0
	***Escherichia coli* K12 MG1655**	■ ■ ■ ■		0
	Escherichia coli BL21	■ ■ ■ ■		0
	Escherichia coli 536	■ ■ ■	X	0
	Escherichia coli ATCC8739	■ ■ ■ ■		0
	Escherichia coli O157:H7	■ ■ ■ ■		0
	***Escherichia coli* CFT073**	■ ■ ■	X	0
	Escherichia albertii TW07627	■ ■ ■		?
	Escherichia albertii KF1	■ ■ ■	X	?
	Escherichia hermannii	■ ■ ■ ■		0
	Escherichia sp. TW09308	■ ■ ■	X	?
	Escherichia vulneris	■ ■ ■		0
	Klebsiella oxytoca	■ ■ ■		95
	Klebsiella pneumoniae	■ ■ ■		98
	Kluyvera ascorbata	■ ■ ■		0
	Raoultella ornithinolytica	■ ■ ■		?
	Salmonella enterica CT18	■ ■ ■	X	0
	***Salmonella enterica* Typhimurium**	■ ■ ■	X	0
	Salmonella bongori N26808	■ ■ ■		0
	Salmonella bongori NCTC12419	■ ■ ■		0

	Shigella flexneri	■ ■ ■	(X)	0
	Shimwellia blattae	■ ■ ■ ■		0
	Trabulsiella guamensis	■ ■ ■ ■		0
Erwiniaceae • *Buchnera* • *Erwinia* • *Pantoea* • *Phaseolibacter* • *Tatumella* • *Wigglesworthia*	*Erwinia pyrifoliae*	■ ■		?
	Erwinia amylovora	■ ■		?
	Erwinia billingiae	■ ■		?
	Erwinia tasmaniensis	■ ■		?
	Erwinia typographi	■ ■		?
	Pantoea agglomerans	■ ■		70
	Pantoea ananatis LMG20103	■ ■		?
	Pantoea ananatis AJ13355	■ ■		?
	Pantoea stewartii	■ ■		?
	Pantoea sp	■ ■		?
	Pantoea sp. A4	■ ■		?
	Pantoea sp. aB	■ ■		?
	Pantoea sp. At9b	■ ■		?
	Pantoea sp. IMH	■ ■		?
	Pantoea sp. PSNIH2	■ ■		?
	Pantoea sp. Sc1	■ ■		?
	Pantoea rwandensis	■ ■		?
	Pantoea vagans	■ ■		?
	Wigglesworthia glossinidia sp Gbr			?
	Wigglesworthia glossinidia sp. Gmo			?
Hafniaceae • *Edwardsiella* • *Hafnia* • *Obesumbacterium*	*Edwardsiella tarda* ATCC15947	■ ■ ■		0
	Edwardsiella hoshinae	■ ■ ■		0
	Hafnia alvei	■ ■ ■ ■		85
Morganellaceae • *Arsenophonus* • *Cosenzaea* • *Moellerella* • *Morganella* • *Photorhabdus* • *Proteus* • *Providencia* • *Xenorhabdus*	*Proteus mirabilis*	■ ■ ■ ■		50
	Proteus penneri	■ ■ ■ ■		0
	Proteus vulgaris	■ ■ ■ ■		0
	Providencia rettgeri Dmel1	■ ■		0
	Providencia rettgeri DSM1131	■ ■		0
	Providencia alcalifaciens	■ ■ ■ ■		0
	Providencia stuartii	■ ■		0
	Providencia rustigianii	■ ■ ■ ■		0
	Providencia burhodogranariea	■ ■ ■ ■		?
	Xenorhabdus bovienii	■ ■		?
	Xenorhabdus nematophila	■ ■		0
Pectobacteriaceae • *Brenneria* • *Dickeya* • *Lonsdalea* • *Pectobacterium* • *Sodalis*	*Brenneria sp.* EniD312	■ ■ ■ ■		?
	Dickeya dadantii 3937	■ ■ ■ ■		?
	Dickeya dadantii Ech586	■ ■ ■ ■		?
	Dickeya dadantii Ech703	■ ■ ■ ■		?
	Dickeya sp. DW 0440	■ ■ ■ ■		?
	Dickeya sp. 2B12	■ ■ ■ ■		?
	Dickeya sp. NCPPB569	■ ■ ■ ■		?
	Dickeya zeae	■ ■ ■ ■		?

			VP
	Pectobacterium carotovorum PC1		?
	P. carotovorum odoriferum		?
	Pectobacterium atrosepticum		?
	Pectobacterium sp. SCC3193		?
	Pectobacterium betavasculorum		?
	Pectobacterium wasabiae		?
Yersiniaceae • *Ewingella* • *Rahnella* • *Samsonia* • *Serratia* • *Yersinia*	*Ewingella americana*		95
	Rahnella aquatilis HX2		100
	Rahnella aquatilis CIP78.65		100
	Rahnella sp. Y9602		?
	Serratia fonticola AUAP2C		9
	Serratia fonticola RB25		9
	Serratia marcescens Db11		60
	Serratia marcescens FGI94		60
	Serratia plymuthica		80
	Serratia proteamaculans		?
	Serratia symbiotica		?
	Serratia sp. DD3		?
	Serratia grimesii		?
	Serratia sp. M24T3		?
	Serratia sp. Ag1		?
	Serratia sp. ATCC39006		?
	Serratia sp. H1n		?
	Yersinia enterocolitica LC20		2
	Yersinia enterocolitica 8081		2
	Yersinia ruckeri		10
	Yersinia pseudotuberculosis		0
	Yersinia aldovae		0
	Yersinia pestis CO92		0
	Yersinia kristensenii		0
	Yersinia massiliensis		0
	Yersinia intermedia		0
	Yersinia frederiksenii		0

no similarity detectable — 100% sequence conservation.

Homologie der Proteine zu den angegebenen *E. coli* Proteinen HyfE, HyfG, HycI und HycE ist durch Rotfärbung angezeigt. Das Vorhandensein von HyfE zeigt einen FHL-2 Komplex an. Die Abwesenheit von HycI indiziert das Fehlen beider Komplexe. Auflistung der Stämme und Farbgebung entsprechend der Datenbank String.db und stellt eine Auswahl aller sequenzierten Enterobakterien-Genome dar.

HycJ indiziert das Vorhandensein eines Extragenes im *hyc*-Operon, welches auf wenige Organismen wie z.B. *Salmonella enterica* Typhimurium und *E. coli* Nissle 1917 (verwandt mit *E. coli* CFT073) beschränkt ist.

VP gibt die Reaktion im Voges-Proskauer Test als % an (100 = 2,3-Butandiolgärung mit Nachweis von Acetoin; 0 = Gemischte Säuregärung). Daten größtenteils entnommen aus *Bergey's Manual of Systematic Bacteriology* (Brenner & Farmer 2015).

Lebenslauf

Name	Constanze Pinske
Nationalität	Deutsch
Geburtsdatum	24.12.1983
Geburtsort	Berlin, Deutschland
ORCiD	0000-0001-6248-2437
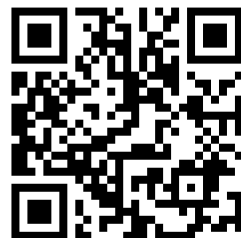
Abbildung 19: QR Code als Link zum ORCiD Profil – kompletter wissenschaftlicher Werdegang

2017-2019	"*For Women in Science*" Fellowship der Deutschen UNESCO-Kommission, L'Oréal Germany und der Christiane Nüsslein-Volhard-Stiftung
Seit 2015	Abteilung für Allgemeine Mikrobiologie, Martin-Luther-Universität Halle-Wittenberg
2012-2015	University of Dundee/UK, School of Life Sciences; *Postdoctoral research assistant* in der Gruppe von Prof. Frank Sargent
2008-2011	Doktorarbeit 'Maturation und Assemblierung von [NiFe]-Hydrogenasen in *Escherichia coli*' in der Abteilung für Allgemeine Mikrobiologie der Martin-Luther-Universität Halle-Wittenberg, unter der Anleitung von Prof. R. Gary Sawers; Verteidigung mit Prädikat *summa cum laude*.
2007-2008	Diplomarbeit 'Maturation von [NiFe]-Hydrogenasen: Strategien zur Isolierung Hydrogenase-negativer Mutanten in *Escherichia coli*' in der Abteilung für Allgemeine Mikrobiologie der Martin-Luther-Universität Halle-Wittenberg, unter der Anleitung von Prof. R. Gary Sawers
2003-2008	Martin-Luther-Universität Halle-Wittenberg; Diplom der Biochemie

Danksagung

Der FHL-Komplex hat bereits seit meiner Doktorarbeit eine große Faszination auf mich ausgeübt. Die kleinen Gasbläschen in den Durham Röhrchen zeugten von einer Aktivität des Komplexes, die man mit bloßem Auge betrachten konnte.

Deshalb gilt selbstverständlich mein allererster Dank meinem Mentor, Dienstvorgesetzen und Chef Prof. R. Gary Sawers, der DER Experte für Hydrogenasen ist. Zahlreiche Manuskripte und Ideen sind über seinen Tisch gegangen und unermüdlich korrigiert und kommentiert worden. Das Oxford Komma wird mir trotzdem immer ein Rätsel bleiben.

Ich bedanke mich bei Frau Prof. Andrea Sinz und Herrn Prof. Gottfried Unden für die Bereitschaft zur Übernahme der Gutachten.

Auch während meiner Postdoc-Zeit in Schottland konnte ich so gut wie selbständig an diesem Komplex weiter forschen und den Zugewinn des Wissens um die FHL Aufreinigung von Prof. Frank Sargent mitnehmen - Cheers.

Für die ‚Aufnahme' in die SPP1927-Familie und die dortige Organisation möchte ich Frau Prof. Silke Leimkühler meinen Dank ausdrücken und insbesondere die damit verbundene finanzielle Unterstützung durch die DFG erwähnen.

Ute Lindenstrauß ist in den letzten Jahren mehr als nur eine geschätzte Mitarbeiterin geworden, denn sie hat mich nicht nur bei der experimentellen Ausführung, sondern auch in Garten-, Familien-, und Urlaubsfragen beraten.

Dorothea Lubek hält den Projekten seit 2015 die Treue und weil ihr auf zwischenmenschlicher Ebene nichts entgeht, ist sie mir seit kurzem zusätzlich die liebste Büronachbarin. Halt weiter durch! Das gleiche gilt für alle weiteren Mitglieder der *E. coli* Forschung wie Michelle Kammel, Alexander Haase und Kerstin Nutschan.

Anna-Luisa Schramm, Patricia Rothe, Stefan Zantop Linares und Janik Telleria Marloth haben meinen Dank und meine Bewunderung für ihre sorgfältig durchgeführten Arbeiten u. a. zum FHL-Komplex insbesondere an der eigenwilligen Elektrode verdient. Es wurden weiterhin Daten von Philipp Skorupa verwendet.

Dr. habil. Stefan König und Dr. habil. Hauke Lilie danke ich für die Kollaboration rund um das HycH Projekt, die Möglichkeit der Nutzung von Geräten und Gasen sowie der Generierung und Auswertung der somit gewonnenen Daten. Dr. Christian Ihling sei für die Durchführung zahlreicher MS Analysen während der letzten Jahre gedankt.

Dr. habil. Ute Lechner und Dr. habil. Basem Soboh haben mir stets mit Tipps zur Karriere geholfen und als Vorbilder gedient.

Erklärung

Hiermit erkläre ich, Dr. Constanze Pinske, an Eides statt, dass die vorliegende Habilitationsschrift selbständig und ohne fremde Hilfe verfasst wurde. Andere als die angegebenen Quellen und Hilfsmittel (Office 2019 Programme, String.db und Google Translate) wurden nicht verwendet und die den benutzten Werken wörtlich oder inhaltlich entnommenen Stellen wurden als solche kenntlich gemacht.

Weiterhin versichere ich, dass ich diese Arbeit an keiner anderen Universität oder Hochschule im In- oder Ausland vorgelegt habe.

Halle, den 01.02.2021

Dr. Constanze Pinske